Ana Margarida Martins Gaspar

Licenciada em Engenharia de Micro e Nanotecnologia

Growth of yttria-stabilized zirconia with 3D printer

Dissertação para Obtenção do Grau de Mestre em

Engenharia de Micro e Nanotecnologias

Orientadora: Doutora Isabel Maria Mercês Ferreira, Professora Associada, Faculdade de Ciências e Tecnologias da Universidade Nova de Lisboa

Júri

Presidente:	Doutor Rodrigo Ferrão Paiva Martins, Prof. Catedrático do Departamento de Ciências dos Materiais, FCT-UNL
Arguente:	Doutor Nuno Miguel Dias Vitorino, Investigador da INNOVNANO
Vogal:	Doutora Isabel Maria Mercês Ferreira, Prof. Associada do Departamento de Ciências dos Materiais, FCT- UNL

Setembro de 2016

FACULDADE DE CIÊNCIAS E TECNOLOGIA
UNIVERSIDADE NOVA DE LISBOA

Growth of yttria-stabilized zirconia with 3D printer

Dedico esta tese à minha família
e em especial ao meu avô Luciano.

Acknowledgment

Em primeiro lugar quero agradecer à minha orientadora, Professora Doutora Isabel Ferreira pelo apoio e suporte que me deu nesta etapa, pela oportunidade de trabalhar neste excelente grupo e por ter sugerido este tema de tese. Apesar de muitas vezes andar a bater com a cabeça nas paredes, sempre me fez ver o lado positivo das coisas e o resultado final foi sem dúvida positivo e recompensador.
Em especial agradeço à Inês Ropio, foi uma ajuda sem dúvida essencial na conclusão desta etapa. Um enorme obrigada é pouco. "Paciência com a nossa menina", paciência e persistência acho que são as duas palavras que mais se adequam a estes últimos meses. Além de todo o apoio e ajuda levo daqui sem dúvida uma amiga.
E claramente não podia deixar de agradecer à Catarina, Joana, Joana, Ana, Paulo, David, Zeca e João-zinho, por me terem acolhido no grupo desde o primeiro dia, ajudado sempre que precisei, por todo companheirismo demonstrado e todas as risadas dadas no laboratório. Não menos importante, um grande obrigado ao Filipe por ter me ter ajudado com um dos meus grandes problemas iniciais desta tese.
Agradeço à INNOVNANO pelo material fornecido e por todo o suporte dado, de outra forma esta tese não existiria.
Um obrigada à Catarina Bianchi, ao Paulo Duarte e ao António Almeida, por me terem fornecido um pouco do seu trabalho (nanopartículas de prata e óxido de grafeno) para poder realizar um dos meus estudos.
Ao Prof. Dr. Rodrigo Martins e à Prof. Dra. Elvira Fortunato por terem criado este excelente curso e por todo o tempo que têm investido para que ele se torne cada vez melhor.
Agradeço a todos os docentes do DCM que se mostraram sempre prestáveis para ajudar em qualquer altura. Tenho de agradecer à Prof. Dra. Célia Henriques, Prof. Dr. Jorge Silva, por terem tirado algum do seu tempo para me ajudarem e auxiliarem na realização dos ensaios biológicos. Ao Prof. Dr. Alexandre Velhinho pela realização dos ensaios de compressão. À Prof. Dr. Margarida Lima pela ajuda na realização das medições pelo método de Arquimedes e disponibilidade que me deu para utilizar o equipamento do laboratório de Cerâmicos. Ao Prof. Dr. João Paulo Borges pela ajuda e principalmente disponibilidade para a utilização dos equipamentos do laboratório de Biomateriais. À Prof. Dr. Alexandra Fernandes e ao Prof. Dr. Pedro Baptista pela disponibilidade demonstrada na realização de ensaios de citoxicidade.

E como não podia faltar tenho de agradecer aos meus amigos, todos eles de alguma forma foram essenciais nesta minha caminhada, sendo que nestes últimos meses alguns deles destacaram-se.
À Sofia que há cinco anos, está a caminhar ao meu lado e nesta fase final foi essencial a sua presença constante e a amizade. Obrigada por todos os jantares, todas as conversas, toda a música motivacional e por alinhares em tudo. Claramente todo o vinho que já foi degustado por nós nestes meses também agradece.
Ao Zé que apesar de estar a quilómetros de distância através das suas magias fez com que o contacto nunca fosse perdido, o apoio estivesse sempre presente e as conquistas (com todos os sentidos que a palavra possa ter) fossem sempre partilhadas.
Ao Almeida que foi uma surpresa e é uma bestinha que teve paciência para me aturar. Apesar de "obrigada" ser se te pedisse para me ires buscar uma garrafa de água e tu fosses, obrigada por todo o apoio e todas as gargalhadas soltas nos últimos meses.
À Andreia que apesar de ser meio desaparecida e uns dias sabermos dela outos não, é uma amiga espetacular com quem se faz grandes loucuras, mas está lá quando é preciso mesmo a quilómetros de distância.
Ao Fofo que só o nome diz tudo, é uma pessoa maravilhosa e apesar de nos últimos meses ter andado do outro lado mundo esteve sempre presente e a interessado pelo que se passava por cá.
Ao Gonçalo por toda a amizade que sempre demonstrou e até mesmo pelas vezes que vêm só apertar-me as bochechas para me chatear.
Ao Jaime que foi o meu companheiro de batalha desde Janeiro, batemos muitas vezes com a cabeça na parede e por incrível que pareça não demos em malucos (completos), vitória.
À Carolina pela boa amiga que é e que os jantares nunca se percam mesmo que a frequência deles mude.

Ao Gabi, que apareceu e ocupou um espaço gigante, aconselho toda a gente a ter um Gabi na vida, vale a pena.
À Ju por todas as vezes que se preocupou comigo (ameaçando mesmo levar-me ao hospital se eu não fosse comprar os medicamentos), pelos jantares e brincadeiras.

Ao Miguel Dias que esteve lá desde o início dos inícios, sempre a comemoramos as vitórias, a aprendemos juntos com as nossas derrotas e que sempre me disse "Aninhas sê feliz". Quem me dera que ainda aqui tivesses e pudéssemos ir comemorar mais esta vitória no sítio do costume.
A todos os meus amigos de Ponte de Sor e circunvizinhos, não vou enumerar ninguém, pois todos são especiais à sua maneira e em grande parte é devido a eles que me tornei quem sou visto que foi ao lado deles e com eles que cresci.

À avó Tina por todas as velinhas que acendeu antes de cada dia importante na minha vida e ao avô Luciano por todo o orgulho que tinha em mim, por cada sorriso de domingo e por eu saber que seria o avô mais orgulhoso do mundo ao ver a sua "Engenheira" a acabar o curso.
Aos tios que sempre se mostraram disponíveis para tudo e sempre torceram por mim. Ao primo por todo o interesse que demonstra quando lhe estou a mostrar algo do meu curso e porque para mim sempre foi uma pessoa a seguir, querendo sempre que tivesse tanto orgulho em mim como eu tenho nele.

E por último mas claramente mais importante, porque o melhor muitas vezes fica para o fim e estes são os verdadeiros pilares da minha vida. Quero agradecer aos meus pais que sempre me mostraram que temos de lutar pelo que quereremos, que nada cai do céu, mas que nem sempre a vida é fácil e tens de ter força para agarrar o touro pelos cornos e não cair. Que me aconselharam da melhor forma sobre tudo e sempre me mostraram que os erros também fazem parte da vida e devemos aprender e crescer com eles. Ao pai Jorge por exemplo por me tirar de casa e me levar para o monte plantar pinheiras. À mãe Zeca por fazer as melhores paparocas do mundo e me fazer sentir em casa mesmo estando longe. São os maiores pais galinhas da história e que são o maior exemplo que alguém pode ter.
À minha irmã Kika por toda alegria que demonstra sempre que chego a casa e por me fazer sentir sempre melhor mesmo nos piores dias. Por todas as grandes conversas antes de dormir, todas as gargalhadas de tirar o fôlego a qualquer um e que fazem soltar a galinha. E porque sendo a irmã mais velha sempre quis que ela tivesse as melhores referências possíveis, esperando sempre fazer parte delas.
Um grande obrigado a todos lá de casa (mãe, pai e Kika) não chega para quantificar o quanto agradeço o facto de sempre lá terem estado quando precisei, por serem sempre o meu grande apoio e a minha força. Obrigada por aturarem o meu mau feitio quando não tem nada a ver com você. E claro, por estarem comigo em cada uma das minhas vitórias fazendo às vezes festas maiores do que as que eu própria faço.

This work was possible due to the partial financing support of the following projects: H2020-ICT-2014-1, RIA, TransFlexTeg-645241; ERC-CoG-2014, ChapTherPV, 647596; and by FEDER funds through the COMPETE 2020 Program and National Funds through FCT - Portuguese Foundation for Science and Technology under the project UID/CTM/50025/2013. And due to 3YSZ nanopowders provided by INNOVNANO.

Abstract

3D printing manufacturing is being widely applied in several areas, including medicine that may be the one with the most promising future. The main advantage of this technology comparing to conventional ones is the possibility to create customizable bioprints for biomedical applications.

In this thesis, the 3D printing conditions of ceramic samples made of 3% mol yttria-stabilized zirconia were studied and optimized. Initially, several pastes were tested in order to choose the one with the best printability, wish resulted in one with binder and another without. Also, geometry studies were performed to achieve samples with optimized mechanical properties. The printed samples were sintered and characterized to understand how the geometry and the sintering temperature influence the mechanical properties. The morphology was observed using optical and electronic microscopy, and the apparent density obtained by Archimedes method. The degradability and biocompatibility of samples were also tested.

The results show that the 3D printed ceramic pieces have compression strength, Young's modulus and porosity comparable to the ones found in literature for human bones confirming its viability for biomedical applications. Tests demonstrate that the samples do not degrade in contact with simulated body fluids, and biological assays confirms its biocompatibility and cells proliferation.

Keywords: 3YSZ pastes; 3D printing; mechanical resistance; sintering; morphology; biocompatibility.

Resumo

A fabricação por impressão 3D é amplamente aplicada em diversas áreas, incluindo na medicina que pode ser a com o futuro mais promissor. A principal vantagem desta tecnologia em comparação com as convencionais, é a possibilidade de criar bioimpressões personalizadas para aplicações biomédicas.

Nesta tese foram estudadas e otimizadas as condições de impressão 3D para amostras cerâmicas de zircónia estabilizada com 3% mol de ítria. Inicialmente, várias pastas foram testadas, a fim de escolher aquela com a melhor qualidade de impressão, resultando numa com ligante e outra sem. Além disso, estudos de geometria foram realizados para obter as amostras com propriedades mecânicas otimizadas. As amostras impressas foram sinterizadas e caracterizadas para compreender como a geometria e a temperatura de sinterização influenciam as propriedades mecânicas. A morfologia foi observada usando microscopia ótica e eletrónica, e a densidade aparente obtida pelo método de Arquimedes. A degradabilidade e compatibilidade de amostras também foram testadas.

Os resultados mostram que as peças 3D impressas tem uma resistência à compressão, módulo de Young e porosidade comparáveis aos encontrados na literatura para os ossos humanos o que confirma a sua viabilidade para aplicações biomédicas. Os testes demonstram que as amostras não se degradam em contacto com fluidos corporais simulados e os ensaios biológicos também confirmam a sua biocompatibilidade e proliferação de células.

Palavras-chave: pasta 3YSZ; impressão 3D; resistência mecânica; sinterização; morfologia; biocompatibilidade.

Abbreviations

2D	Two-dimensional
3D	Three-dimensional
3YSZ	3% mol yttria-stabilized zirconia
4YSZ	4% mol yttria-stabilized zirconia
8YSZ	8% mol yttria-stabilized zirconia
AM	Additive manufacturing
AP	Apparent porosity
BTE	Bone tissue engineering
c	Cubic phase
CC	Control cells
CC-	Negative control cells
CC+	Positive control cells
CAD	Computer aided design
CM	Control medium
CP	Calcium phosphate
E	Young's modulus
ECM	Extracellular matrix
FPDs	Fixed partial dentures
m	Monoclinic phase
m_d	Mass of the sample
m_i	Mass of the immersed sample
m_w	Mass of the wet sample
NASA	National Aeronautics and Space Administration
QD-LEDs	Quantum dot-Light emitting diodes
RP	Rapid prototyping
RT	Room temperature
SBF	Simulated body fluid
SEM	Scanning electron microscopy
SFF	Solid-freeform
SOFC	Solid oxide fuel cell
STL	Stereolithography
t	Tetragonal phase
T	Temperature
TEM	Transmission electron microscopy
XRD	X-ray diffraction

Symbols

σ	Stress
σ_{Max}	Maximum stress
ε	Strain
°C	Degree Celsius
ρ	Density
ρ_a	Apparent density
ρ_{li}	Density of the immersion liquid
Ag	Silver
AgNPs	Silver nanoparticles
C	Carbon
HA	Hydroxyapatite
L	Litre (SI) - mL, µL
g	Gram
GO	Graphen oxide
h	Hour
m	Meter (SI) - cm, mm, µm
min	Minutes
mol	mole
PBS	Phosphate-buffered saline
TCP	Tricalcium phosphate
Y_2O_3	Yttrium oxide or yttria
YSZ	Yttria-stabilized zirconia
ZrO_2	Zirconium dioxide or zirconia

Table of Contents

List of Tables

List of Figures

Objectives

The main goal of this work was to investigate the viability of ceramic samples produced by 3D printing using 3% mol yttria-stabilized zirconia nanopowders developed by INNOVNANO and evaluate their mechanical properties and biocompatibility for possible biomedical applications.

The development of this work required an intensive and exploratory study since it was the first time that extrusion 3D printing process was used to obtain ceramic samples at CENIMAT/I3N and FCT-UNL. Therefore, the first challenge was to produce a 3D printable paste containing the INNOVNANO nanopowder mixed with a solvent and the second one to achieve the sample geometry with the highest mechanical properties. Finally, the biocompatibility and the degradation behaviour of these samples were evaluated.

1. Introduction

The attempt to print 3% mol yttria-stabilized zirconia (3YSZ) nanopowders synthesized by a Portuguese company, INNOVNANO has been done by the first time in this work. This is one of the commercial products developed by this company for ceramic components and coating applications where exceptional wear-resistance, high component and flexural strength, and excellent durability are needed. Although this material is being already used for dental applications, for instance, the combination of printing by a 3D plotter and the use of nanometric YSZ powders has never been tried as far as we have searched. In the following is explained and reviewed the 3D printing processes, and the bioceramics already investigated and tested.

1.1. 3D printer

The 3D printing has gained much attention in the last years and in many areas of manufacturing. It already started replacing some of the traditional processes because 3D printers greatly facilitate manufacturing process, reduces consuming of raw materials and its waste. There is ongoing a huge increase on the research field across many areas, such as engineering, manufacturing, art, education and medicine. [1,2] Specifically 3D printing techniques/methods provide a powerful tool to fabricate complex 3D structures.

The 3D printing also mentioned as additive manufacturing (AM), rapid prototyping (RP), or solid-freeform technology (SFF), was described in 1986 by Charles Hull. [1,3] In 1993, Michael Cima and Emanuel Sachs patented the first device termed "3D printer" to print plastic, metal, and ceramic parts.[3]

There are many types of 3D printing, but the basic concept of all 3D printers is simple, firstly is required a 3D dataset, originating from medical imaging sources or CAD programs. Then, 3D dataset has to be converted into 2D data by a special slice algorithm. Thus, a digital model is supplied to the printer, which interprets the digitally supplied coordinates derived from the STL file. STL file is a sequence of 2D horizontal cross sections, which allows the 3D object to be printed in consecutive layers of the desired material (layer-by-layer, observed in Figure 1.1), starting at the base.

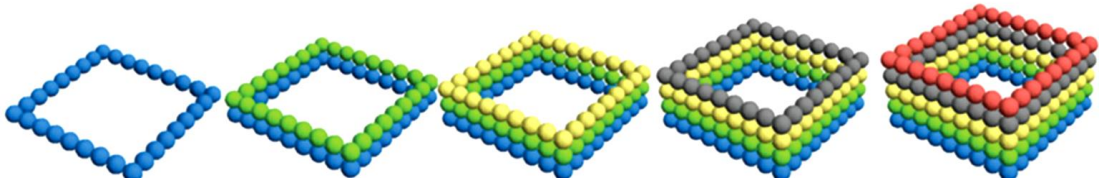

Figure 1.1 Three representations of manufacturing layer-by-layer. [4]

The concept behind 3D printing is not innovative, considering that many organisms have the same layer-by-layer structure. For example, when molluscs that have seashells begin to grow, calcium carbonate is successively added to the outer shell, the reason behind the possibility to observe lines of growth in seashells, which is basically a construction layer-by-layer as in 3D printing (see Annex 1). [5] Nature is a source of inspiration for humanity and nowadays is possible, in industrial-scale, to have 3D printers capable to fabricate an object as large as a car, a house, and many others.

As mentioned there is an assortment of 3D printing methods (different methods in Table 1.1), and all of them operate upon similar principles. Firstly, an STL file is created and the digital coordinates provided by the STL file are sent to the 3D printer, which traduces the slicing in trajectories and layers. This process uses the principle of multilayer deposition, which consists in the material extrusion through a nozzle in several layers to construct the object from the STL file. The object is gradually printed from the bottom to the top, through the layer build-up. [6]
3D printing involves many technologies, depending of the material and of its hardening system, such as the sintering or melting by laser, the binder or resin jetting, or the filament depositing. [7]

Table 1.1 Comparisons of 3D printing methods for the scaffolds manufacturing. [2–4,65,66]

Method	Principle	Advantages	Disadvantages	Resolution (XY/Z) [μm]
Stereolithography (SLA)	UV initiated curing of defined photoresin layer.	Very high resolution (submicron scale). Speed of fabrication. Smooth surface finish. Available cell and biology materials. Complex internal features can be obtained.	Materials must be photopolymers. Expensive cost. Support system is necessary for overhang and intricate objects. Only available with UV curable liquid polymer.	70−250/ 1−10, <1
Inkjet Printing	Powder-liquid binding; Polyjet technology (hybrid between SLA and Inkjet) allows inkjet printing of photoresins.	Versatile in terms of usable materials. No support is necessary for overhang or complex structures.	Potential toxicity (incompletely removed binders). Low mechanical strength prints compared to laser sintering. Time Consuming (Post-processing).	20−50/50
Selective Laser Sintering (SLS)	Laser induced heating of powder particles.	Provides scaffolds with high mechanical strength. Powder bed provides support for complex structures. Fine resolution. High-strength object. Variety of materials. No need for support.	Limitation on materials (must be shrinkage and heat resistant). Very high temperature required (up to 1400°C). Expensive and time consuming (processing and post processing. Impossible to print cells or biological materials. Rough surface. Limitation to powder form.	50/1−2
Fused Deposition Modeling (FDM)	Extrusion of molten thermoplastics.	Low cytotoxicity vs direct 3D printing. Relatively inexpensive (printers and materials). No need for platform/support.	Limitation on materials (often requires thermoplastics). Materials used are non-biodegradable. Requires support structure for overhangs and complex shapes. Post-processing may be necessary. Low Resolution.	250/50
Bioplotting	Uses a nozzle extrusion system of thermally or chemically treated materials.	Prints viable cells. Soft tissue applications. Mild condition of process allows drug and biomolecules (proteins and living cells) plotting.	Limitation on nozzle size (Must not be cytotoxic during processing). Requires support structure for printing complex shapes. Heating/post-processing needed for some materials restricts. The biomolecule incorporation.	-

3D printing gives people powerful new tools of design and production. This technology has been driven rapidly by advances in computing power, new design software and new materials. The computer is a critical point in the 3D printing process, with no instructions from a computer, the printer is stopped.[10] Until now, three-dimensional printing has mostly been used to create replicas of natural and man-made structures, such as implants, toys or art statues. 3D-printing is being applied in various areas such as:

biological applications (e.g. biomedical engineering, tissue scaffolding and surgical preparation) [1,9], pharmaceuticals [12], forensic science, education, chemical applications (e.g. micro/macrofluidics, electronics, scaling and custom Labware) [3], culinary [13] and even personalized consumer products at home (e.g. bicycle parts and jewellery). [1] It is also being used in automotive and aerospace industries for printing prototypes of car and airplane parts and applications in gun prototyping and manufacturing processes for the military. [3,12] On board the Mars Rover, NASA has several custom-made 3D printed metal parts, that could not have been manufactured by anything other than a 3D printer, since it has complicated shapes of curves and inner hollows. [10] The Boeing's premium airplane, the 787 Dreamliner, has at least thirty-two different 3D printed parts. [10] Another current application is the 3D printing of quantum dot-based light emitting diodes (QD-LEDs) that exhibit pure and tunable colour emission properties. [15]
With advanced 3D printing techniques, it will be possible to manufacture nano/microscale complex structures that are not feasible by other manufacturing techniques.

Initially, 3D printing technologies were designed for non-biological applications, as the deposition of metals, ceramics and thermoplastic polymers and generally involved the use of organic solvents, high temperatures or crosslinking agents that are not compatible with living cells and biological materials. Nowadays, due to recent advances in the 3D printing technology, cell biology and materials science, it is already possible to print biocompatible materials, cells and tissue engineering scaffolds. [1,6,14] This technique is called 3D bioprinting and has captured increasing attention in the past years since it offers the possibility of implants fabrication at room temperature and hence the incorporation of organic, biologically active, or hydrated molecules within the bulk of the implant.[14,15] This type of 3D printing, has already been used in medical applications such as the production of dental implants, personalized prosthesis (e.g. vascular grafts, tracheal splints) [18] and for the generation and transplantation of several tissues [18], as multilayered skin, bone [19], craniofacial reconstruction [20], heart tissue [1] and cartilaginous structures [1,19]. The 3D bioprinted biomaterials can serve as an artificial extracellular matrix (ECM) for the cells (scaffold), giving structural support and allowing cellular attachment. [6] The interactions between cells and an underlying biomaterial are important for the promotion of cell adhesion, proliferation and function.
Over the past 15 years, printers have been increasingly utilized for biomedical applications in various areas of medicine and tissue engineering. 3D printing has been used to research and testing models to surgical planning, device manufacturing and tissue or organ replacement. [14,18,20,21] The most important application in medicine has been the fabrication of geometrically accurate models for surgery planning. Klammert et al. [17] utilized the 3D printing technique for the fabrication of individual cranial models according to patient data obtained by computed tomography. [17]

The number of people suffering of illnesses or traumas, such as heart attacks, strokes, and joint degeneration is increasing. This way, 3D printing technology emerged as a promising tool to fabricate scaffolds with high precision, accuracy and high degree of complexity, where details can be performed at micrometre scale. Some advantages of using 3D printing are the ability to fabricate versatile scaffolds with complex shapes, capable of a homogenous cell distribution, and the ability to mimic the ECM. The disadvantages are the availability of biomaterials with the stability and desired properties for 3D printing and the production time that it takes to fabricate scaffolds. [4]
For a successful design of a tissue engineering scaffold, several characterization criteria are required: morphology (e.g. porosity, pore size and surface area); mechanical properties (e.g. compressive and tensile strength); bulk properties (e.g. degradation and its relevant mechanical properties); surface properties (e.g. surface energy, chemistry and charge); biocompatibility and biodegradability. [1,22–24] Porosity is defined as the fraction (i.e. percentage) of the total volume occupied by voids. [26] Two very important criteria are biocompatibility and biodegradability, ensuring that scaffolds have nontoxic degradation by products. [4] These should be also readily metabolized and rapidly cleared from the body.[1] The mechanical stability must be structurally sound so as to withstand daily activity and normal body movements. [4]
Composite materials are important for 3D printing because they can increase mechanical strength and can perform more intricately designed scaffolds. [4]

Bones perform several vital functions within the body, for example primarily structural support and protection of bodily organs. [27] This way, majority of research on 3D printed scaffolds has been concerned with bone tissues. [4] The scaffolds serve as three-dimensional templates for initial cell attachment and subsequent tissue formation. For this reason, it is important to ensure the cell ingrowth into the structure. [18] Bone tissue has strong capability for regeneration in non-critical size bony defects and repair after fractures. [28] Nowadays, there is a need for bone replacement materials used in bone tissue engineering (BTE). [28] The biocompatibility of materials is one of the most important prerequisite for their use as a scaffold.

Bone is a dynamic and complex organ. The main role of the bone network is in providing the necessary mechanical support, movement and protection, with other roles ranging from blood production, to storage of mineral materials, pH regulation and housing multi progenitor cells. [6] Bone is not uniformly dense, it is able to bear heavy loads, withstand large forces and to flex without fracture within certain limits. The bone ECM is comprised of two main zones with very different morphological properties: a relatively dense outer layer (cortical or compact bone), which surrounds a less dense and porous (cancellous or trabecular or spongy bone), which in turn is filled with a jelly tissue: the bone marrow, Figure 1.2. [6,20] Cancellous bone is a highly porous bone matrix, with interconnected porosities between 50–90% and visible macropores in the range of 500–1000μm and is positioned between shells of cortical bone. Cortical bone has a compact solid-like structure, with enclosed vascular Haversian canals, having a low porosity between 3–12%, and pores smaller than 500μm and in humans, 80% of the bone is cortical. [6] The bone ECM is constantly changed by the cells that reside in it, where osteoblasts are responsible for producing and mineralizing new bone matrix, osteocytes work on maintaining the matrix, and osteoclasts are responsible for resorbing the matrix. Thus, in a bone substitute designing, it is necessary to control the porosity and mechanical properties. This means that an ideal bone substitute must have a heterogeneous porous structure, with varying physical and mechanical characteristics. [6]
Scaffolds are biocompatible structures of natural or synthetic origin, which can mimic the ECM of native bone and provide a 3D environment in which cells become attached and proliferate. A porous scaffold allows cell spreading and an effective transport of nutrients, oxygen, waste, as well as growth factors, favouring continuous ingrowth of bone tissue from the periphery into the inner part of the scaffold.

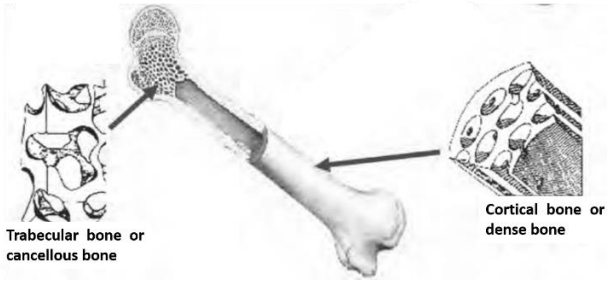

Figure 1.2 Cortical and cancellous bone in human femur. [27,28]

Table 1.2 Range of mechanical properties for human cancellous and cortical bone. [6,29,30]

Bone type	Compressive strength (MPa)	Young's modulus (GPa)
Cancellous bone	4-12	0.01-0.5
Cortical bone	130-225	3-30

The generality of biomaterials which have been applied in the field of bone tissue engineering are dense material, and therefore they can't be used to inducing new bone ingrowth to the grafted materials. Ideal bone substitutes should promote new bone formation to fill the voids and, considering that in this thesis, ceramic materials were chosen, due to its excellent properties. [19]

Studies say that the high level of porosity and pore interconnectivity (ideal for a bone substitute) can be limited by the mechanical strength requirements, mainly in the case of load bearing applications. [6] Engineering ceramics are becoming increasingly important in the nowadays-industrial landscape, thanks to the exceptional combination of good mechanical, thermal and chemical properties. [33]

Figure 1.3 Advantages of 3D printing.

1.2. Bioceramic

Bioceramics are a class of advanced ceramics that are produced by sintering or melting inorganic raw materials to create an amorphous or crystalline solid body. They are biocompatible, can be inert, bioactive and degradable in a physiological environment, and are chemically similar to the inorganic component of hard tissues, which makes it an ideal biomaterial. In this way, bioceramics can be used in medical and dental applications, mainly as implants and replacements. Porous final products are mainly used for scaffolds. However, it is brittle, with poor tensile strength, which makes it unsuitable for load-bearing applications. [6,24,32,33]
Bioceramics used for tissue engineering may be classified as nonresorbable (relatively inert), bioactive or surface active (semi-inert) and biodegradable or resorbed (noninert). Materials that are classified as bioceramics include alumina, zirconia, calcium phosphates, silica-based glasses or glass ceramics and pyrolytic carbons. [24,32]
A general weakness of 3D-printed (porous) bioceramic implants is their brittle nature and relatively low mechanical performance. However, implant pores can be infiltrated with polymers to alter strength, fracture resistance and biodegradation speed. [17]
Ceramics are typically consolidated from powders by sintering or deposited in thin films, because they are difficult to process. Ceramics have great proprieties as high temperature capability, environmental resistance, and high strength, however, they have some disadvantages as the porosity and inhomogeneity introduced during processing that may initiate cracks and a little ability to resist to fracture. [36]
Commonly investigated ceramics for bone regeneration can be classified into two categories: bioactive calcium phosphates (such as HA and TCP) or biopassive ceramics (such as alumina and zirconia). [6]

1.2.1. Zirconia

Zirconia is an inorganic material, highly biocompatible and was introduced in 1985 as an alternative material to alumina for ceramic femoral heads, due to demonstrated enhanced mechanical properties. [26,33,35]
Zirconium oxides or zirconia (ZrO_2) has high mechanical properties, thermal insulation, ionic conductivity and low toxicity, which is an inert material and cannot be degraded in vivo. However, the mechanical properties of sintered ZrO_2 are known to be far greater than that of a cortical bone. In fact, the sintered 100% ZrO2 substrate has a flexural strength 200 MPa. [31,37] Nowadays it is used as material for e.g. body-implants, dental crowns, stamping dies, oxygen sensors and several micro components. [33]

ZrO_2 presents three polymorphs at successive temperature ranges: monoclinic (below approximately 1170°C), tetragonal (~1170–2370°C) and cubic (~2370–2680°C). [36–38]

$$m - ZrO_2 \overset{1170°C}{\longleftrightarrow} t - ZrO_2 \overset{2370°C}{\longleftrightarrow} c - ZrO_2 \overset{2680°C}{\longleftrightarrow} melt \qquad (1.1)$$

As most of the oxide ceramics, zirconia is inherently brittle, however this can be refined using doping elements, thus improving their characteristics. This is achieved by the addition of small amounts of yttria oxide (Y_2O_3) in the zirconia, this oxide is also commonly used to stabilize cubic zirconia. Femoral heads of zirconia can typically tolerate 250 kN, a generally superior value to what is possible with alumina or metal femoral heads. Zirconia is also used for dental applications due to aesthetic and mechanical benefits. [34,35]

1.2.1.1. Yttria-stabilized zirconia (YSZ)

Yttria-stabilized zirconia (YSZ) is an oxide material resistant to corrosion and radiation, it has high fracture strength, flexural strength (~950MPa) [37,41] , Young modulus (210 GPa) [36], fracture toughness (~10 MPa $m^{1/2}$) [35,39] and chemical stability (chemical inertness). The presence of oxygen vacancies allows yttria to become a fast-ion conductor at elevated temperatures [40,41], which also reveals good thermo-mechanical stability and low toxicity and density. [42,43]
Yttria has a wide range of applications, for example orthopedic applications such as hip and knee joints and, recently was introduced into prosthetic dentistry for the fabrication of crowns and fixed partial dentures (FPDs), for these applications is used 3YSZ. [45] However, as YSZ ceramics are bioinert, they do not directly bond to natural bone in hip–joint replacements. [42]
The YSZ has been used for fabricating the femoral head of total hip joint prosthesis and has two advantages over the alumina. One is the finer grain size and a well-controlled microstructure without any residual porosity of the YSZ. The other is the higher fracture strength and toughness due to the phase transformation toughening process. [36]
Furthermore, YSZ is used in no biological applications (used 3YSZ), grinding material (used 3YSZ), mainly as thermal barrier coatings (used 4YSZ), gas sensors (used 4YSZ) and solid oxide fuel cell (SOFC) electrolytes (used 8YSZ). [42,47,48]
The aim of this work is to produce 3D samples of 3% mol yttria-stabilized zirconia with 3D printing, using the nanopowder sintered by INNOVNANO, that uses a unique technique in the world, therefore, there is no information in the literature about the combination of both nanopowders and 3D printing.

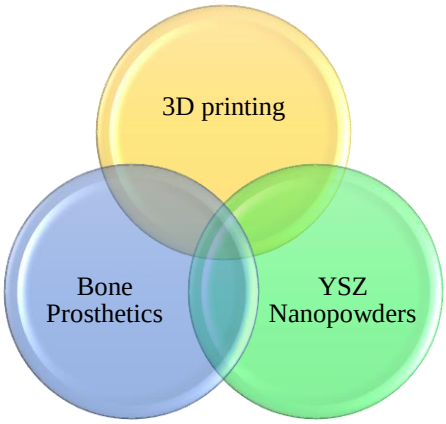

Figure 1.4 Representative scheme of the three areas covered in this thesis.

2. Materials and Methods

2.1. 3D printing procedure

The printing process, performed by a homemade adapted printer, uses a *123D Design* software (CAD program), see images in Annex 2 and the files are saved in STL format. The STL file is sliced and prepared to print in C*ure* software. Considering that 3D printing is a layer-by-layer process it is mandatory to study parameters such as layer height, fill density, print speed and scanning speed (parameters can be seen in detail in Annex 3). After setting the appropriate parameters, the file is saved in G programming language (G-code) to be read directly by the printer. Additionally, during printing is needed to control the starting position of the z-axis control, the extrusion rate (ranging from 100 to 2000 mm/min) and the size of the nozzle used.

A viscous solution, containing surfactant and/or binder, is mixed under magnetic stirring (Agimatic-N, P-Selecta) at approximately 50ºC until completely dissolve. 3YSZ nanopowders (provided by INNOVNANO, 3YSZ-Tetragonal Zirconia) are added to the previous solution and are manually mixed to form a homogeneous paste able to be printed and to form a solid object with the shape and size defined by the design. This production process is schematized in Figure 2.1.
Before the printing process, the paste is placed inside the modular heads extruder; the file with the model to be printed is selected and some parameters are manually adjusted in the printer, such as the z-axis and the speed to print/extrude the paste. The printing finally starts and this process is conducted at room temperature (RT) under atmosphere conditions.
The obtained sample is dried at 55°C in a hotplate (IKA®RCT basic, safety control) and then it is placed inside the oven (Nabertherm P330). Sintering is carried out mainly at 1400ºC for 2h [46], to ensure the complete removing of surfactant and the binder of the sample, except for the sintering temperature study where it was changer for 1100 to 1450°C temperature sintering time 2h. The ramp used was 2°C/min.

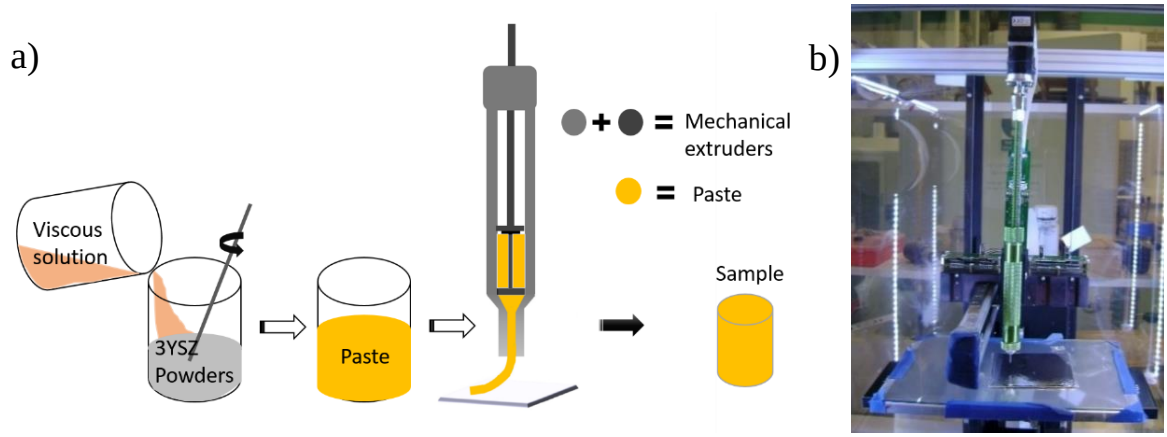

Figure 2.1 a) Representative scheme of paste production and its printing process; and b) Printer extruder.

2.2. Structural and morphologic analyses

The morphology and the elementary composition of the samples were characterized by a scanning electron microscope (SEM - Hitachi S2400 with Bruker light elements EDS, at MicroLab-Electron Microscopy Laboratory of *Instituto Superior Técnico*). The samples surface was observed in an inverted optical microscope (Leica DMi8, at Lab 213, DCM, FCT-UNL). For SEM analysis, the printed sample was placed in the sample holder using a carbon ribbon and then covered with a very thin layer of gold.

The composition of pastes was determined by Raman microscopy (Labram 300 Jobin Yvon spectrometer, equipped with a solid state laser operating at 532 nm, at Lab 217, *Departamento de Conservação e Restauro*, FCT UNL). The laser beam was focused with 50× Olympus objective lens. The analysis was performed using a small amount of sample in powder.

X-ray diffraction (XRD - PANalytical X'Pert PRO equipped with an X'Celerator detector using CuKα radiation at 45 kV and 40 mA, in a Bragg–Brentano configuration) was used to analyse the crystalline phases present in the sintered pieces. XRD patterns were collected over the angular 2θ range 15°–80°, with a scanning step of 0.03° at CENIMAT-I3N, FCT-UNL.

2.3. Mechanical tests

The σ_{Max} and E of the hallow cylinder shape sintered samples, with external ϕ= 7 mm and internal open ϕ= 5 mm and height of 7 mm, were measured by the universal testing machine (Shimadzu AG-50kNG, Thermal and Mechanical Testing Laboratory-CENIMAT) at a loading rate of 0.5 mm/min and SHIMADZU Autograph (in *Instituto Pedro Nunes*, Coimbra) at loading rate of 0.3mm/min. Other shapes as shown in Figure 3.2 were also tested using the same conditions.

2.4. Density and Degradation

The density of the sintered samples was determined by the Archimedes immersion method in water (it is an indirect method, as can be seen in the protocol of Annex 4). To obtain a more reliable value, three replicas were made for each paste, and each one had its own 3 measurements.
By Archimedes method when the porous ceramic sample is in contact with water, it enters inside the porous due to capillary forces. The water absorbed is determined by measuring the weight percentage of sample when the maximum water is absorbed. It is assumed that all water in the open pores remain there. However, it should be noticed that the Archimedes method is an indirect method and only the open porosity is determined, so the calculated densities do not reflect all the possible porosity of samples.

For the degradation assays, the samples (a total of 40) were placed in individual vials, each one filled with 7 mL of simulated body fluid (SBF, the procedure of the SBF production can be seen in Annex 5). Then the vials were placed in the oven (Memmert) at 37°C and different samples were analysed after 1 day, 1 week, 2 weeks and 4 weeks of immersion in SBF. The samples degradation was characterized by observing changes in their dimensions, porosity, optical microscopy images, change of phase and mechanical properties in respect to the initial condition.
The degradation was also analysed by placing the samples during 73 hours in boiling water and water vapour (photography of experimental set-up can be seen in Annex 6), After that, the variations in samples dimensions and weight were verified, and the phase of zirconia was determined by XDR.

2.5. Biological tests

In the *Departamento de Física* and *Departamento de Ciências da Vida* of FCT UNL, were carried out cytotoxicity assays and cell adhesion/proliferation tests, the last one were performed only in the *Departamento de Física*. For both tests were printed 10 samples. See procedures used in Annex 7 and Annex 8.

3. Results and Discussion

The results here presented reflect the work performed during a period of 6 months and had the goal of producing ceramic materials through a 3D printing process and evaluate their mechanical properties and biocompatibility for possible biomedical applications. Therefore, the work has been conducted by several tasks: preliminary studies; samples geometry; influence of sintering temperature; mechanical tests; degradability tests; pastes enhancement; pastes mixture and bioactivity tests.

3.1. Preliminary tests

The printing process of ceramics at CENIMAT/DCM was initiated previously to this work, so several preliminary studies had to be performed such as: the extrusion rate of the paste; the printing speed of the nozzle; the layer height and the nozzle size. These parameters are key factors that may affect the printing quality (precision of printing) but they also depend of each type of printer. As the printer used is adapted in house (homemade) the study of previous parameters was not included in this thesis, including the tests to find the most suitable paste to print, since the parameters must be different for each specific printer. Two pastes were selected to produce the samples with different geometries: one of them is composed by a solvent containing a binder and the other without it, Figure 3.1.

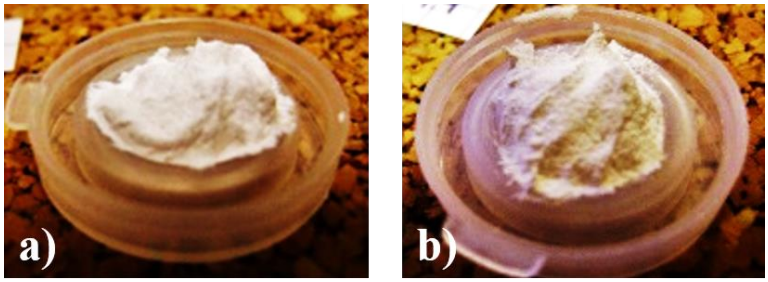

Figure 3.1 a) Paste without binder and b) Paste with binder, both used to print.

The speed of extruders rotation (rate x/y), the printing head speed and layer height can affect the fill density. The appropriate pastes for printing should have some requirements, such as, the use of a small particle size, good dispersion of the particles and suitable rheological behaviour due to the high pressure in the nozzle that as to be very thin to augment the resolution of the printed samples.

The following step was the study of different geometries to understand the performance of the 3D printer available for this study. The choice of the best geometry has into account the maximum resolution for each one, the object definition and reproducibility, and possible scale-up.

3.2. Samples geometry

Samples of different geometries were printed with pastes containing a binder or without it, previously selected, in order to understand how the binder influences the objects resolution, the mechanical performances and the porosity after sintering. All the printer parameters were kept constant (i.e.: extrusion rate x/y). The samples preparation compasses two main steps: first the paste is printed forming an object that is very fragile, and then it follows a sintering step to obtained a solid, stable and rigid ceramic object. These were analysed in terms of porosity, volume constrain after sintering and mechanical properties.

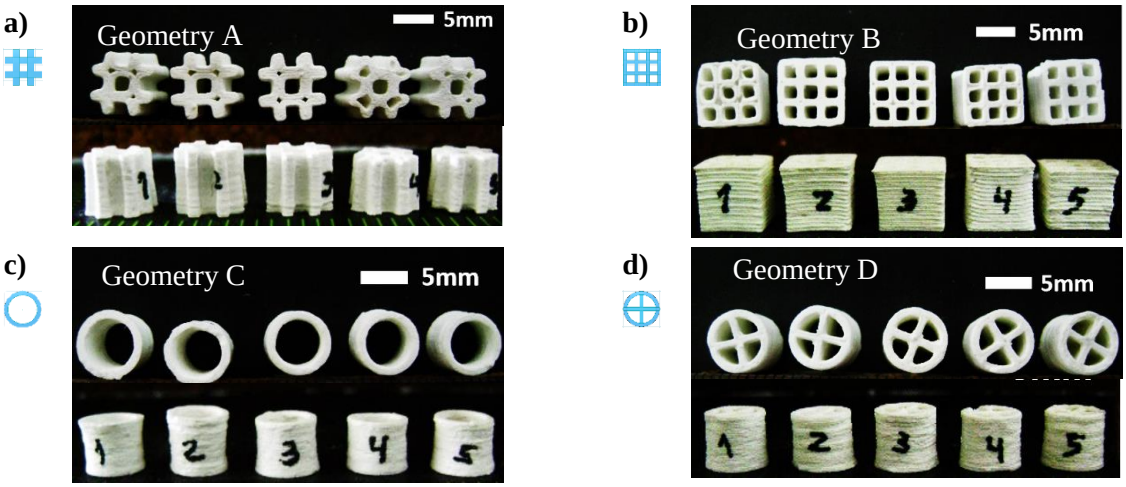

Figure 3.2 Photograph of samples prepared to the mechanical tests and the respective geometries and sizes; a) Geometry A, b) Geometry B, c) Geometry C, and d) Geometry D.

Four different shapes were tested as shown in photos above. The set of 5 samples, all of them with approximately 7 mm height, shown in Figure 3.2 were used in the mechanical tests to have enough samples for a minimum required statistic. The compression tests were done in the universal testing machine in CENIMAT. From the obtained data, which is the force and stroke, the stress–strain graphs were plotted as shown in Figure 3.3. The maximum compressive stress (σ_{Max}) value and the Young's modulus (E) were calculated according the equations shown below. The mean values of the results for each set of 5 samples are displayed in Table 3.1.

The stress and strain relation is given by,

$$\sigma = \varepsilon E \Rightarrow E = \frac{\sigma}{\varepsilon} \tag{3.1}$$

where E is the Young's modulus, σ represents the stress and ε the strain. This way, de E is calculated through linear regression.
The stress (σ) represents the pressure at any point in a body submitted to a load and is expressed as:

$$\sigma = \frac{F}{A} \tag{3.2}$$

where F is the force and A, the supporting area. The material will experience deformation under certain stress. [31] The strain (ε), can be expressed as:

$$\varepsilon = \int_{L_0}^{L_1} \frac{dL}{L} = \ln \frac{\Delta L}{L} \tag{3.3}$$

where L represents the original length and ΔL the increment of length.[31]
From the stress–strain curve is then possible to determine the main mechanical properties of any materials by performing uniaxial compressive tests. [48]

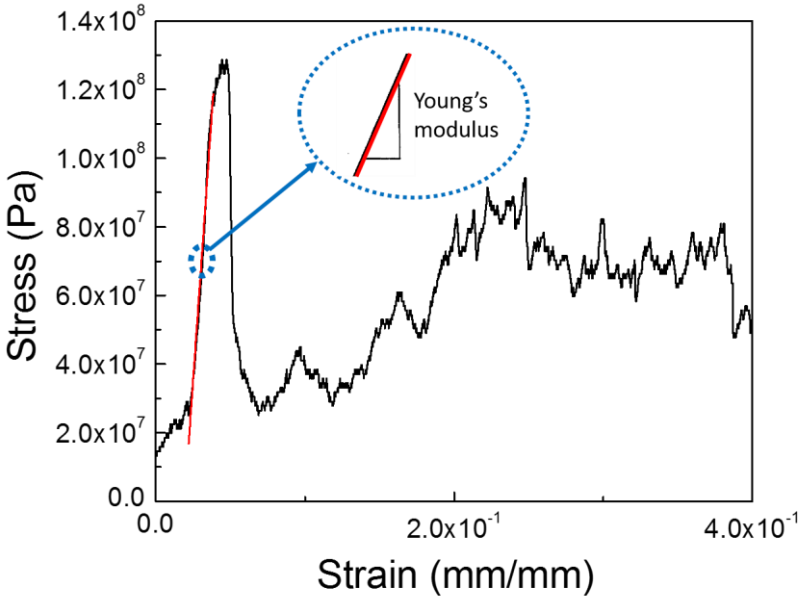

Figure 3.3 An example of a resulting graph of compression tests. This graph of the stress-strain corresponds to the sample C, printed with the without binder paste. Through linear regression (red line) withdraws the value of E (y=-1.19011E8+6.180E9x), E=6.18 GPa.

Table 3.1 Results of compressive stress and Young's modulus for different geometries of samples printed with the without binder paste and paste with binder (see Annex 9).

		Sample A	**Sample B**	**Sample C**	**Sample D**
Without binder	σ_{Max} [MPa]	62.677±18.255	39.172±24.028	156.297±45.034	126.670±72.453
	E [GPa]	2.554±0.881	1.346±0.496	6.630±0.843	4.537±3.154
With binder	σ_{Max} [MPa]	32.166±32.106	49.280±12.373	57.614±32.247	88.250±29.419
	E [GPa]	1.566±1.326	2.270±0.475	3.878±1.934	3.767±0.368

The results show a great influence of samples geometry and paste constitution in both σ_{Max} and E. The hollow cylinder which seemed the most fragile one has the best performance in terms of compression resistance. This must be related with the printing process of this specific geometry. Normally, the samples are produced by additive process i.e., they are formed line over line and in the case of this cylinder the process is continuous, while for the others geometries the lines are crossed and this introduces possible fragilities in the structure. On the other hand, the binder adversely influences the mechanical properties, allowing the production of a paste with less components.

3.3. Influence of sintering temperature

To understand the role of the sintering step on the mechanical properties and also the porosity of samples these ones were sintered in the temperature range of 1100ºC to 1450ºC, using the same annealing ramp (advised by the powder manufacturer), only changing the T parameter. Table 3.2 shows the set of samples prepared for the sintering temperature study for both pastes.

Due to its fragility, the dimensions of non-sintered samples were measured using the *ImageJ* software and the sintered samples were measured with a digital profilometer (POWERFIX® - Profi $_+$ - ELECTRONIC DIGITAL CALLIPER).

Table 3.2 Images of the sintered samples at different temperatures, a) 1100°C, b) 1200°C, c) 1300°C, d) 1400°C and e) 1450°C (Table A.4 of Annex 10).

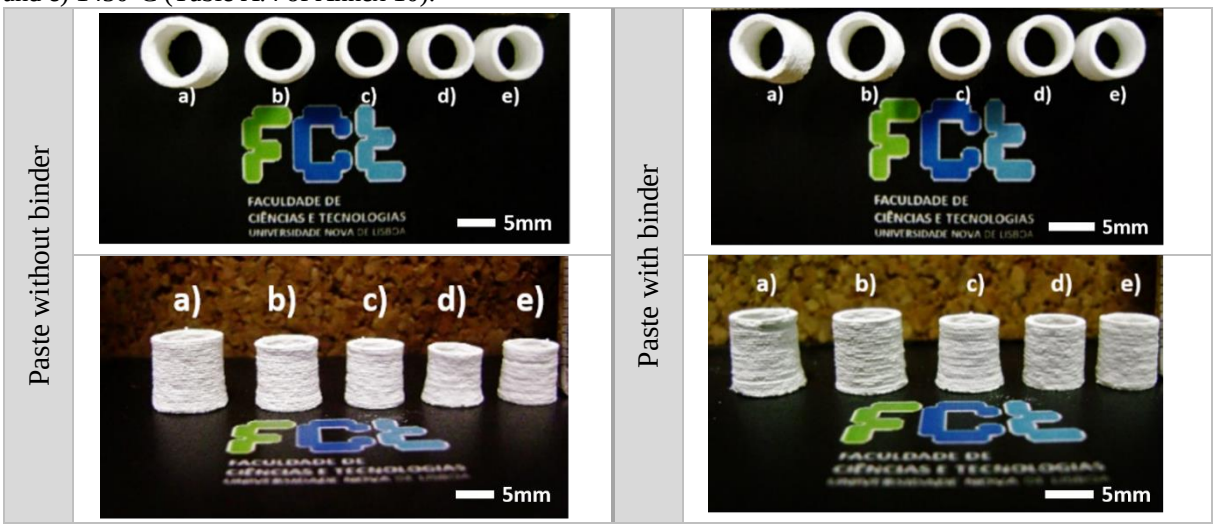

The samples sizes after the respective sintering cycle are displayed in Table A.4 of Annex 10. The shrinkage variation as a function of temperature is shown in Figure 3.4 for the pastes studied. The microscopy images of the corresponding samples, Table 3.3, are also included on the top of figure.

Table 3.3 Photographs obtained from an inverted optical microscope corresponding to the samples of pastes with and without binder produced with different sintering temperatures (Table A.5 and Table A.6 of Annex 10).

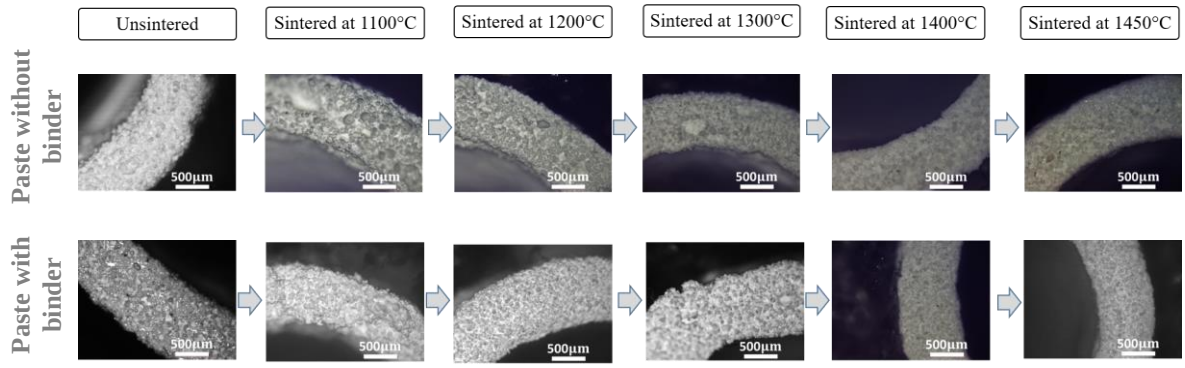

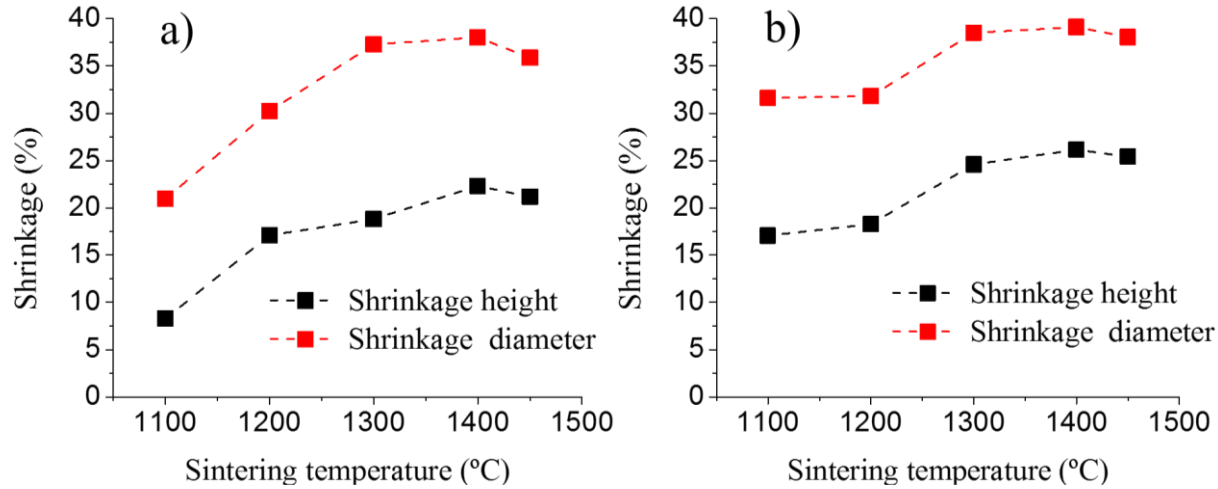

Figure 3.4 Shrinkage percentages as a function of sintering temperatures: a) Samples printed using pastes without binder; b) Samples printed using pastes with binder.

As shown in Figure 3.4, between 1100ºC and 1400ºC the sample's shrinkage increases with increasing sintering temperature. The shrinkage rate depends on the existence of a binder in the paste, although it reaches a maximum of 38% at sintering temperature of 1400ºC for both pastes in one direction, the parallel to the printing line (in the samples diameter). A difference of about 16% between the shrinkage ratio of height and the diameter of the cylinder samples was observed. In fact, the shrinkage is higher along the diameter cause the contact area between grains is higher across the printed filament (higher aggregation of 3YSZ grains), while between filaments the contact interface is comparatively more reduced. The sample printing process is performed layer-by-layer, thus there is a greater surface area between the layers which prevents the aggregation and so, there is less shrinkage of the sample height, as illustrated in Figure 3.5. Another result from this study is the binder influence. The binder is expected to enhance the homogeneity of the paste and so during the annealing cycle it contributes to enhance the densification and the shrinkage increases even at lower sintering temperatures.

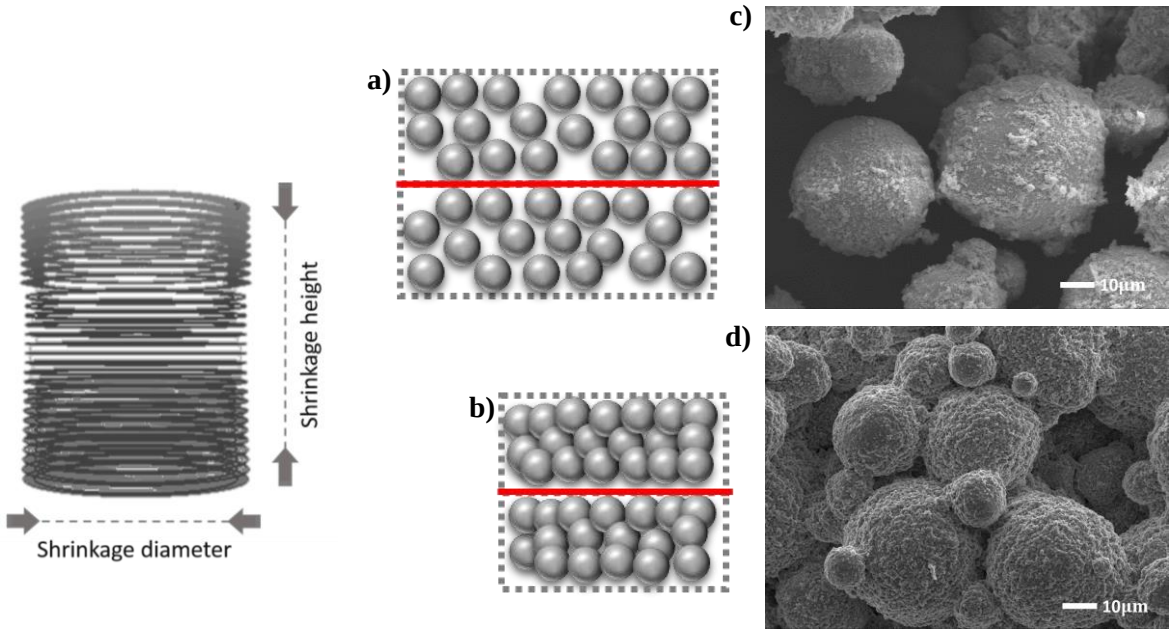

Figure 3.5 From left to right - Schematics of shrinkage directions; a) and c) Schema and respective SEM image representative of the paste non-sintered; b) and d) Schema and SEM image representing the sintered sample with grains aggregation. The red lines represent the critical area for the aggregation of particles, corresponding to the surface between two successive printed layers.

Comparing the SEM imagens of Figure 3.5 it is possible to confirm the sintering effect due to the 3YSZ nanograins aggregation. Typically, the 3YSZ nanograins form large spherical-like agglomerates in the range of a few micrometres to dozens of micrometress (micrograins). After sintering, both micrograins and nanograins aggregate, which gives strength to the printed sample.

Generically, the sintering process of ceramics without any applied load, results in samples with a low level of densification and consequently, in a higher porosity, which is an advantage for the application of this work. Due to the small sample sizes and to the limiting access to other techniques, after sintering, the porosity was measured using the Archimedes method, an indirect method, because of the small sample sizes. The density of ceramic samples calculated by Archimedes method can be seen in Table 3.4.

Table 3.4 Density and porosity as a function of sintering temperatures for samples printed using pastes with and without binder.

	Sintering temperature [ºC]	ρ [g/cm^3]	Porosity [%]
Without binder	1400	3.6411±0.1798	28.56±3.53
	1450	3.6318±0.0248	30.75±5.88
With binder	1400	3.4478±0.2074	37.45±5.35
	1450	3.3648±0.0740	42.49±0.83

The density and porosity results of Table 3.4 show in general a higher porosity of samples printed with paste with binder and a corresponding lower density. This was expected cause during the sintering process the binder carbonizes leaving behind an open space. In the future, this will permit to control the porosity of samples for a specific application.

Nevertheless, the samples strength is proportional to the porosity, i.e., the higher the porosity, the lower the strength of the material. So, it is expected that porosity influences the linear shrinkage, porosity and pore size, and thus σ.

3.3.1. Comparison of compression tests

The obtained compression results of the several samples are shown in Table 3.5, samples measured in two equipment; samples produced with and paste without binder ; samples sintered at different temperatures.

Table 3.5 Comparison of results of several compression tests and samples replica.

 Sintering temperature [ºC]		σ_{Max} [MPa]	E [GPa]
Paste without binder	**1300** (CENIMAT)	6.977±1.423	0.480±0.182
	1300 (IPN)	2.050±0.071	0.585±0.566
	1400 (CENIMAT)	156.297±45.034	6.630±0.843
		57.640±24.620	3.240±2.090
		29.300±4.580	1.070±0.430
	1400 (IPN)	20.625±11.939	1.918±0.951
	1400 (IPN) **1h speed 40 rpm**	36.750±2.616	2.831±0.432
	1400 (IPN) **4 weeks in SBF**	27.900±2.404	2.580±0.058
	1450 (CENIMAT)	54.570±33.080	4.300±1.490
	1450 (IPN)	9.200±0.990	0.705±0.274
Paste with binder	**1300 (**CENIMAT)	6.205±5.098	0.885±1.054
	1400 (CENIMAT)	57.614±32.247	3.878±1.934

Note: These tests were done on the SHIMADZU Autograph (in IPN) and Shimadzu AG-50kNG, Thermal and Mechanical Testing Laboratory-CENIMAT.

The mechanical results were obtained by different machines (at CENIMAT and Instituto Pedro Nunes-IPN, Coimbra) since it was observed a random range of values for samples produced with the same printing parameters and the same paste. Therefore, a possible problem with equipment was excluded. However, some problems in both equipment may remain, in particular the size of samples that are too

small for the equipment used. Some authors have concluded that the variation of some parameters such as strain rate, frequency and grip and slack adapter influence the measurements of the mechanical properties of human bone (tibia), leading to dispersion of values. [49]
Other possible explanation for the random dispersion of values is that in this preliminary study the samples were produced with pastes mixed manually and due to agglomerates of nanopowder particularities the homogenization of these could not be achieved.

Compression tests performed in CENIMAT were made with sets of 5 samples, whereas tests made at IPN were performed in series of 2 samples.
As can be seen from Table 3.5, the compression values have a great dispersion among themselves. The case that the dispersion is most evident is in compression results of paste without binder sintered at 1400°C, where for the same replicas values have an enormous dispersion values. This dispersion can have various causes, such as the way that the sample is printed and/or the way that the paste is mixed. The last mentioned cause, as shown in Section 3.7, causes a more homogeneous morphology of the sample, which results in a better dispersion and uniformity of the nanopowder grain size, enhancing a lower variance in reproducibility and in the compression values.
To have enough statistics for the compression results would be needed to print at least 30 samples of each series, which was unpractical since this is an exploratory study and it was wanted to explore as many parameters as possible within the limited period of time to do the same.

The SEM images of samples sintered at 1400ºC and 1450ºC are displayed in Table 3.6. Although it is obtained a lower density in the samples sintered at higher temperatures no remarkable difference can be detected from the surface morphology. The samples after sintering are formed by grains aggregation with a very large range of sizes. It is important to refer that after sintering some of the agglomerated large grains seem to collapse, meaning that they (or some of them) might be somehow hollow inside, which can be a characteristic of the 3YSZ nanopowders of INNOVNANO.

The 3YSZ nanopowders of INNOVNANO have sintering temperatures from 1200°C [50], lower than for many ‘conventional’ powders, however, the mechanical properties are improved with the increasing of temperature up to 1400°C. [45,49–54] For lower sintering temperatures the samples are too fragile to be manipulated, maybe sintering has been incomplete at these temperatures (1100ºC, 1200ºC and 1300ºC) for the sintering time used, or it is just not enough to promote grains aggregation.

With the increase of the sintering temperature, the interconnection between the 3YSZ nanopowder grains is enhanced and consequently, the porosity is lower and the compression strength is enhanced, as can be seen from the results in Table 3.4 and Table 3.6 with exception the sintering temperature of 1450ºC.

The sintering temperature of 3YSZ influences the shrinkage, evidenced by the fact that the samples sintered at 1450°C have a higher dimension than the samples sintered at 1400°C. Further studies such as dilatometry should be performed to confirm the origin of these results.

Table 3.6 SEM images of samples printed using pastes containing binder or without sintered at 1400ºC and 1450ºC.

	Sintering at 1400°C	Sintering at 1450°C
Without binder	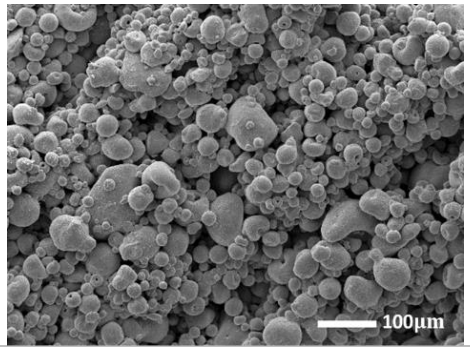	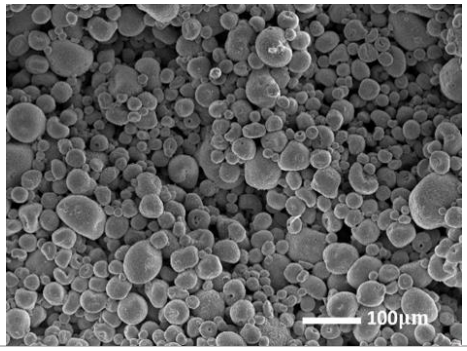
	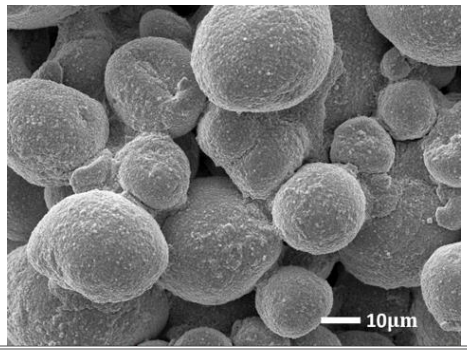	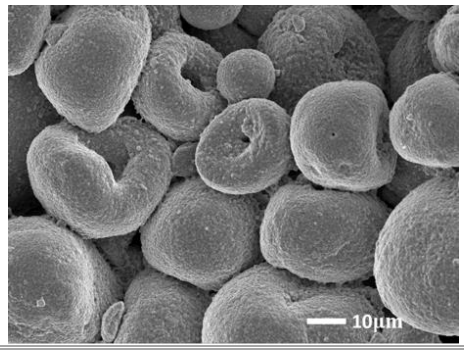
With binder	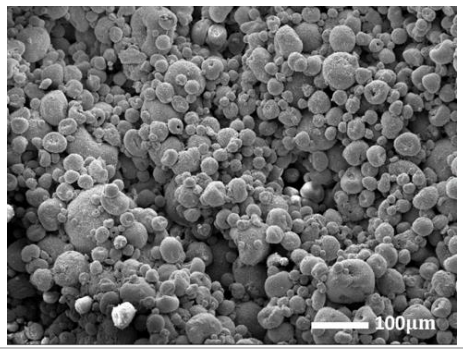	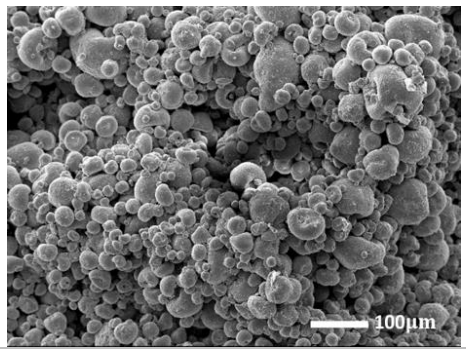
	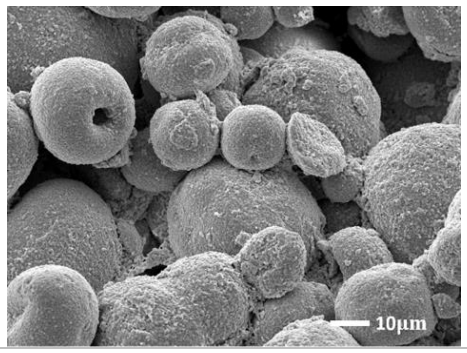	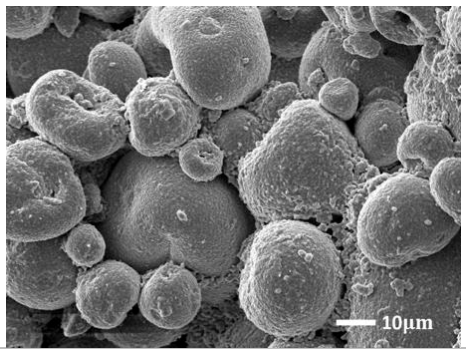

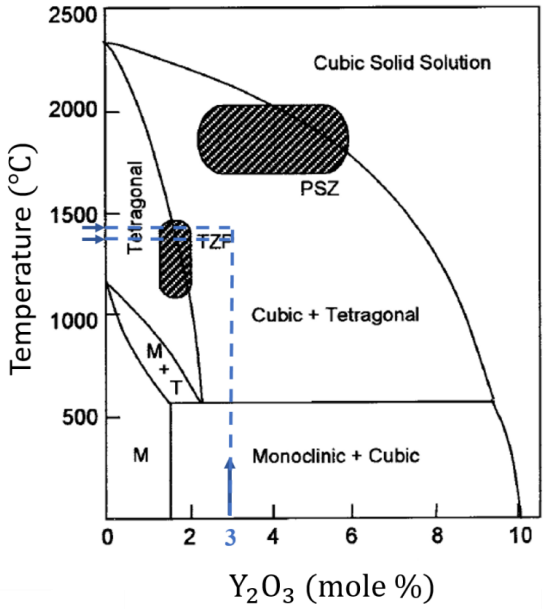

Figure 3.6 ZrO_2–Y_2O_3 equilibrium phase diagram. The blue dashed lines show the critical range of sintering temperatures (1400ºC and 1450ºC) of 3 mol % yttria-stabilized zirconia, relative to the shrinkage and porosity of sample with temperature. Adapted from [57].

Through Raman spectroscopy, assays characteristic bands of the material can be identified, Figure 3.7. Samples printed from pastes without binder sintered at different temperatures (1400ºC and 1450ºC) were analysed and identified the different phases. The 1400ºC and 1450ºC 3 mol% Y_2O_3 present two phases: a cubic phase and a tetragonal phase (both cubic and tetragonal phases can be retained in the microstructure), as shown in the phase diagram in the Figure 3.6. [39,55,56]. The YSZ has five characteristic bands at 145, 255, 315/328, 460/470, 607/610 and 640 cm^{-1} which are indicative of a tetragonal phase. [37,57] Raman spectrum of cubic zirconia consists of a single broad peak at ~617 cm^{-1}. [39,56]

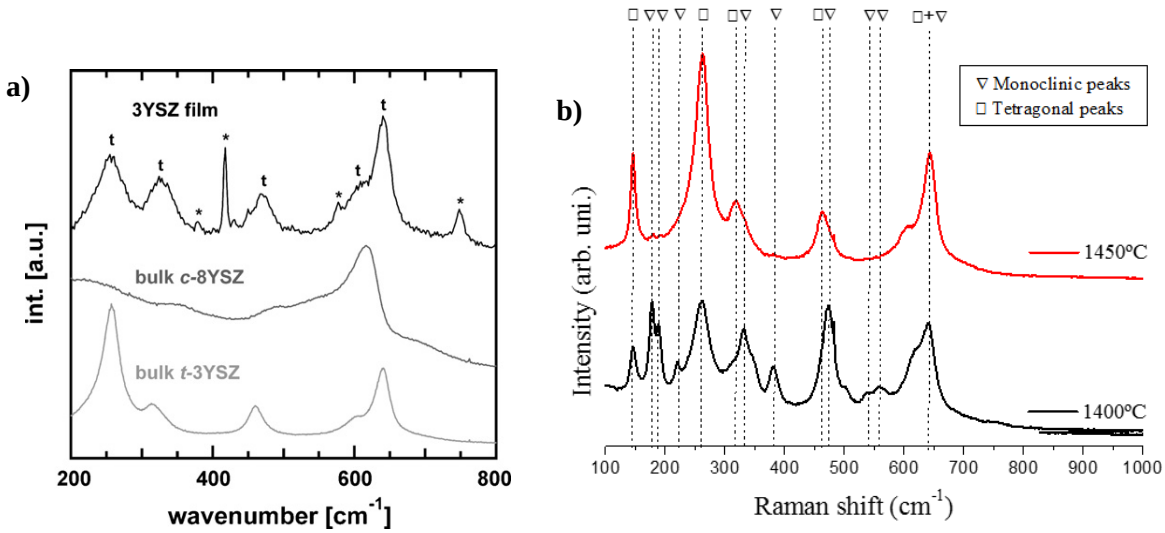

Figure 3.7 a) Micro-Raman spectra of 3YSZ from reference [38]; b) Raman spectra of samples printed using pastes without binder sintered at 1400°C and 1450°C.

According the phase diagram, as explained above, it was expected that by analysing Raman spectrum of samples sintered at 1400°C it would appear peaks of tetragonal and/or cubic phase. Nevertheless, in samples sintered at 1400°C most of the Raman peaks are related to the monoclinic phase, and only three belong to the tetragonal phase. One possible reason is the fact that samples analysed by Raman were

obtained by destroying/crushing the sintered samples and this can cause a phase change from tetragonal to monoclinic as reported by other authors.[60]

The Raman spectrum of the sintered sample at 1450ºC, show mainly the tetragonal phase, but this sample powder used for performing Raman analysis has been sintered in the powder form, with no fracture of the material after the sintering. This may explain the differences on both spectra which must be explored in the future work. Otherwise, it reveals that to obtain tetragonal zirconia stabilized with yttria using the temperature ramp performed we may need to perform the annealing at 1450ºC instead at 1400ºC.

Another difference of samples sintered at 1400°C or sintering at 1450ºC is the volume expansion of the ones sintered at 1450ºC, which still is contrary to expected from the Raman spectra and so, it is not possible to reach any conclusion for this phenomenon. Future work is also needed identify the origin of this expansion.

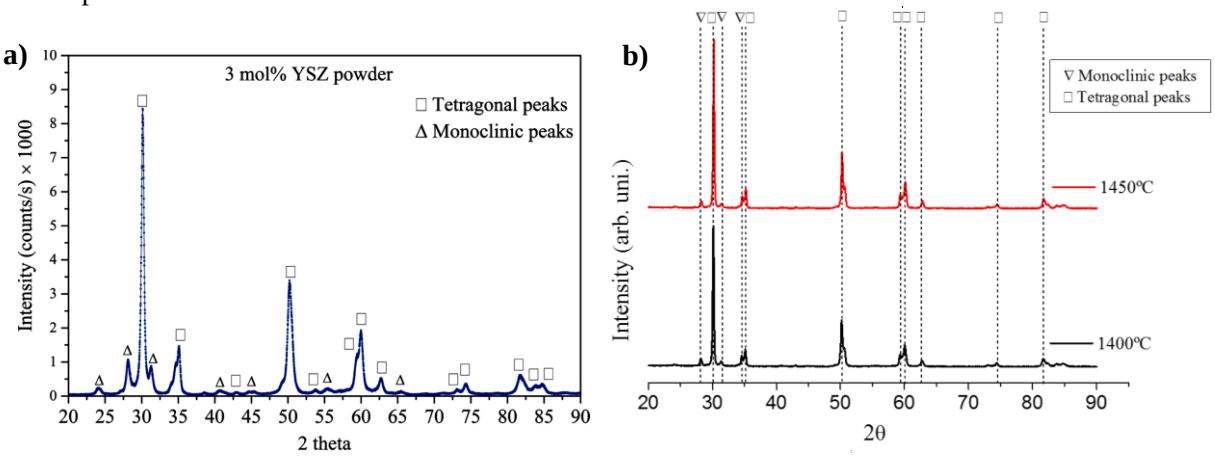

Figure 3.8 a) Literature XRD of 3 mol% YSZ powder in monoclinic phase and tetragonal phase [37]; b) Phase identification results zirconia sintered 1400ºC and 1450ºC by XRD patterns.

Through the XRD spectrum (Figure 3.8) can be seen that the samples sintered at both temperatures have mostly peaks of the tetragonal phase. However, it should be noted that the samples for this analysis were not fractured, so there was no transformation of t→m phase due to fracture of the ceramic piece.

3.4. Degradability

The ZrO_2 faces instability problems with water, the OH^- groups diffuse from surface to interior through vacancies leading to an oxidation of zirconia and phase transformation from tetragonal to monoclinic being the mechanical strength reduced. [59] The introduction of Y works as a phase stabilizer in percentages below 10% mol, although in several reports this transformation still exists and can alter remarkably the mechanical properties of the material. Therefore, and considering possible biomedical applications namely the implantable ones, such as dental, or bones replacement, the samples will be permanently in contact with body fluids. Thus, we performed a study where the samples have been immersed in SBF solution for 4 weeks and their mechanical properties have been analysed. The samples produce with pastes containing binder and without it were immersed in the SBF solution and kept at 37ºC in a muffle. Several pieces (about 40 samples) were tested with frequent analysis of their degradation but no variation of size or density was observed up to 4 weeks. Determination of changes in degradation of sample was characterized by size variation, density and compression strength and Young's modulus (see conditions of degradability tests in Annex 11).

Table 3.7 Changes in dimensions for some samples (printed with paste without binder), during 4 weeks in SBF.

	Samples sintered before SBF				Samples sintered after SBF			
	Height (h) [mm]	Diameter (d) [mm]	Wall (w) [mm]	Weight [g]	Height (h) [mm]	Diameter (d) [mm]	Wall (w) [mm]	Weight [g]
1	6.93±0.01	6.71±0.01	0.87±0.01	0.335±0.005	6.90±0.01	6.70±0.01	0.87±0.01	0.335±0.005
2	6.92±0.01	6.71±0.01	0.89±0.01	0.340±0.005	6.93±0.01	6.71±0.01	0.88±0.01	0.335±0.005
3	6.81±0.01	6.55±0.01	0.92±0.01	0.335±0.005	6.79±0.01	6.52±0.01	0.92±0.01	0.330±0.005
4	6.83±0.01	6.54±0.01	0.82±0.01	0.330±0.005	6.82±0.01	6.54±0.01	0.89±0.01	0.340±0.005
5	6.90±0.01	6.60±0.01	0.91±0.01	0.345±0.005	6.85±0.01	6.59±0.01	0.92±0.01	0.340±0.005

The Table 3.7 results show that there was no change in dimensions or weight of pieces before and after 4 weeks immersed in SBF.

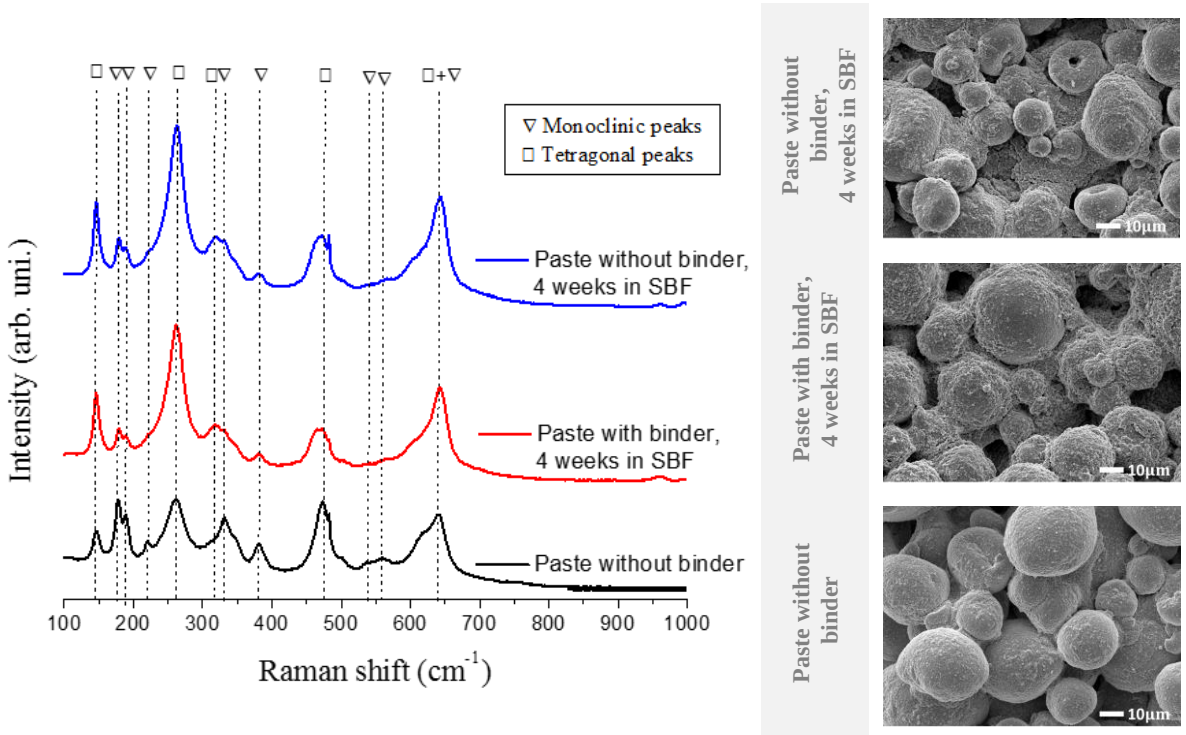

Figure 3.9 Comparison of Raman spectra of the samples that have been in SBF during 4 weeks and the sample without being immersed in SBF, and the corresponding SEM images of the analysed samples.

Table 3.8 Density results and phase of zirconia of samples printed from pastes with and without binder, before and after 4 weeks in SBF.

	Without binder		With binder	
	Without being in SBF	4 weeks in SBF	Without being in SBF	4 weeks in SBF
ρ [g/cm^3]	3.6411±0.1798	3.6651±0.0301	3.4478±0.2074	3.3833±0.049
YSZ main phase	tetragonal	tetragonal	NA	tetragonal

Note: see the graphics XRD for phase identification in the Figure A.27 in Annex 12.

As can be seen in the previous table (Table 3.8), there is no variation in the density of samples that were 1 month (4 weeks) in SBF comparatively with those that have not been immersed in SBF. Therefore, no mass loss is observed. The microscope imagens displayed in Table 3.9 did not reveal either surface morphology alteration. The Raman spectra of samples not immersed in SBF show a higher monoclinic phase than the others that were in SBF, Figure 3.9. This was not expected and the only possible reason is if the furnace has high gradient of temperature that some pieces are at higher/or lower temperature than the expected leading to an incomplete phase transformation during the sintering process. This is something to be identified in future work and could also explain the large variation in the values of

mechanical strength for the samples produced in the same conditions, as shown in previous sections (Section 3.3).

The results obtained by XRD, Table 3.8, confirm the presence of the tetragonal phase in the samples, after SBF, what demonstrate that samples in contact with body fluids at 37 ºC have a low degradation or none.

Table 3.9 Comparison of samples surface morphology for the different number of days in SBF.

	Days in SBF				
	0	1	7	14	30
Without binder	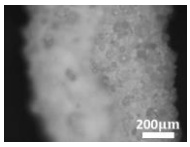	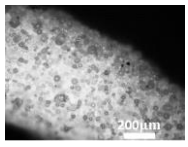	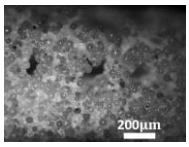	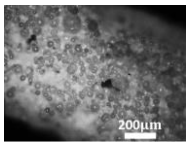	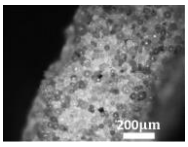
With binder	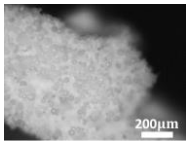	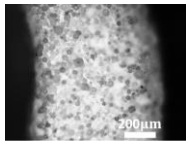	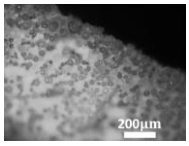	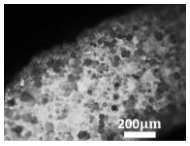	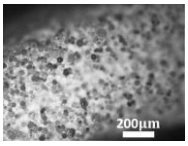

From all values presented above, no significant changes in the samples before and after the SBF are observed.

When comparing the values, it can be observed once more that the binder is not important in the manufacture of samples. Therefore, in further studies, the binder can be removed, becoming the process of fabrication even more economical than initially expected.

Table 3.10 Comparison of the two compression results.

	Not immersed in SBF	**Immersed 4 weeks in SBF**
σ_{Max} [MPa]	20.625±11.939	27.900±2.404
E [GPa]	1.918±0.951	2.580±0.058

Note: These tests were done on the SHIMADZU Autograph (in IPN).

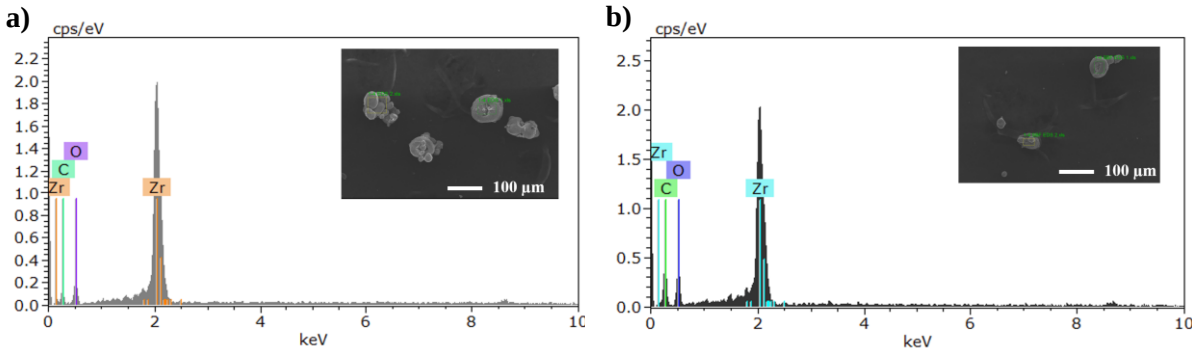

Figure 3.10 EDS spectrum, a) Samples not immersed in SBF 1.4; b) Samples immersed 4 weeks in SBF.

Despite the enormous dispersion values of the mechanical tests, using the compression results (Table 3.10) the σ_{Max} and E have not decreased, meaning that no remarkable degradation of the sample after one month in SBF is observed. This conclusion is supported by the analysis of EDS spectrum (Figure 3.10) where the appearance of new compound, for example salts, is absent.

Once the samples are not degraded in SBF and since approximately 70% of human body is composed by water, a deeper study of degradability with water of printed samples of zirconia was performed. A sample was placed in boiling water (~100°C) for 73 hours and during this time there was another sample receiving only water vapour. In total, one of the samples remained in water during 196 hours at 25°C.

XRD analysis was performed to analyse the phases present before and after water test. The water is responsible for a transformation of zirconia from tetragonal to monoclinic phase, indicating that occurs degradation due to the presence of water molecules. [31]
Studies have demonstrated that water radicals penetrate in zirconia lattice (Figure 3.11) and during an exposure to a humid atmosphere, diffusion of water radicals is facilitated by the presence of numerous vacancies. Most likely, the oxygen from the water is located on vacancy sites, and the hydrogen is placed on an adjacent interstitial site. Zirconia in the aging/degradation can be caused by the roughness and micro-cracking. Roughening happen due to the transformation at the surface and is associated with volume expansion. [29,38]
In 1981, it was found that zirconia stabilized with yttria ceramic in the presence of humidity would has a slow transformation of the tetragonal to the monoclinic phase because of the presence of cracks. [59] And this way, the ZrO_2, undergoes a 3.25% volume expansion on transformation which results in the catastrophic failure of pure ZrO_2 bodies and a reduction in strength of the ceramic. [61]

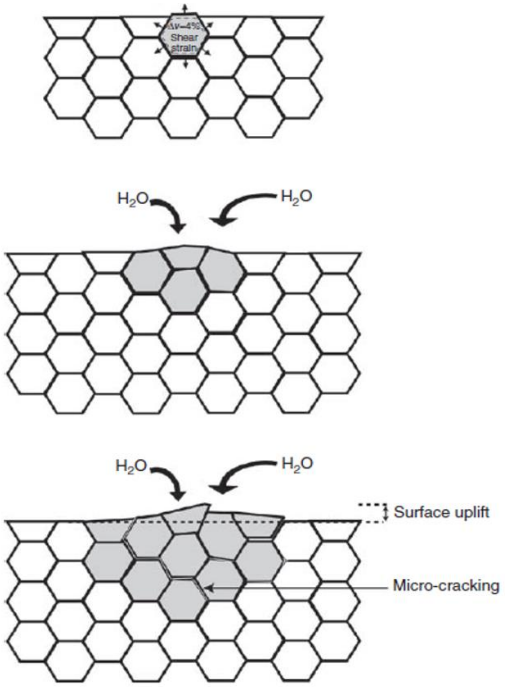

Figure 3.11 Schematic representation of ageing at the surface of zirconia. The water diffuses in the lattice and then propagates to the neighbours, which leads to the aging and consequently the roughening and micro-cracking at the surface. [31]

The increase of internal stresses associated with the penetration of water species inside the lattice is likely to trigger the initiation of transformation t→m. The idea is that OH^- ions diffuse into the zirconia lattice, filling oxygen vacancies, and reducing the stabilization of the tetragonal phase. [38,57]
The pieces used in this study of degradation were measured and weighed (Table 3.11) before and after and XRD performed.

Table 3.11 Samples being 73h in boiling water and water vapour.

	Samples as produced				**Samples after test of water**			
	Height (h) [mm]	Diameter (d) [mm]	Wall (w) [mm]	Weight [g]	Height (h) [mm]	Diameter (d) [mm]	Wall (w) [mm]	Weight [g]
water	6.90±0.01	6.60±0.01	0.88±0.01	0.305±0.005	6.89±0.01	6.60±0.01	0.89±0.01	0.305±0.005
water vapour	7.05±0.01	6.77±0.01	0.84±0.01	0.310±0.005	7.05±0.01	6.76±0.01	0.84±0.01	0.305±0.005

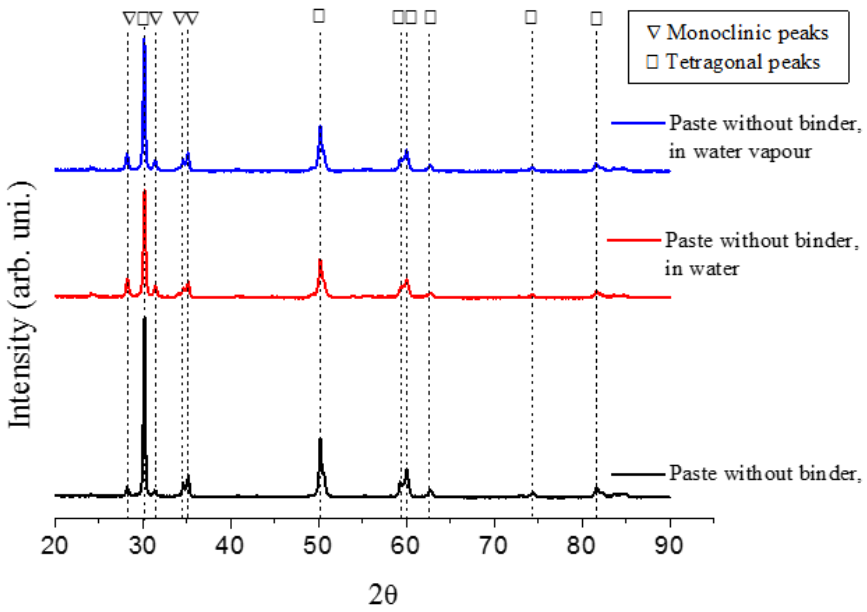

Figure 3.12 XRD patterns of printed samples sintered and samples sintered but being immersed in water or water vapour .

From XRD patterns all samples are on the tetragonal phase, Figure 3.12. [36,60] The samples were in boiling water and soaking up with water vapour at high temperatures that causes the pores of the sample become more exposed (more open porosity), which facilitates the penetration of water radicals in samples of 3YSZ printed. Thus, as the samples were 196 hours in water, of which 73 hours in boiling water, it was expected the occurrence of a transformation, of the tetragonal phase to the monoclinic phase. The XRD spectrum show no degradation due to water, at least there is no phase transformation, however further work is necessary to conduct compression tests to see if there was no degradation of mechanical strength. This study was performed after being observed no degradation in samples immersed in SBF at body temperature, so it was important to verify if the pieces also resist to more extreme water conditions. However, to have a fully confirmation of the YSZ samples stability further studies should also include longer periods in water and compression tests.

3.5. Pastes enhancement

From the previous results, we choose the paste that led to the production of samples with the best mechanical properties. To the selected 3YSZ paste without binder, AgNPs and GO were added to find how it influences the biological tests and the mechanical properties. The GO solutions and AgNPs were synthetized by other colleagues working in the research group and therefore their synthesis was not included in this work. The addition of GO had the purpose to enhance the mechanical strength to compression as reported in literature [64,66] while AgNPs had the purpose to enhance the antiseptic and antimicrobial activity. [65]

3.5.1. Graphene oxide (GO)

To the solution of 3YSZ paste was added different concentrations of GO solution (0.035, 0.1, 0.05 and 0.5 mg/mL) and the objective was to reinforce the ceramic. [64,65] Graphene has characteristics as, high mechanical strength, and it is applied to many different kinds of tissue engineering, including but not limited to bone, cartilage, and nerve. [6] The GO concentrations tested were low because the literature refers the improvement of the mechanical properties with such low concentrations and these also guarantee no colour modification of pastes and therefore of sintered samples. [6] As the GO introduction did not influence the viscosity of pastes only the higher percentage was used for printing samples. These were sintered at the same conditions and the microscopy images are shown in Table 3.12.

Table 3.12 Comparison of 3YSZ +0.5 GO paste non-sintered and sintered (analysis with inverted optical microscope), see Annex 13.

3YSZ+0.5 GO non-sintered	3YSZ + 0.5 GO sintered
	
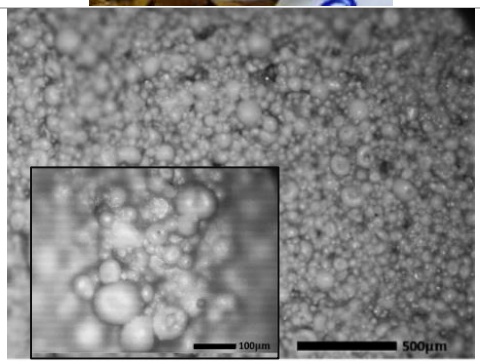	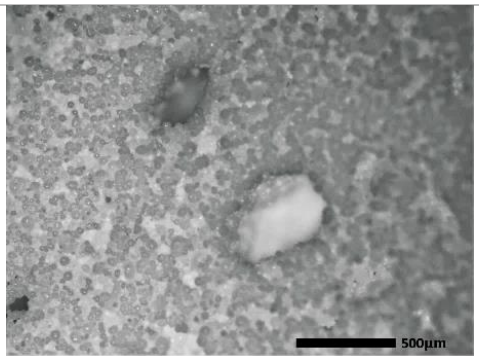

3.5.2. Silver nanoparticles (AgNPs)

AgNPs were added to 3YSZ paste and then used for printing the samples. The photograph of non-sintered paste and its observation through the microscope are shown in the images of Table 3.13. Compared with other nanomaterials, silver nanoparticles have an excellent antibacterial action and low cytotoxicity to human cells in low concentrations, therefore were introduced in order to understand if their use enhances the biocompatibility. [67]

Table 3.13 Comparison of 3YSZ+AgNPs paste non-sintered and sintered (analysis with inverted optical microscope), see Annex 14.

3YSZ+Ag NPs non-sintered	3YSZ+ Ag NPs sintered
	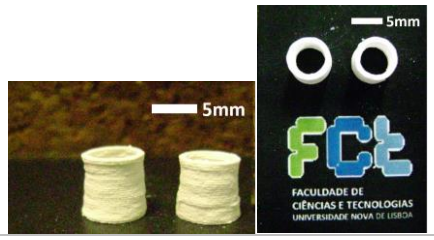
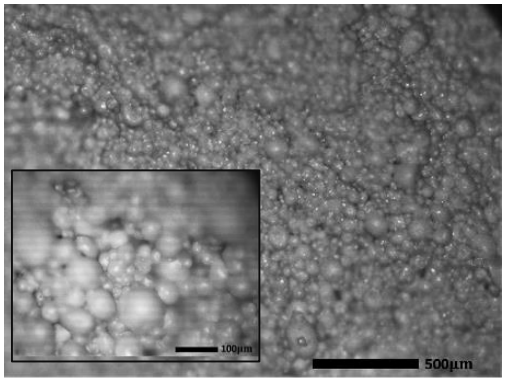	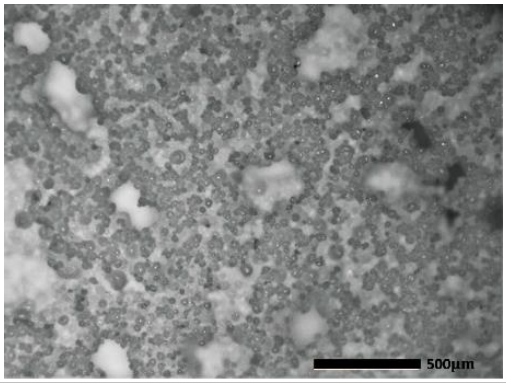

3.6. Samples comparison

Table 3.14 Comparison of densities of samples printed with the 3YSZ paste without binder; 3YSZ+0.5 GO; and 3YSZ+AgNPs.

Paste without binder	ρ [g/cm^3]
3YSZ	3.6411±0,1798
3YSZ+0.5 GO	3.6719±0.0401
3YSZ+AgNPs	3.6591±0.0430

Through the Archimedes method it can be concluded that the density values observed in Table 3.14 are approximately equal in all samples printed with three different pastes.

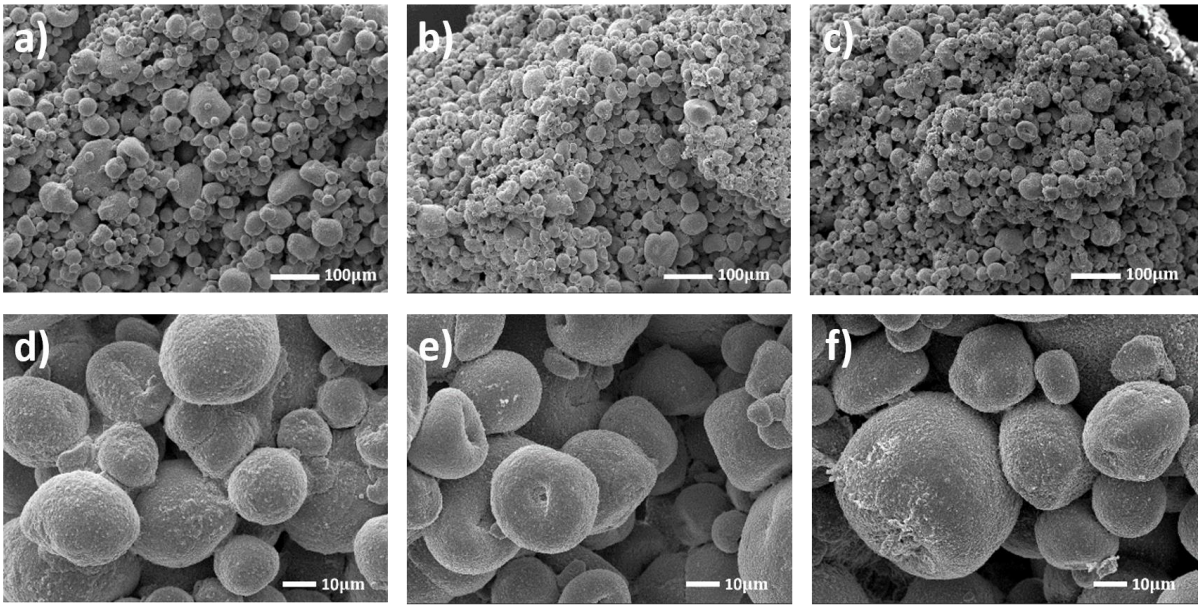

Figure 3.13 SEM images of sintered samples printed with the different pastes a) and d) 3YSZ, b) and e) 3YSZ+ 0.5 GO sintered, c) and f) 3YSZ+ AgNPs.

From the results obtained in the inverted optical microscope and through the images obtained by SEM (Figure 3.13), all the samples seem to have the same morphology. Therefore, we performed the Raman and EDS tests and the results of these were used to find out if the elements (GO and AgNPs) are still in the paste after sintering or contain only 3YSZ.

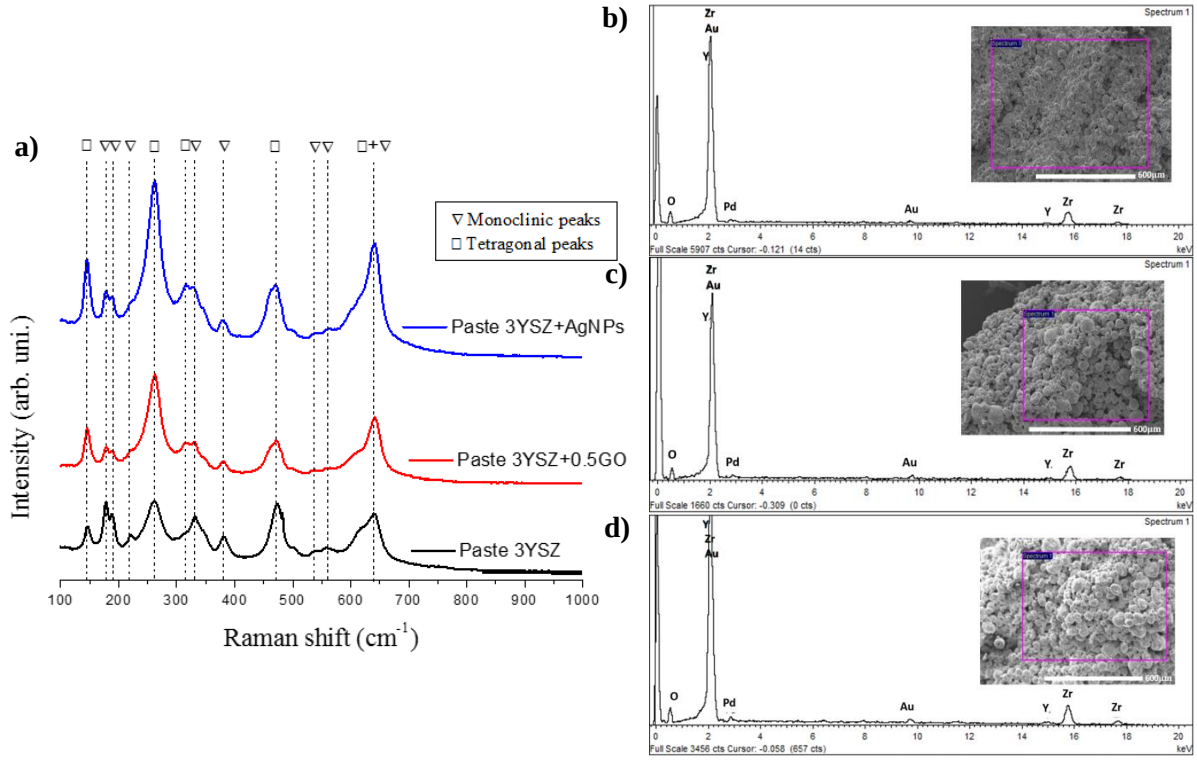

Figure 3.14 a) Raman spectra of samples printed with the paste 3YSZ, paste 3YSZ+0.5GO and the paste 3YSZ+AgNPs; EDS spectrum of b) Samples printed with paste 3YSZ , c) Samples printed with the paste 3YSZ+0.5 GO, d) Samples printed with paste 3YSZ+AgNPs. The traces of Au and Pd comes from the coating for SEM analysis (see Annex 15).

As seen by Raman and EDS spectra (Figure 3.14), after sintering there is no vestiges of silver or any change in the composition caused by the GO (for example, the presence of carbon), since all three samples have the same four characteristic peaks of 3YSZ (255, 328, 470 and 640 cm^{-1}) in the Raman spectra. [38] By EDS results can be seen that the elemental composition is approximately equal in the three samples. Therefore, it means that the concentration of both elements can be so low that the measurement equipment cannot identify them, or they may have disappeared during sintering. In future the percentages of these elements should be increased so that the printed samples benefit from the advantage of the GO and AgNPs.

3.7. Pastes mixture

All the previous studies were made with the pastes being mixed manually, in a goblet. The influence of the way that the paste is mixed was tested by using an artisanal adaptation of a controlled motor rotation, Figure 3.15. Although it is not the best scientific way to do the mixtures, it was the fast one to test this parameter without buying expensive equipment. Then the samples performed with pastes mixed manually and made with two mixing velocities were compared in terms of performances.

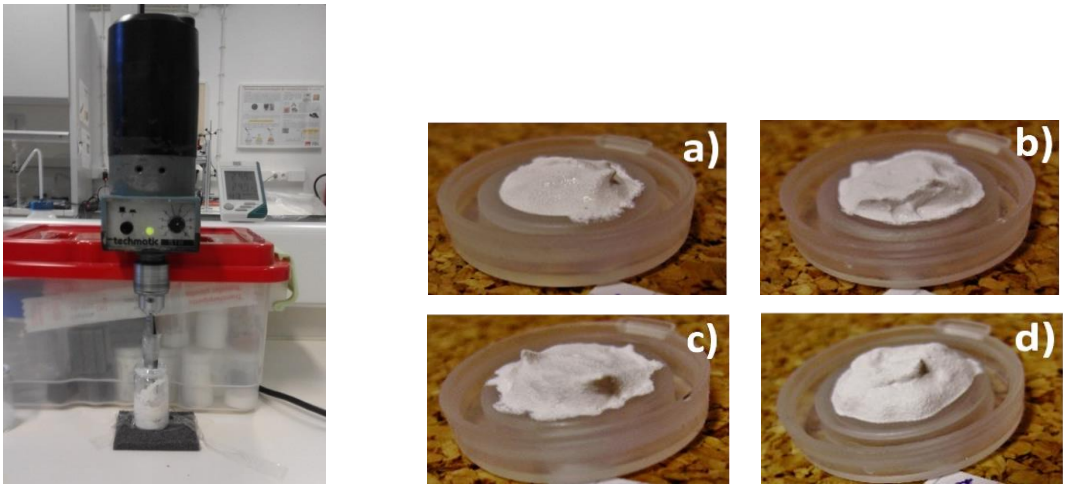

Figure 3.15 Left image - the set-up used for mixing the pastes; right images – photographs of pastes obtained at different speeds and times a) 1h at 10rpm, b) 1h at 40rpm, c) 1h and 30min at 10rpm, d) 1h and 30min at 40rpm.

Table 3.15 Comparison of samples obtained with pastes mixed: manually, 1h at 10rpm and 1h at 40rpm.

Manually	1h at10rpm	1h at 40rpm
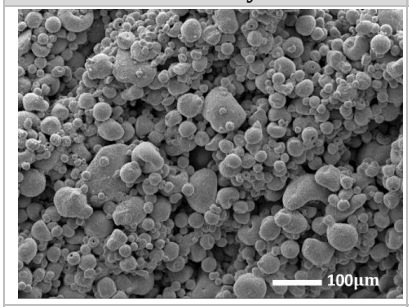	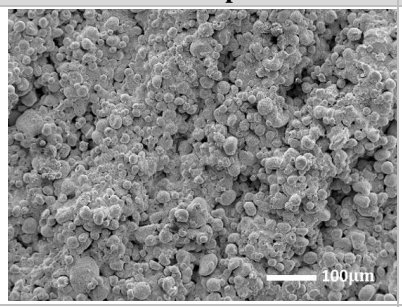	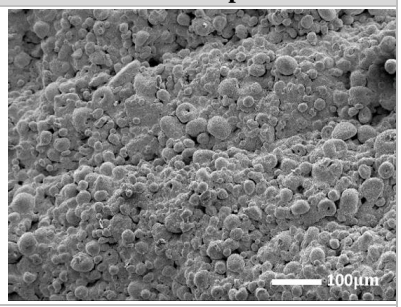
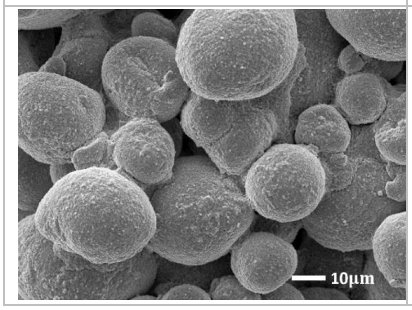	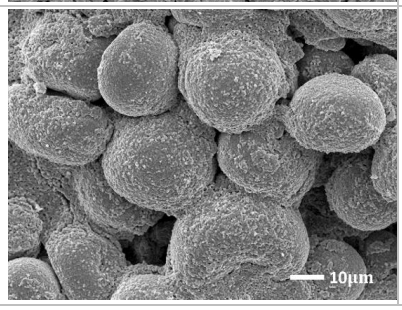	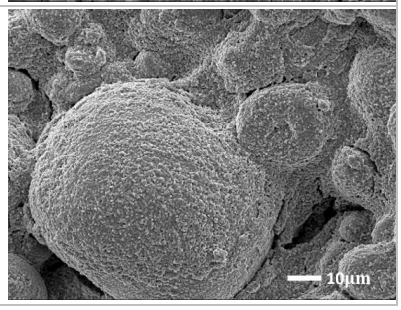

From the SEM images (Table 3.15) it is evidenced that by performing the mixing of the paste with the set-up developed for the purpose, the agglomerates of 3YSZ nanopowders decrease in size and have a higher aggregation during sintering. With the increase of speed can be observed an improvement of particles de-agglomeration and a final enhancing of surfaces homogeneity. This enhanced the aggregation it's confirmed by mechanical tests, because mechanical properties were improved and more than that the standard deviation decreased remarkably, as can see in Table 3.16.

Table 3.16 Comparison of compression results of printed hallow pieces produced with pastes mixed differently.

	Manually	1h at 40rpm
σ_{Max} [MPa]	20.625±11.939	36.75±2.616
E [GPa]	1.918±0.951	2.831±0.432

Note: These tests were done on the SHIMADZU Autograph (in IPN).

As expected the samples mixed at a constant velocity (40rpm) for 1 hour have better compressive strength values and a lower variance in the measurements results. So, further detailed study with reproducible equipment for mixing the pastes and different type of mixture processes should be considered.

Note that when mixing manually, even when by the same person, the conditions of mixing are very different from day to day, with no possible control. And it is reflected, for example, in the dispersion values of the mechanical results, which are much higher in the paste mixed manually.

3.8. Biomedical applications

Among others possible applications for those materials being studied in the last sections, the mechanical properties achieved make them suitable for biomedical applications. Table 3.17 compares the best results obtained within literature values for the human bones.
As discussed in Section 3.2, due to the values obtained in σ_{Max} and E the geometry that stood out was the hollow cylinder of the paste without binder (showing the best values).

Table 3.17 Comparison of mechanical proprieties of hollow cylinder samples vs human bone. [6,29,30]

	$\boldsymbol{\sigma_{Max}}$ [MPa]	**E** [GPa]
Cylinder hollow of 3YSZ (maximum value obtained)	156.297±45.034	6.630±0.843
Cancellous bone	4-12	0.01-0.5
Cortical bone	130-225	3-30

Bones perform several vital functions within the body, for example primarily structural support and protection of bodily organs. [68] This way, the mechanical stability must be structurally sound so as to withstand daily activity and normal body movements. [4] As can be seen from Table 3.17 the values of the mechanical properties are within the range values of human bone, in other words, these pieces can probably withstand the forces that will be imposed daily.
Being the best mechanical properties obtained in hollow cylinder of the paste without binder their use as cortical bone could be a possibility if they pass durability and biological tests. Cancellous bone can be also produced with this technique as their mechanical properties are less demanding and the required porosity of these bones is achieved by an adequate change of 3D printing parameters.

Table 3.18 Porosities of the bone and printed 3YSZ hallow cylinder pieces. [6,65]

		Porosity [%]
Bone type	Cancellous bone	50–90
	Cortical bone	3–12
Cylinder hollow of 3YSZ	Sintered at 1400°C	28.56±3.53
	Sintered at 1450°C	30.75±5.88

As seen, the result of porosity of the samples sintering to 1400ºC is good (28.56±3.53%) and lies closer to the porosity of cortical bone to that of cancellous bone, as the values of compression tests, Table 3.18. This way the samples generated by 3D printing in this study can be used for bone tissue engineering. These pieces can also be used as scaffolds, i.e., the patient-derived cells can be seeded onto the samples and due to its good porosity the proliferation of the cells is enhanced (study of proliferation later). Samples serve as 3D templates for initial cell attachment and subsequent tissue formation.
As referred in the introduction, in humans, 80% of the bone is cortical and its main function is mechanical stability. [30] This way the 3D pieces printed with paste with can create 80% of bone implants.
The degradation rate is an important parameter in this study. The rate of materials degradation is usually matched with the rate of tissue regeneration to ensure that the scaffold can still provide the necessary support for cells to the completely regeneration of the tissue. For applications in prosthesis, the material must not degrade. [6] In Section 3.4 it was proved that the printed pieces do not degrade confirming that the printed pieces can be used as implants/prostheses bones.

3.8.1. Biological tests/Biocompatibility tests

For adhesion and cell proliferation tests, the samples were printed in the same way as the cylinders but with a coin shape (filled in spiral) to facilitate the proliferation of cells that remain on top of the samples, as can be seen in the Figure A.30, Annex 16. In all tests, human cells were used.

3.8.1.1. Cytotoxicity

Cytotoxicity tests were performed in two different labs. The first one was held at the *Departamento de Física* and the second one at the *Departamento de Ciências da Vida* of FCT UNL.

An indirect method was used, where the samples have been in contact with a culture medium that is subsequently transferred to the wells containing cells. The resazurin is often used as an indicator of cell viability because it is reduced to resofurin only by the cells metabolically active. The cell viability can be evaluated by the ratio between the resazurin converted to resorufin, comparing the absorptions of these compounds present in wells where have been the samples and cell control wells. The relative viability is used in cell adhesion studies.

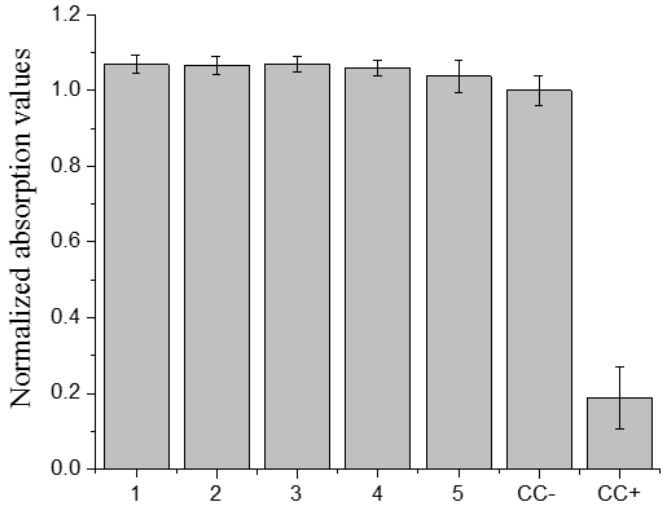

Figure 3.16 Absorption values for the different dilutions of samples printed with paste without binder and the cells control.

Table 3.19 Cell viability for different dilutions of samples tested (Figure A.31, Annex 16).

Dilutions	Cell viability [%]
1	106.88±2.44
2	106.67±2.34
3	106.88±2.02
4	105.95±1.98
5	103.75±4.15

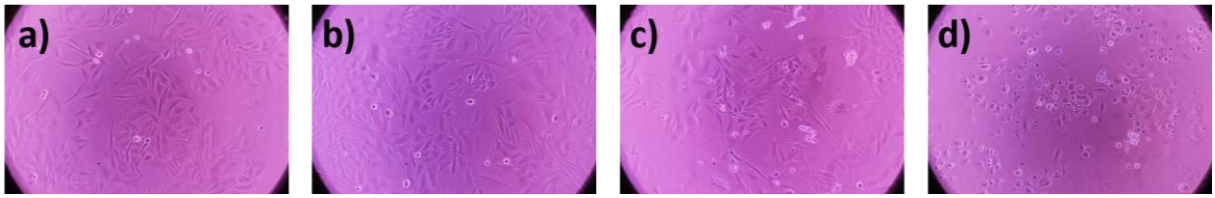

Figure 3.17 a) Cells in the medium with the concentration of 0.5 g/mL (well 1D), b) Cells in medium with the concentration of 0.03125g/mL (well 5C), c) Negative control cells (CC-), living cells, d) Positive control cells (CC+), dead cells.

Through the graphs and the previous table (Figure 3.16 and Table 3.19) it can be concluded that the printed samples are non-toxic, the cell viability is higher than 100% in all studied cases. This means that in just few hours the cells immediately begin to proliferate.
The cytotoxicity and cell adhesion of the same samples were also analysed but, this time, with a direct method.

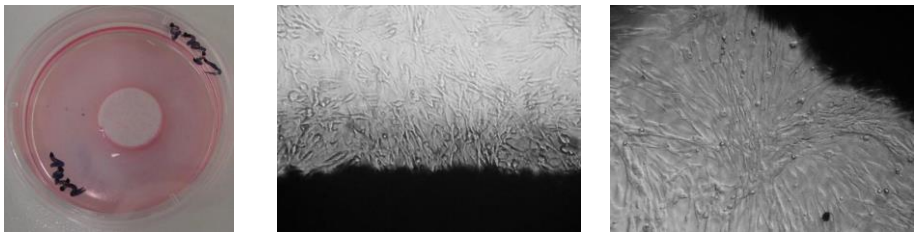

Figure 3.18 Sample in medium with cells.

In this method, the sample is in direct contact with the cells medium (see Figure 3.18). Cells viability in this test is even better than the obtained in the previous method, it reached 116±5.5%. These results are in accordance with the ones obtained by the indirect method, confirming the non-toxicity of the samples, which also may promote the cells growth.

3.8.1.2. Adhesion and cell proliferation

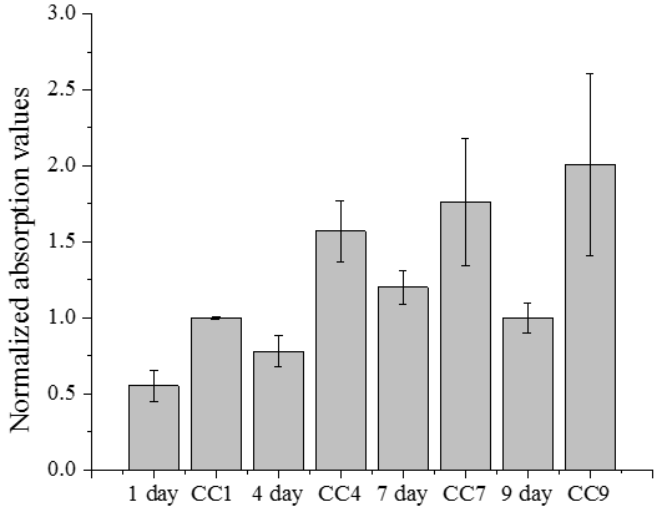

Figure 3.19 Absorption values for different days of printed samples; 1 day represent adhesion and rest of days are proliferation.

Table 3.20 Cell viability of samples for different days .

Days	Cell viability [%]
1 day (adhesion)	55.43±10.11
CC $_{1\ day\ (adhesion)}$	100±1.00
4 day (proliferation)	78.39±9.64
CC $_{4\ day\ (proliferation)}$	156.72 ±20.33
7 day (proliferation)	119.72±11,14
CC $_{7\ day\ (proliferation)}$	175.84±41.85
9 day (proliferation)	100.60±10.41
CC $_{9\ day\ (proliferation)}$	201.21±59.66

Note: CC represent cells control.

As can be observed in Figure 3.19 and Table 3.20 on the first day the cells adhered to the pieces/samples, with 54% of cells in relation to cells that were initially placed in the surface of the samples.
By analysing the three measurements of absorption in different days, it was observed that there was cell proliferation on the surface of the samples, with a big growth until the 7th day, existing on the 9th day a decrease in cell viability.
In the future, it will be needed to perform more proliferation assays and for more days in order to get a higher precision of the results and to understand why the cells viability decreases after the 7th day of culture or if it was an exceptional case. If this decline continues for the 9th day it will be necessary to investigate its cause and if it can be related with the samples constitution.

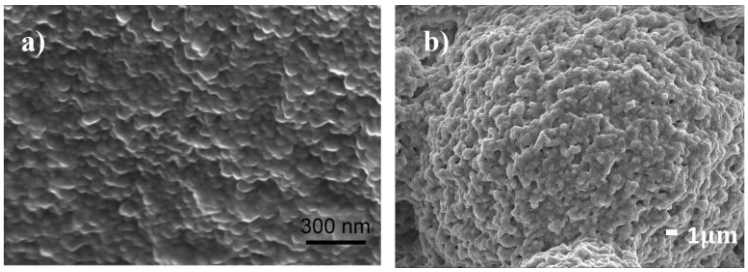

Figure 3.20 a) 3YSZ of literature [53]; b) Sintered 3D printed piece.

The good cells proliferation can be due to a high surface roughness, as can be seen in the images of Figure 3.20 comparing the surface morphology of YSZ sintered pieces with one from literature, where a more compact structure is observed.

4. Conclusions and Future perspectives

4.1. Conclusions

This study was important to initiate a new field of research inside the Energy Materials group and also at DCM/CENIMAT in 3D printing of ceramic pieces. In this thesis, in particular, was studied the 3D printing of pastes made of 3% yttria-stabilized zirconia nanopowders supplied by INNOVNANO, a Portuguese company devoted to the production of ceramic nanopowders by an innovative patented method.
From the different challenges embraced at the beginning of this research work, all have been successfully achieved.

In a preliminary study, were obtained the favourable conditions of the printer and the appropriate pastes to be printed. Two pastes have been selected to further studies, one with binder and another without it. With the selected pastes were studied the influence of pieces' geometry on the mechanical properties, and from this study we concluded that the hollow cylinder had the best mechanical strength and Young modulus, because it is literally printed layer upon layer. From there, the following studies were conducted only with the hollow cylinders.

Then, various sintering temperatures were studied and we concluded that the better compressive strength results were obtained with the sintering temperature of 1400ºC. So, the sintering temperature is important to optimize the mechanical properties of the final pieces and to obtain tetragonal zirconia the temperature used should be 1400-1450ºC. The linear shrinkage, porosity and pore size, and thus σ are influenced by the sintering temperature, so, it is possible to adjust sintering temperature also to control porosity. Comparing the paste with binder with paste without binder, the presence of binder does not morphologically change the sample and improvements do not happen in mechanical properties, this way the pastes without binder are most suitable ones.

One of the problems reported in the literature for ZrO_2 is its instability in water, if there is oxidation of zirconia there is a transformation from tetragonal to monoclinic phase and there is a loss of mechanical strength. Since the objective of these samples is for biomedical applications, they were subjected to human body simulated conditions, i.e., pieces were immersed in SBF solution for 1 month at body temperature (37-38ºC) what did not change the tetragonal phase of the samples. This was confirmed by Raman and XRD measurements in different set of samples.
As no degradation was observed in samples in SBF solution, some studies where carried out with pieces immersed in boiling water and in water vapour during 73 hours. No remarkable alteration was detected by Raman, volume variation or samples morphology. These results can demonstrate a reduction in mechanical strength, however in this test the samples were exposed to extreme conditions, conditions which the human body will never be exposed.
Even in the results of the different sintering temperatures, was demonstrated that when higher the shrinkage, the better are the mechanical properties and lower the porosity is. Lower porosity also becomes favourable, since it means that there is less possibility of degradation of the sample with water because there will be fewer places where water can penetrate.

The addition of AgNPs and GO have shown none or a minor influence on the overall properties of samples, not even vestiges of C from GO or Ag from AgNPs were detected by EDS, and Raman reveal no alteration on the predominant tetragonal phase of YSZ after sintering. Therefore, in the percentages of GO and AgNPs used, these were inconsequent for the properties of the printed ceramic pieces.

The mechanical tests of samples performed have shown a high dispersion of values, although it is known that ceramic pieces always present a wide dispersion of values due to incontrollable defects and its propagation, therefore large number of pieces (at least 30) is recommended to have accurate measurements. In this case, due to time constrains and due to exploratory character of the study, only 5 pieces were measured. However, we have obtained pieces with very high mechanical properties considering that the material has about 30% porosity (28.56±3.53%). Besides that, we also identify ways to reduce this dispersion of values such as mechanical mixing of the nanopowders.
It was created an assembly to optimize the mixing of the paste (the manufacture of the paste) where were tested two speeds and two times and through morphologic analysis and compression was possible to conclude that the 3YSZ agglomerates decrease in size, leading to a better resistance in compression.

Overall, in this study was demonstrated the possibility to produce YSZ ceramic pieces by using the 3D printing. The better mechanical strength obtained of 156.297±45.034MPa and Young modulus values of 6.630±0.843GPa enable their use for bone implants, adding the fact that pieces may have bone geometry, adapted to each patient. The produced samples reveal also to be biocompatible with human cells (SAOS cells) and its proliferation was demonstrated as well.
The overall results are encouraging to reproduce real bones by 3D printing YSZ of identical geometry. Through cytotoxicity assays was demonstrated that samples are not toxic to the human cells and these are able to adhere and to proliferate on the surface of the sample 3YSZ manufactured by 3D printing, because of the high surface roughness.

4.2. Future perspectives

Although the objectives of this thesis have been successfully concluded it opened also several research topics for further work. Indeed, new student from *Universidade Egas Moniz*, Flávia Neto, will continue the biological assays with the 3YSZ printed ceramic pieces. For that, 28 samples were printed, 18 samples for tests on alkaline phosphatase activity 7 days, 14 days and 28 days (x2), to perform the evaluation of the osteoblast response to the material surface 7 days 14 days 28 days (x2) and histology, SEM and TEM 7 days, 14 days and 28d (x2) and 10 of 28 samples were printed for implantation in rabbits. This will allow defining the implantation viability of the printed samples.

From the performed study, it is clear that more tests are needed to overcome some problems. The scalability of the process must be proved. For this work very small pieces were printed due to economy of time and materials, but it is necessary to print larger samples and evaluate their feasibility namely concerning the porosity versus mechanical properties. With larger sample would be possible to measure the porosity of the samples by a direct method, such as helium pycnometer, thus being able to accurately measure the porosity.

The way the pastes are mixed have shown to be important for the final mechanical properties of samples, so a deeper study on this must be performed and again correlate it with the mechanical properties as well as with porosity.

During this work the sintering was performed in the same conditions for all samples. A detailed study on the influence of sintering cycle (temperature versus time) should be explored to adequate that to the geometry of samples produced and this way save energy and time in the sintering step. Furthermore, avoiding the influence of any temperature gradient inside the furnace is of extreme importance to have reproducibility of results. Thus, a temperature mapping inside furnace should be performed prior to any further study. Besides that, to have mechanical results more accurate and reproducible large number of replicas should be produced, at least 30.

The deterioration of YSZ samples with water should be further studied, after having a process completely reproducible and ensuring that the same samples are analysed before and after aging with water. This will avoid possible differences of samples in same production run, or between different runs. In this case, these results will not confirm the stability observed in the obtained preliminary results so new additives should be included in the pastes. Further studies with AgNPs and GO with higher concentration can be tried or even different Y concentrations in ZrO_2 powders, besides other possibilities.

Tetragonal zirconia is known to be bioinert and thereby fibrous layer may form around the implant and induce aseptic loosening. If this condition is also found in the pieces produced, inorganic coatings on the material surface can overcome the instability and promote direct attachment to bone tissue. Calcium phosphate (CP) based materials, such as hydroxyapatite (HA) and tricalcium phosphate (TCP) are considered to be bioactive and thus stimulate bone regeneration [44].

Another possible field of application for the materials developed is orthodontics. Statistics show that 100% of adults have dental caries while dental disease is cumulative with age, leading to loss of teeth. The mandible and maxilla of the edentulous naturally atrophy with time, becoming much thinner and more susceptible to fracture. [6] So, teeth printing is one of the future objectives, because it has been proven that the material is not toxic, does not degrade and the cells can proliferate in it.
As a final remark it is important to notice that although a preliminary study has been developed within this thesis, it has enormous possibilities of reaching a successful real application in the near future.

References

[1] S. V Murphy and A. Atala, "3D bioprinting of tissues and organs.," *Nat. Biotechnol.*, vol. 32, no. 8, pp. 773–785, 2014.

[2] A. E. Jakus, A. L. Rutz, and R. N. Shah, "Advancing the field of 3D biomaterial printing," *Biomed. Mater.*, vol. 14102, no. 11, pp. 1–11, 2016.

[3] B. C. Gross, J. L. Erkal, S. Y. Lockwood, C. Chen, and D. M. Spence, "Evaluation of 3D Printing and Its Potential Impact on Biotechnology and the Chemical Sciences," *Anal. Chem.*, vol. 86, pp. 3240–3253, 2014.

[4] A. Do, B. Khorsand, S. M. Geary, and A. K. Salem, "3D Printing of Scaffolds for Tissue Regeneration Applications," in *Advanced Healhcare Materials*, 2015, pp. 1–21.

[5] J. Horvath, *Mastering 3D Printing*. 2015.

[6] L. G. Zhang, J. P. Fisher, and K. W. Leong, *3D Bioprinting and Nanotechnology in Tissue Engineering and Regenerative Medicine*. 2015.

[7] J. Gardan, A. Makke, and N. Recho, "A Method to Improve the Fracture Toughness Using 3D Printing by Extrusion Deposition," in *Procedia Structural Integrity 2*, 2016, pp. 144–151.

[8] C. M. O. Brien, B. Holmes, S. Faucett, and L. G. Zhang, "Three-Dimensional Printing of Nanomaterial Scaffolds for Complex Tissue Regeneration," *TISSUE Eng. Part B*, vol. 0, no. 0, 2014.

[9] S. Bose, S. Vahabzadeh, and A. Bandyopadhyay, "Bone tissue engineering using 3D printing," *Mater. Today*, vol. 16, no. 12, pp. 496–504, 2013.

[10] M. Lipson, Hod; Kurman, *Fabricated: The New World of 3D Printing*, vol. XXXIII, no. 2. 2014.

[11] E. K. O. Brien, D. B. Wayne, K. A. Barsness, W. C. Mcgaghie, and J. H. Barsuk, "Use of 3D Printing for Medical Education Models in Transplantation Medicine : a Critical Review," *Curr Transpl Rep*, 2016.

[12] G. Jonathan and A. Karim, "3D printing in pharmaceutics : A new tool for designing customized drug delivery systems," *Int. J. Pharm.*, vol. 499, pp. 376–394, 2016.

[13] F. C. Godoi, S. Prakash, and B. R. Bhandari, "3d printing technologies applied for food design : Status and prospects," *J. Food Eng.*, vol. 179, pp. 44–54, 2016.

[14] S. A. Khaled, J. C. Burley, M. R. Alexander, J. Yang, and C. J. Roberts, "3D printing of five-in-one dose combination polypill with defined immediate and sustained release profiles," *J. Control. Release*, vol. 217, pp. 308–314, 2015.

[15] Y. L. Kong, I. a Tamargo, H. Kim, and E. Al, "3D Printed Quantum Dot Light-Emitting Diodes," in *Nano letters*, 2014, no. October 2015.

[16] A. Sha and A. Atala, "Printing Technologies for Medical Applications," *CelPress*, vol. 22, no. 3, pp. 254–265, 2016.

[17] E. Vorndran, C. Moseke, and U. Gbureck, "3D printing of ceramic implants," *MRS Bull.*, vol. 40, pp. 127–136, 2015.

[18] S. Mohanty, L. Bashir, J. Trifol, P. Szabo, H. Vardhan, R. Burri, C. Canali, M. Dufva, J. Emnéus, and A. Wolff, "Fabrication of scalable and structured tissue engineering scaffolds using water dissolvable sacrificial 3D printed moulds," *Mater. Sci. Eng. C*, vol. 55, pp. 569–578, 2015.

[19] C. Bergmann, M. Lindner, W. Zhang, K. Koczur, A. Kirsten, R. Telle, and H. Fischer, "3D printing of bone substitute implants using calcium phosphate and bioactive glasses," *J. Eur. Ceram. Soc.*, vol. 30, pp. 2563–2567, 2010.

[20] C. Colasante, Z. Sanford, E. Garfein, and O. Tepper, "Current Trends in 3D Printing ,

Bioprosthetics , and Tissue Engineering in Plastic and Reconstructive Surgery," *Curr. Surg. Reports*, vol. 4, no. 6, 2016.

[21] M. Kesti, C. Eberhardt, G. Pagliccia, D. Kenkel, D. Grande, A. Boss, and M. Zenobi-wong, "Bioprinting Complex Cartilaginous Structures with Clinically Compliant Biomaterials," *Adv. Funct. Mater.*, vol. 25, pp. 7406–7417, 2015.

[22] V. Mironov, V. Kasyanov, and R. R. Markwald, "Organ printing : From bioprinter to organ biofabrication line," *Curr. Opin. Biotechology*, vol. 22, pp. 1–7, 2011.

[23] I. Ozbolat and Y. Yu, "Bioprinting Toward Organ Fabrication : Challenges and Future Trends," *IEEE Trans. Biomed. Eng.*, vol. 60, no. 3, pp. 691–699, 2013.

[24] A. C. Jones, C. H. Arns, D. W. Hutmacher, B. K. Milthorpe, A. P. Sheppard, and M. a. Knackstedt, "The correlation of pore morphology, interconnectivity and physical properties of 3D ceramic scaffolds with bone ingrowth," *Biomaterials*, vol. 30, no. 7, pp. 1440–1451, 2009.

[25] M. A. Knackstedt, C. H. Arns, T. J. Senden, and K. Gross, "Structure and properties of clinical coralline implants measured via 3D imaging and analysis," *Biomaterials*, vol. 27, no. 13, pp. 2776–2786, 2006.

[26] G. Khang, M. S. Kim, and H. B. Lee, *A manual for biomaterials/ scaffold fabrication technology*, no. 4. 2007.

[27] S. C. Cox, J. A. Thornby, G. J. Gibbons, M. A. Williams, and K. K. Mallick, "3D printing of porous hydroxyapatite scaffolds intended for use in bone tissue engineering applications.," *Mater. Sci. Eng. C. Mater. Biol. Appl.*, vol. 47, no. FEBRUARY, pp. 237–47, 2015.

[28] R. Shao, R. Quan, and X. Huang, "Evaluation of porous gradient hydroxyapatite / zirconia composites for repair of lumbar vertebra defect in dogs," *J. Biomater. Appl.*, vol. 0, no. 0, pp. 1–10, 2016.

[29] M. Vallet-Regí and D. Arcos, *Biomimetic Nanoceramics in Clinical Use From Materials to Applications*. 2008.

[30] N. M. B. K. Willems, G. E. J. Langenbach, V. Everts, and A. Zentner, "The microstructural and biomechanical development of the condylar bone : a review," *Eur. J. Orthod.*, vol. 36, no. December 2013, pp. 479–485, 2014.

[31] T. Kokubo, *Bioceramics and their clinical applications*. 2012.

[32] L. Hench, *An Introduction to Bioceramics*. 2015.

[33] M. Faes, M. Faes, H. Valkenaers, F. Vogeler, J. Vleugels, and E. Ferraris, "Extrusion-based 3D Printing of Ceramic Components," in *Procedia CIRP 28*, 2015.

[34] G. Khang, *HANDBOOK OF: Intelligent Scaffolds for Tissue Engineering and Regenerative Medicine*. 2012.

[35] B. D. Ratner, A. S. Hoffman, F. J. Schoen, and J. E. Lemons, *Biomaterials Science: An Introduction to Materials in Medicine*. 1997.

[36] J. Park and R. S. Lakes, *Biomaterials: An Introduction*, Third Edit. 2007.

[37] A. Sondhi, O. Okobiah, S. Chattopadhyay, T. Shibata, and T. W. Scharf, "X-ray absorption spectroscopy studies on the carbothermal reduction reaction products of 3 mol% yttria-stabilized zirconia," *J. Appl. Crystallogr.*, vol. 47, pp. 1512–1519, 2014.

[38] P. Institut, I. Physics, and N. Materials, "Yttria-stabilized zirconia thin films by pulsed laser deposition : Microstructural and compositional control," *J. Eur. Ceram. Soc.*, vol. 30, pp. 489–495, 2010.

[39] J. Chevalier, L. Gremillard, and S. Deville, "Low-Temperature Degradation of Zirconia and Implications for Biomedical Implants," *Annu. Rev. Mater. Res.*, vol. 37, pp. 1–32, 2007.

[40] M. Chatee, M. H. Shariat, and J. T. S. Irvine, "Investigation of electrical and mechanical properties of 3YSZ / 8YSZ composite electrolytes," *Solid State Ionics*, vol. 180, pp. 56–62, 2008.

[41] A. V Bandura, D. G. Sykes, V. Shapovalov, T. N. Troung, J. D. Kubicki, and R. A. Evarestov, "Adsorption of water on Yttria-stabilized Zirconia," *J. Phys. Chem.*, vol. 2, pp. 22526–22533, 2015.

[42] S. a M. Tofail, *Biological Interactions with Surface Charge in Biomaterials*. 2011.

[43] G. Pia, L. Casnedi, and U. Sanna, "Porosity and pore size distribution in fl uence on thermal conductivity of yttria-stabilized zirconia : Experimental fi ndings and model predictions," *Ceram. Int.*, vol. 42, pp. 5802–5809, 2016.

[44] K. Pardun, L. Treccani, E. Volkmann, P. Streckbein, C. Heiss, G. Li, G. Marletta, and K. Rezwan, "Mixed zirconia calcium phosphate coatings for dental implants : Tailoring coating stability and bioactivity potential," *Mater. Sci. Eng. C*, vol. 48, pp. 337–346, 2015.

[45] Z. Wu, N. Li, W. Zhao, and J. Yan, "Low Temperature Degradation of Y-TZP Ceramic for Dental Applications," *Adv. Mater. Interfaces*, vol. 873, pp. 241–249, 2014.

[46] L. Hu and C. Wang, "Effect of sintering temperature on compressive strength of porous yttria-stabilized zirconia ceramics," *Ceram. Int.*, vol. 36, pp. 1697–1701, 2010.

[47] V. Esposito, C. Gadea, J. Hjelm, D. Marani, Q. Hu, K. Agersted, S. Ramousse, and S. H. Jensen, "Fabrication of thin yttria-stabilized-zirconia dense electrolyte layers by inkjet printing for high performing solid oxide fuel cells," *J. Power Sources*, vol. 273, no. 1, pp. 89–95, 2015.

[48] D. François, *Structural Components :Mechanical Tests and Behavioral Laws*. 2008.

[49] A. Kemper, C. Mcnally, E. Kennedy, S. Manoogian, V. Tech, W. Forest, and I. Biomechanics, "The material properties of human tibia cortical bone in tension and compression: implacations for the tibia index," no. 1976, pp. 1–12, 1998.

[50] P. Newbatt, "Product Information Sheet - 3YSZ - INNOVNANO."

[51] P. Von Dollen and S. Barnett, "A Study of Screen Printed Yttria-Stabilized Zirconia Layers for Solid Oxide Fuel Cells," *Am. Ceram. Soc.*, vol. 88, pp. 3361–3368, 2005.

[52] E. Choi, J. Lee, S. Lee, S. Kim, S. Jeon, S. H. Cho, S. C. Oh, M. K. Jeon, S. K. Lee, H. W. Kang, and J. Hur, "Stability of yttria-stabilized zirconia during pyroprocessing tests," *J. Nucl. Mater.*, vol. 475, pp. 57–61, 2016.

[53] I. G. Tredici, M. Sebastiani, F. Massimi, E. Bemporad, A. Resmini, G. Merlati, and U. Anselmi-tamburini, "Low temperature degradation resistant nanostructured yttria-stabilized zirconia for dental applications," *Ceram. Int.*, vol. 42, no. 7, pp. 8190–8197, 2016.

[54] H. A. N. Minfang, T. Xiuling, and S. Wu, "The Properties of YSZ Electrolyte Sintering at 1300°C," *J. Wuhan Univ. Technol.*, pp. 775–778, 2008.

[55] P. Dahl, I. Kaus, Z. Zhao, M. Johnsson, and M. Nygren, "Densification and properties of zirconia prepared by three different sintering techniques," *Ceram. Int.*, vol. 33, pp. 1603–1610, 2007.

[56] J. Of and P. Sources, "A Study of the Process Parameters for Yttria- Stabilized Zirconia Electrolyte Films Prepared by Screen-Printing," *J. Power Sources*, vol. 106, pp. 1065–1073, 2006.

[57] R. Hannink and P. M. Kelly, "Transformation Toughening in Zirconia- Containing Ceramics," *J. Am. Ceram. Soc*, vol. 83, no. 3, pp. 461–487, 2000.

[58] J. Chevalier, S. Deville, E. Münch, R. Jullian, and F. Lair, "Critical effect of cubic phase on aging in 3mol% yttria-stabilized zirconia ceramics for hip replacement prosthesis.," *Biomaterials*, vol. 25, no. 24, pp. 5539–45, Nov. 2004.

[59] T. Duong, A. M. Limarga, and D. R. Clarke, "Diffusion of Water Species in Yttria-Stabilized Zirconia," *J.Am. Ceram. Soc.*, vol. 92, no. 11, pp. 2731–2737, 2009.

[60] D. R. Clarke and F. Adar, “Measurement of the Crystallographically Transformed Zone Produced by Fracture in Ceramics Containing Tetragonal Zirconia,” *Crystallogr. Transform. Zo. Prod. by Fract. Ceram.*, pp. 284–288, 1982.

[61] K. Kobayashi, H. Kuwajima, and T. Masaki, “Phase Change and Mechanical Properpies of ZrO2_Y2O3 Solid Electrolyte After Ageing,” *Solid State Ionics*, vol. 3/4, pp. 489–493, 1981.

[62] R. Srinivasan, R. J. De Angelis, G. Ice, B. H. Davis, and G. Ice, “Identification of tetragonal and cubic structures of zirconia using synchrotron x-radiation source,” *J. Mater. Res.*, vol. 6, no. 6, 1991.

[63] K. Markandan, J. K. Chin, and M. T. T. Tan, “Recent progress in graphene based ceramic composites : a review,” in *Materials Research Society 2016.*, 2016.

[64] R. Kiran, F. Garcia, B. Milsom, M. Reece, and M. Anglada, “Processing and characterization of high-density zirconia – carbon nanotube composites,” *Mater. Sci. Eng. A*, vol. 549, pp. 50–59, 2012.

[65] G. Franci, A. Falanga, S. Galdiero, L. Palomba, M. Rai, G. Morelli, and M. Galdiero, “Silver Nanoparticles as Potential Antibacterial Agents,” *Molecules*, vol. 20, pp. 8856–8874, 2015.

[66] J. Shin and S. Hong, “Fabrication and properties of reduced graphene oxide reinforced yttria-stabilized zirconia composite ceramics,” *J. Eur. Ceram. Soc.*, vol. 34, pp. 1297–1302, 2014.

[67] I. Science and B. Qi, “Synthesis and characterization of silver nanoparticle and graphene oxide nanosheet composites as a bactericidal agent for water disinfection,” *J. Coilloid Interface Sci.*, vol. 360, pp. 463–470, 2011.

[68] S. C. Cox, J. A. Thornby, G. J. Gibbons, M. A. Williams, and K. K. Mallick, “3D printing of porous hydroxyapatite scaffolds intended for use in bone tissue engineering applications.,” *Mater. Sci. Eng. C*, vol. 47, pp. 237–247, 2015.

[69] T. Bulletin, “CellTiter-Blue ® Cell Viability Assay,” 2016.

[70] P. Zrimsek, J. Kunc, M. Kosec, and J. Mrkun, “Spectrophotometric application of resazurin reduction assay to evaluate boar semen quality,” *Int. J. Androl.*, vol. 62, pp. 57–62, 2004.

Annex

Annex 1

Figure A.1 3D printing in nature, seashells. [5]

Annex 2

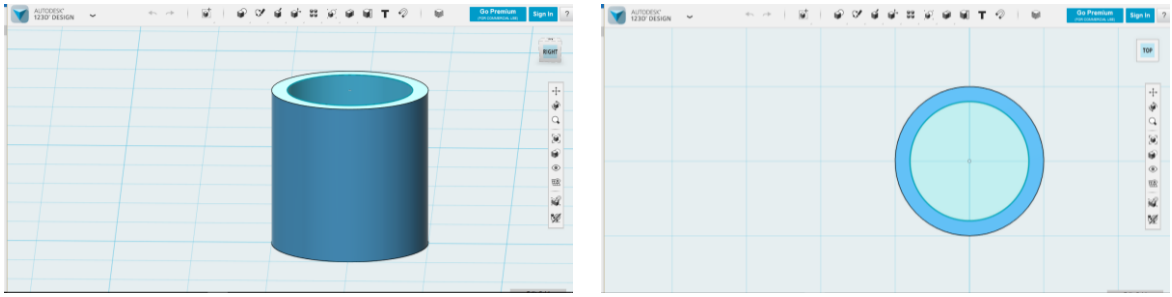

Figure A.2 Example of design created in *123D Design* software.

Annex 3

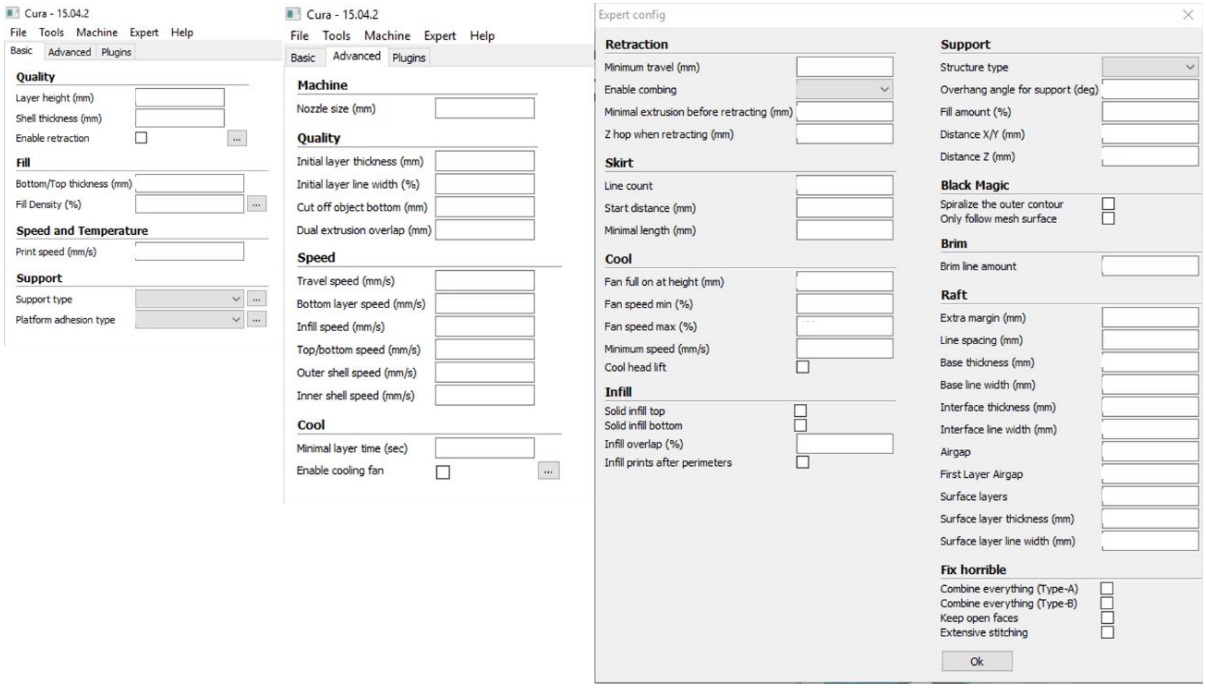

Figure.A.3 Parameters of the *Cura* software.

Annex 4

The Archimedes method is used to determine the bulk density of sintered samples. Procedure of method of Archimedes (based on protocol INNOVNANO - Code: PMT-Lab-10; Edition: 1st; Date: /2012).

Protocol of method of Archimedes (based on a protocol provided by INNOVNANO)

1. Place the samples in boiling water at 110±1°C for 3 hours (put a condenser for water not evaporate).

Figure A.4 Assembly used for the samples in boiling water for 3 h at 110±1°C

2. Prepare the experimental device to evaluate the mass of the sample when immersed, as shown in below image.

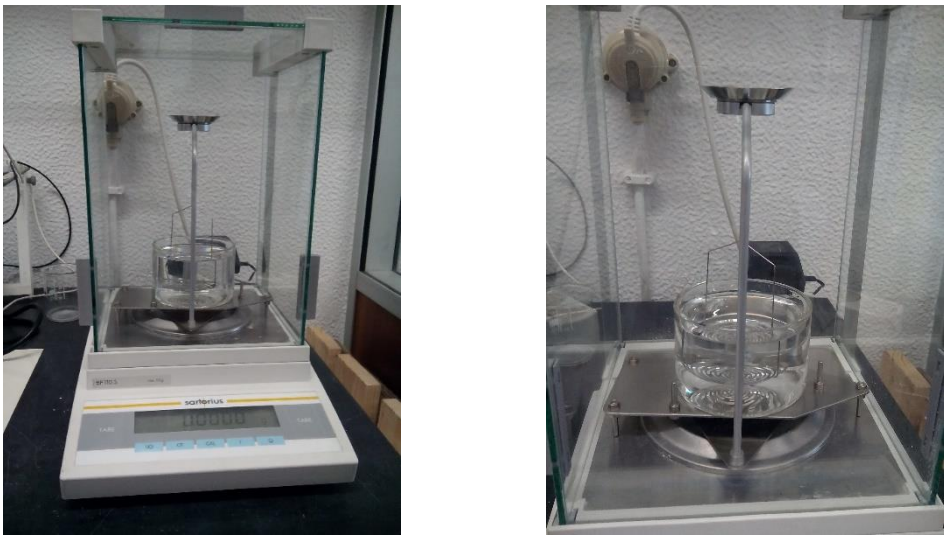

Figure A.5 Experimental device for measure the mass of the immersed sample.

3. Remove the excess water droplets in the sample and place it in the basket sample holder.
   3.1. When removing the sample from the basket, avoid removing water from the container, so that the disruption of the water level is negligible.
   3.2. Tare the balance of analytical precision after removing the sample.
4. Prepare the water absorption device, wetting it, to evaluate the wet mass of samples.
   4.1. The excess water in the sample should be removed so that droplets are not on their surfaces. What should be done in the wet area of the absorption device.
   4.2. Weigh relatively quickly to prevent evaporation of the water within the pores of the sample.

Figure A.6 Water absorption device.

5. Dry the samples at a temperature above 110°C for 30 minutes, or put in oven at 37°C for 12 hours in order to remove the pore water.
6. Weigh the dry samples.

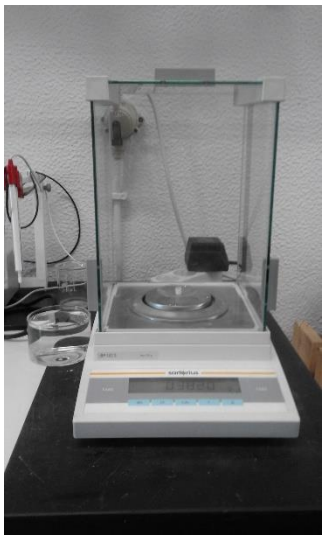


Figure A.7 Assembly for measure the mass of the dry sample.

7. Calculation of apparent density:

$$\rho_a = \frac{m_d}{m_w - m_i}\,\rho_{li} \qquad \text{(A.1)}$$

, where ρ_a is the apparent density of the sample, m_d the mass of the dry sample, m_w mass of the wet sample, m_i the mass of the immersed sample and ρ_{li} the density of the immersion liquid (water) temperature at which the measurements were made.

Calculation of apparent porosity:

$$\mathrm{AP} = \frac{\mathrm{m_w} - \mathrm{m_d}}{\mathrm{m_w} - \mathrm{m_i}} 100 \qquad \text{(A.2)}$$

, where AP is the apparent porosity of the sample, m_d the mass of the sample dry, m_w mass of the wet sample and m_i the mass of the immersed sample.

Annex 5

SBF procedure

Table A.1 Preparation of 1L of tris-HCl-buffered SBF with $[HCO_3^-]$ = 27mol:

Order	Reagent	Quantity [gpl]	Ion	SBF [nM]
1 – S15	NaCl	6.547	Cl^-; Na^+	142
2 – S16	$NaHCO_3$	2.268	Na^+; HCO_3^-	125
3 – P10	KCl	0.373	K^+; Cl^-	27
4 – S22	$Na_2HPO_4.2H_2O$	0.178	Na^+; HPO_4^{2-}	5
5 – M02	$MgCl_2.6H_2O$	0.305	Mg^{2+}; Cl^-	1.5
6	1M HCl	15 ml	H^+; Cl^-	2.5
7 – C08	$CaCl_2.2H_2O$	0.368	Ca^{2+}; Cl^-	1
8 – S21	Na_2SO_4	0.071	Na^+; SO_4^{2-}	0.5
9 – T03	$(CH_2OH)_3CNH_2$	6.057	-	-
10	1M HCl	Tritate to PH 7.4 at 37°C	-	-

Experimental procedure:

1) The reagents are added one by one, after complete dissolution in 700mL of distilled water.
2) In total we used 40 mL of HCl.
3) After addition of 9° reagent (Tris), solution was heated from room temperature to 37°C.
4) Water was added to make 1L of solution.
5) SBF have got valid for 1 month at 5°C.

Annex 6

For the degradation test, the sample was placed in boiling water during 73 hours and a condenser was used for water not evaporate.

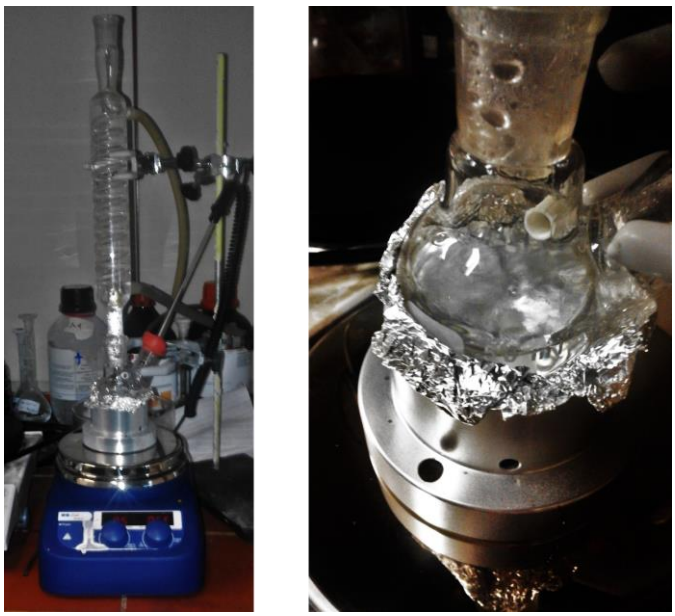

Figure A.8 Assembly to study the degradation of 3YSZ with water.

Annex 7

Cytotoxicity procedure

Resazurin is a non-fluorescent blue dye that is reduced to resorufin by cells. The resorufin is a rose fluorescent compound and through the change of color can be determined by measuring the change in absorbance. This variation is proportional to the number of viable cells present, see Figure A.9. The graph shows the absorbance spectra of resazurin (absorbance peak occurs at 601 nm) and resorufin (has the maximum absorbance at 571 nm), Figure.A.10.

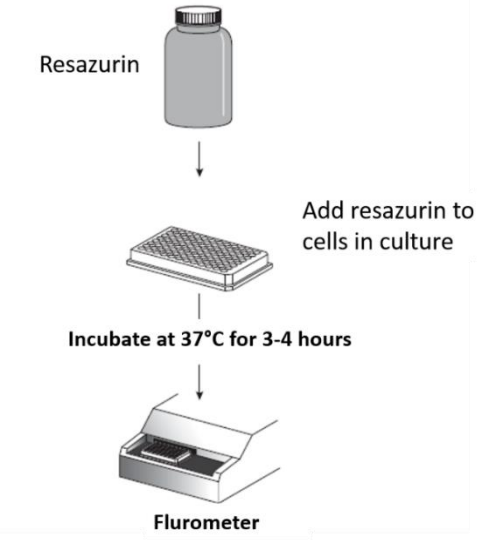

Figure A.9 Scheme for multiwell plate (96 well) compatible with fluorescent plate readers. Adapted from [69].

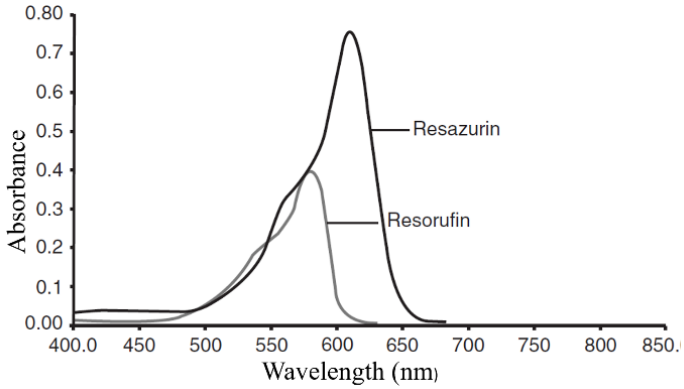

Figure.A.10 Absorbance spectra for resazurin and resorufin. Adapted from [70].

The cells are initially adhered to the bottom of a vial where they were saved. To be able to use these cells in culture must be freed from the vial background, so that trypsin was added in the vial.
For performing the cell count, a sample of the suspension was added to a hemacytometer to estimate the cell density.

In multiwell plate (96 well plate) that was previously prepared are SAOS cells with 6k cells per well. The density in each row is half the density on the preceding line. Each well of a 96 well plate has a diameter of 6 mm corresponding to an area of 0.283 cm^2 (≅ 0.3 cm^2).

1st - Was used one sample to produce the extract (the others are for adhesion/proliferation tests).

Weigh and record the mass (m) of the sample using: $m_{1.4}$= 0.9306g

2nd - The sample are sterilized in 70% ethanol. 15 min more 3 washes with distilled water

3th - Production of extracts.

Adjust the volume of medium to be 0.5 g/mL.

Place the medium without serum and serum is added only at the end (should be at a concentration of 10% fetal bovine serum) will put each set of sample at the following volume (v) of serum free medium:

$$v = (m/g) \times \frac{(900/\mu L)}{0{,}5} \Rightarrow v_{1.4} = 1675.01\mu L$$

In an identified falcon, put the respective sample and volume.

Once the solution is placed in the wells, the cells were placed in an incubator at 37°C for 24 hours, Figure A.11.

After 24 hours of contact of the cells with the conditioned medium, a resazurin solution (PrestoBlue®) with medium was performed. Next, after aspiring the wells, it was added 100 µL solution to each well. It is very important to be pipetted exactly 100 µL to each well, the uncertainty of the results will be greater the higher the dispersion of pipetted volume. The plate was again placed in the incubator at 37°C for 3 hours to metabolize resazurin. The plates are incubated at 37°C to allow cells to convert resazurin to resorufin. After the incubation, the absorbance (also called optical density) of the medium at 570 nm and 600 nm was read in a microplate reader. (BioTek ELx800).

Table A.2 Dilutions used in study of cytotoxicity.

Dilutions	Concentrations
1	0.500000 g/mL
2	0.250000 g/mL
3	0.125000 g/mL
4	0.062500 g/mL
5	0.031250 g/mL
6	0.015625 g/mL

Note: We made several dilutions in case the samples are toxic to realize from that concentration stopped being.

	1	2	3	4	5	6	7	8	9	10	11	12
A	3YSZ	3YSZ	3YSZ	3YSZ	3YSZ							CM
B	3YSZ	3YSZ	3YSZ	3YSZ	3YSZ							CM
C	3YSZ	3YSZ	3YSZ	3YSZ	3YSZ							CM
D	3YSZ	3YSZ	3YSZ	3YSZ	3YSZ							CM
E	3YSZ	3YSZ	3YSZ	3YSZ	3YSZ						CC+	CM
F											CC-	CC+
G											CC-	CC+
H										CC-	CC-	CC+

Figure A.11 Representative scheme of 96 well plate used, 3YSZ is the medium with waste samples printed using the paste without binder, CM is control medium, CC+ is positive control cells (dead cells) and CC- is negative control cells (living cells).

Annex 8

Cell adhesion/proliferation

The procedure is similar to that performed when the study of the cytotoxicity.

In this assay, we used 6 replicas to the adhesion/proliferation test and two samples in the medium control (CM).

After placing the samples in the wells and before placing the medium and cells on these it is necessary to sterilize the sample. For that, the samples were washed with ethanol (500µL per well), which remained at rest for 15 minutes, following up two washes with distilled water and ending with a washing with phosphate-buffered saline (PBS), always with the 500µL volume per well.

For the multiwell plate (48 well plate) were prepared a culture with SAOS cells with 30k cells per well. Each well of a 48 well plate has a diameter of 9 mm corresponding to an area of 0.64 cm^2.

Are needed a total of 500k cells, after performing the count were to 540k cells, thus the volume posed is:

$$v = \frac{500\text{kcells} \times 1\text{mL}}{540\text{kcells}} + 11575\mu\text{Lmedium} \Rightarrow \text{v} = 925\mu\text{L} + 11575\mu\text{Lmedium}$$

The cell medium was distributed by wells with the samples and by wells with the cell control (CC). In the next day, the samples are changed for other wells, as shown in Figure A.12 to be possible to count the cells that were adhered to in the deep end where the sample is selected and to know the approximate number of cells that were adhered to the sample, since each well have approximately 30K cells. And in this way, it is calculated cell adhesion.

	1	2	3	4	5	6	7	8
A	3YSZ	3YSZ	3YSZ	3YSZ	3YSZ	3YSZ	CC	CC
B							1.4CM	1.4CM
C							CC	CM
D								
E							CC	CM
F								

Figure A.12 Representative scheme of 48 well plate used, 3YSZ is where the samples printed using the paste without binder, CC is control cells and CM is control medium. The arrows represent the well where moved the samples to be able to count the cells adhering to the sample.

The plates were incubated at 37°C to allow cells to convert resazurin to resorufin. After the incubation, 150µL of solution were removed from each well and placed in a 96-well plate for absorbance reading (also called optical density) of the medium at 570 nm and 600 nm in microplate reader. (BioTek ELx800).

After the reading of the absorbances is necessary to vacuum and wash the wells of 48-well plate with PBS and then place 500µL of the new medium. One day, four, seven and nine days later the absorbance is measured again by repeating the above procedure below to be able to calculate the cell proliferation.

Annex 9

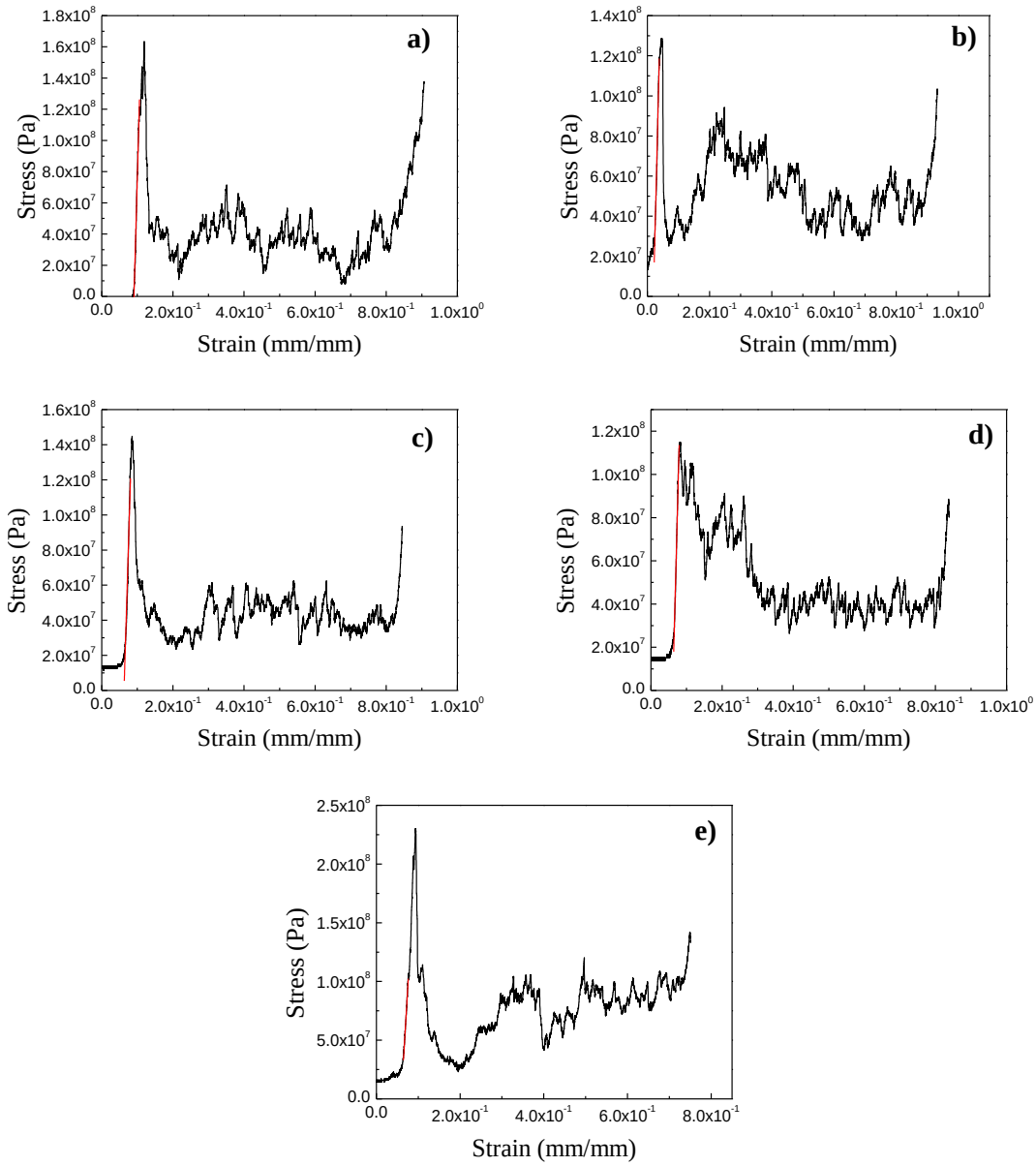

Figure A.13 Graphs of compression tests of samples printed with the paste without binder and geometry C, a) Sample 1, b) Sample 2, c) Sample 3, d) Sample 4 and e) Sample 5.

Through the stress-strain graphs we can obtain the values of σ_{Max} and E and calculate the mean value, as can be seen in Table A.3.

Table A.3 Results of samples printed using pastes without binder, series of sample geometry C.

	σ_{Max} [MPa]	E [GPa]
1	163.340;	8.079;
2	128.586;	6.180;
3	144.686;	6.641;
3	114.823;	6.251;
4	230.051	6.000
Mean	156.297±45.034	6.630±0.843

Annex 10

Table A.4 Results of size of samples made using pastes with and without binder at different temperatures.

	Sintering temperature [°C]	Height [mm]	Diameter [mm]
Without binder	Non-sintered	8.83	10.65
	1100	8.10±0.01	8.42±0.01
	1200	7.32±0.01	7.43±0.01
	1300	7.17±0.01	6.68±0.01
	1400	6.86±0.01	6.60±0.01
	1450	6.96±0.01	6.83±0.01
With binder	Non-sintered	9.68	11.25
	1100	8.03±0.01	7.69±0.01
	1200	7.91±0.01	7.67±0.01
	1300	7.30±0.01	6.92±0.01
	1400	7.15±0.01	6.85±0.01
	1450	7.22±0.01	6.97±0.01

Note: The measurements of samples of the non-sintered paste are performed trough *ImageJ* software.

Table A.5 Samples printed with the paste without binder sintered different temperatures.

Non-sintered	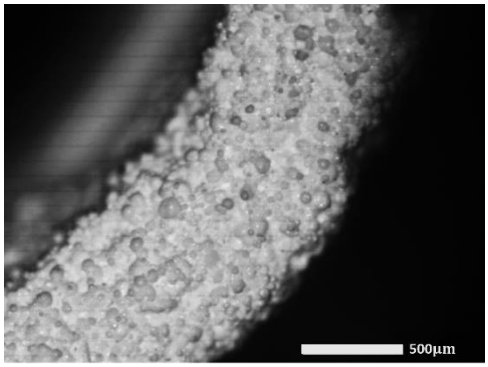	NA

Sintered at 1100°C	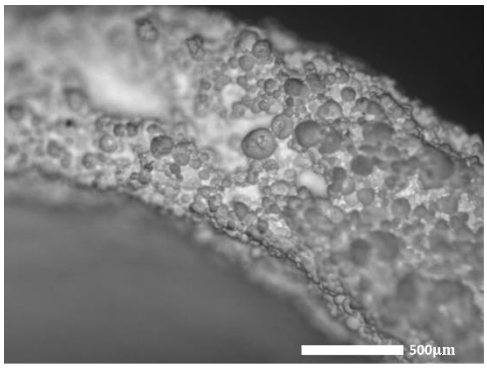	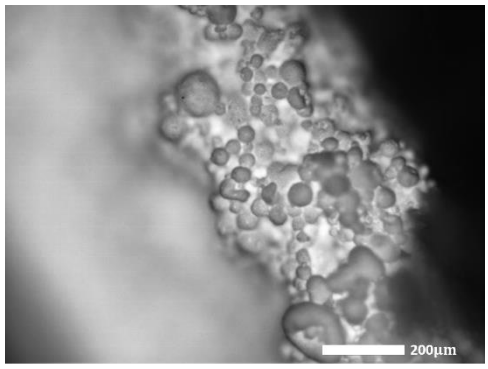
Sintered at 1200°C	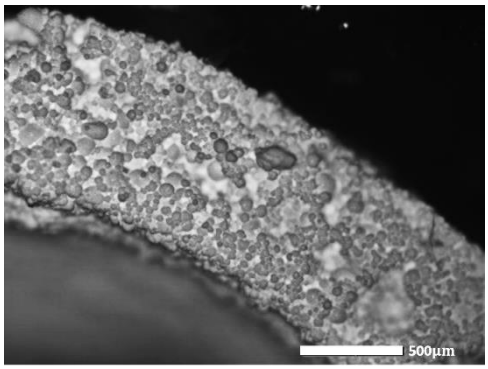	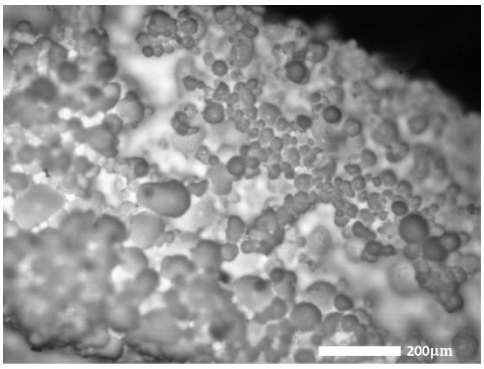
Sintered at 1300°C	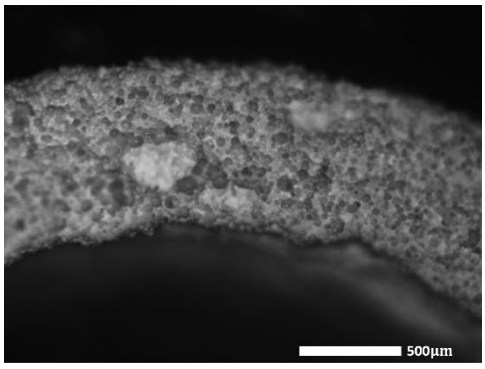	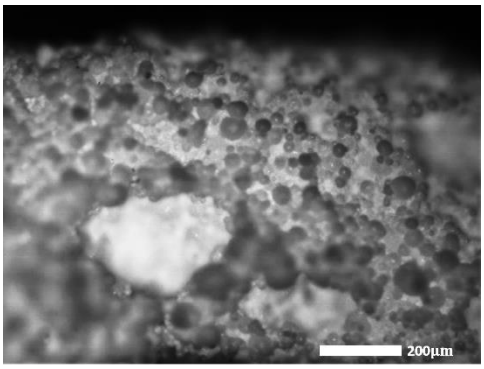
Sintered at 1400°C	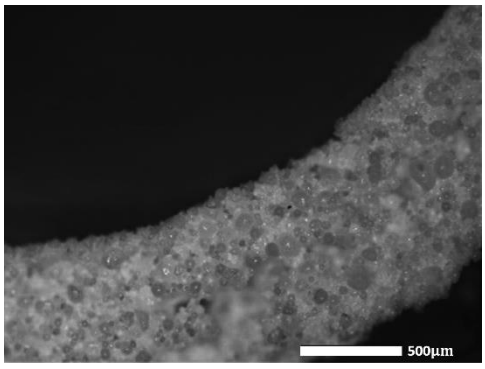	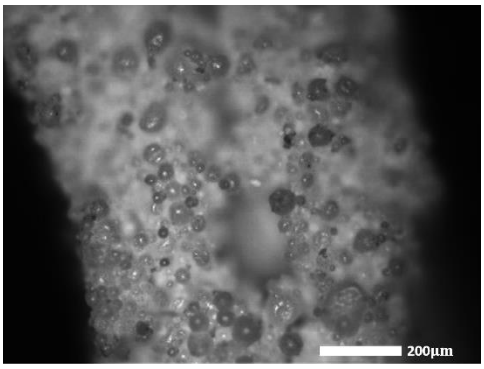

Sintered at 1450°C	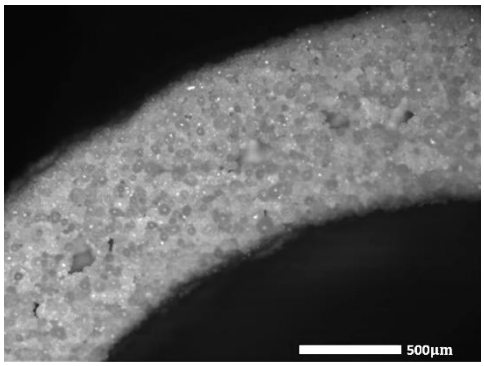	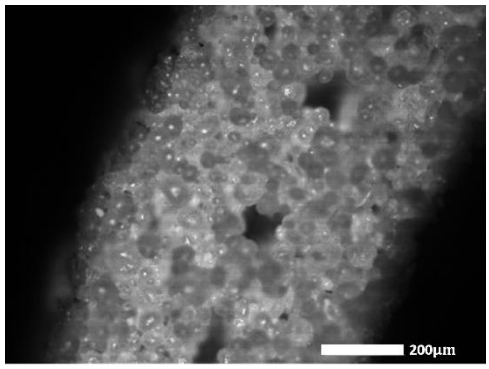

Table A.6 Samples printed using the paste with binder sintered at different temperatures.

Non-sintered	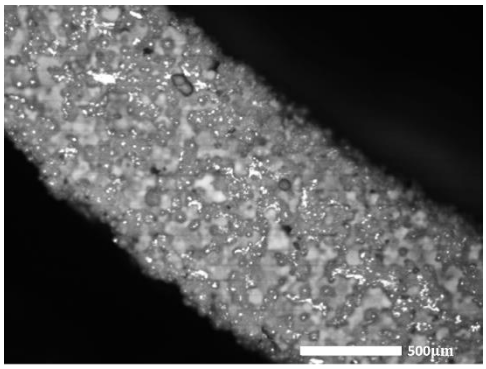	NA
Sintered at 1100°C	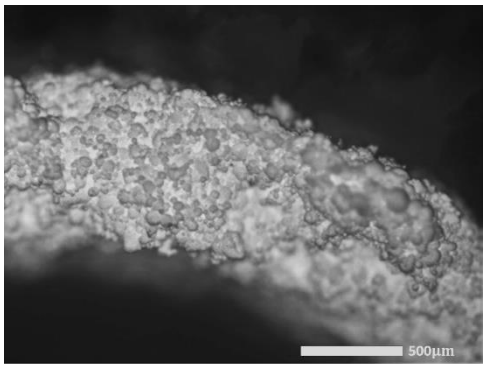	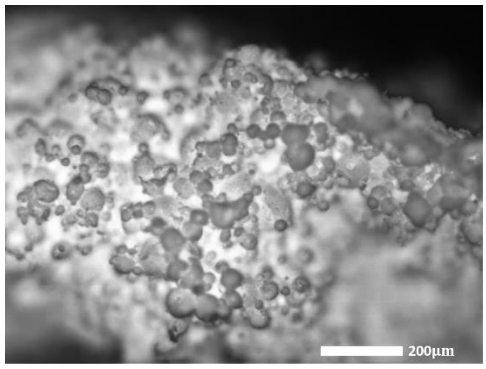
Sintered at 1200°C	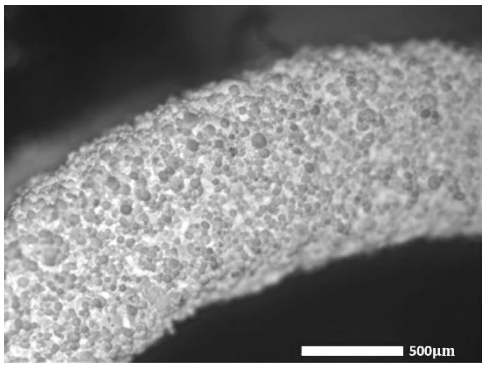	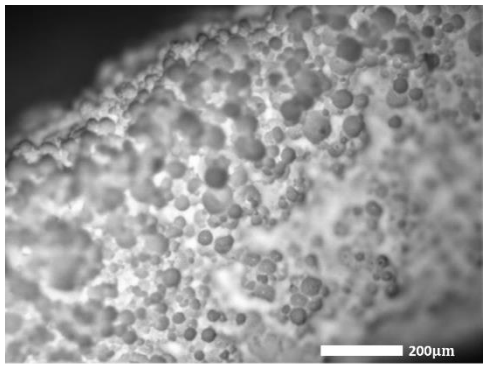

Sintered at 1300°C	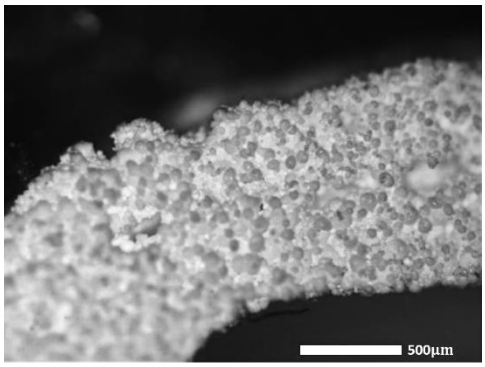	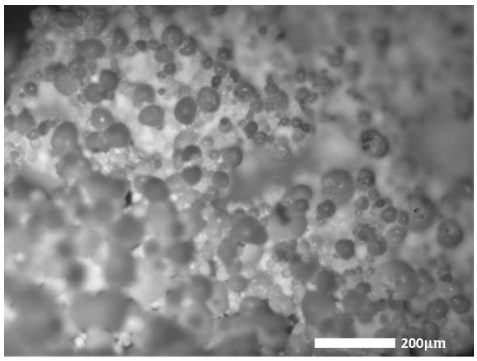
Sintered at 1400°C	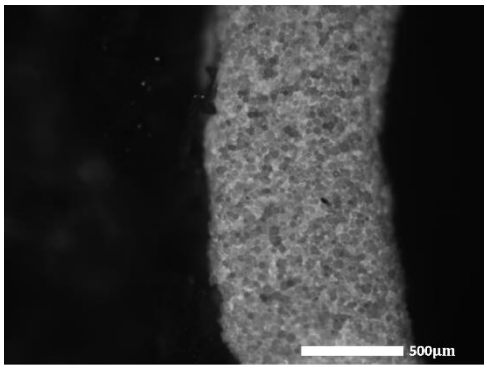	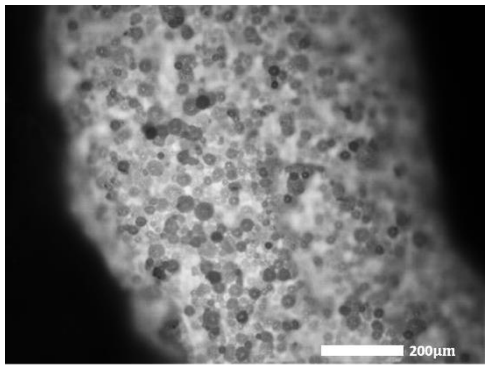
Sintered at 1450°C	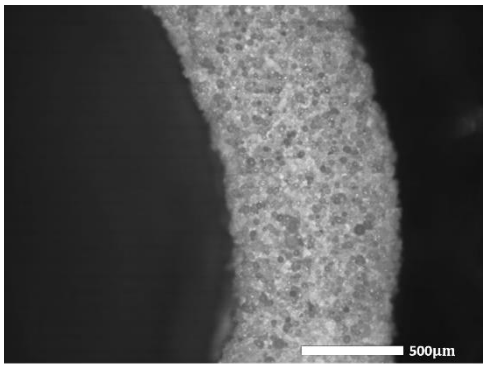	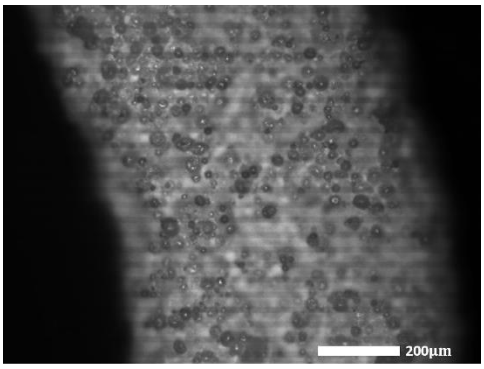

Annex 11

Conditions of degradability tests

- Printing a total of 40 samples:
  - Without being in SBF,
  - 1 day in SBF,
  - 1 week in SBF,
  - 2 weeks in SBF,
  - 4 weeks in SBF (1 month).
- Oven at 37°C (body temperature).
- Renew the SBF every week (7ml of SBF in each vial).

Figure A.14 5 series of cylindrical samples.

Figure A.15 a) Oven ate 37 °C and b) Samples in the vials with 7mL of SBF.

- Measuring, weighing and see samples under the microscope before and after the tests.
- Realize the compression tests after the samples come out of the oven.

• Paste without binder →Without being in SBF

Table A.7 Results of samples printed using pastes not containing binder without being in SBF.

	Samples sintered before SBF				**Samples sintered after SBF**			
	Height (h) [mm]	Diameter (d) [mm]	Wall (w) [mm]	Weight [g]	Height (h) [mm]	Diameter (d) [mm]	Wall (w) [mm]	Weight [g]
1	6.15±0.01	7.87±0.01	8.10±0.01	-	6.15±0.01	7.87±0.01	8.10±0.01	-
2	6.64±0.01	7.55±0.01	7.61±0.01	-	6.64±0.01	7.55±0.01	7.61±0.01	-
3	5.08±0.01	7.64±0.01	7.76±0.01	-	5.08±0.01	7.64±0.01	7.76±0.01	-
4	6.39±0.01	7.69±0.01	7.87±0.01	-	6.39±0.01	7.69±0.01	7.87±0.01	-
5	7.11±0.01	6.85±0.01	6.92±0.01	-	7.11±0.01	6.85±0.01	6.92±0.01	-

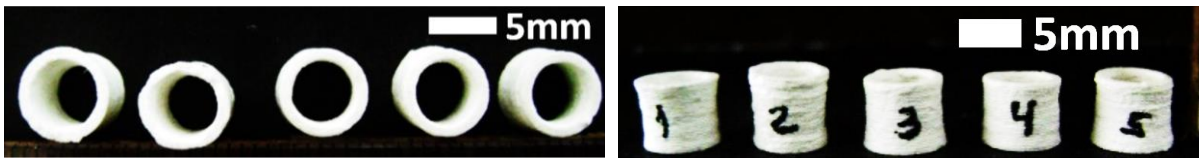

Figure A.16 Samples without being in SBF.

Table A.8 Samples printed from paste without binder not immersed in SBF.

Bottom view	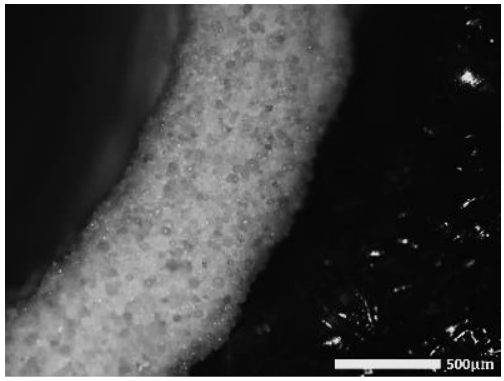	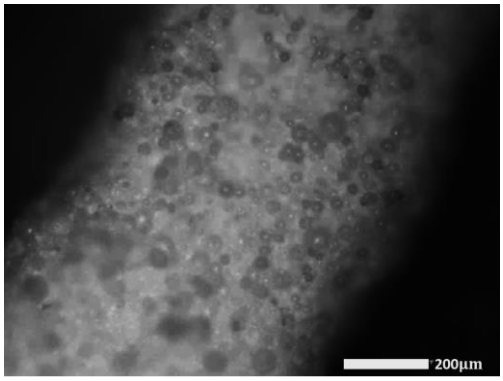
Side view	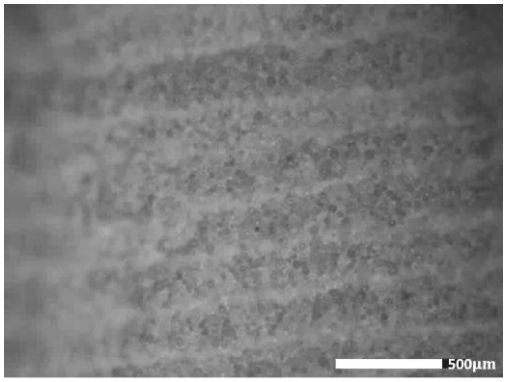	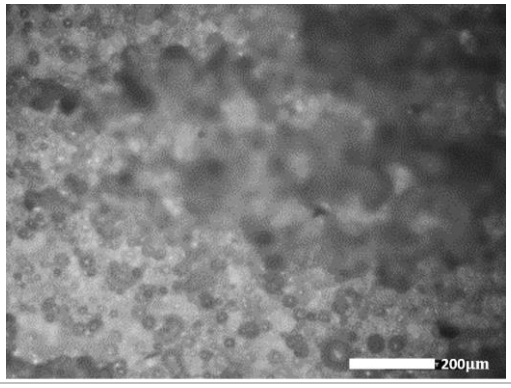

- Paste without binder - 1 day in SBF

Table A.9 Results of samples printed from pastes without binder, 1 day in SBF.

	Samples sintered before SBF				**Samples sintered after SBF**			
	Height (h) [mm]	Diameter (d) [mm]	Wall (w) [mm]	Weight [g]	Height (h) [mm]	Diameter (d) [mm]	Wall (w) [mm]	Weight [g]
1	6.78±0.01	6.75±0.01	0.95±0.01	0.325±0.005	6.78±0.01	6.75±0.01	0.96±0.01	0.330±0.005
2	6.81±0.01	6.67±0.01	0.93±0.01	0.325±0.005	6.82±0.01	6.75±0.01	0.93±0.01	0.330±0.005
3	6.85±0.01	6.36±0.01	0.93±0.01	0.325±0.005	6.82±0.01	6.38±0.01	0.94±0.01	0.330±0.005
4	7.07±0.01	6.62±0.01	0.91±0.01	0.320±0.005	7.09±0.01	6.63±0.01	0.91±0.01	0.320±0.005
5	6.80±0.01	6.82±0.01	0.94±0.01	0.325±0.005	6.82±0.01	6.84±0.01	0.93±0.01	0.325±0.005

No weight loss after SFB.

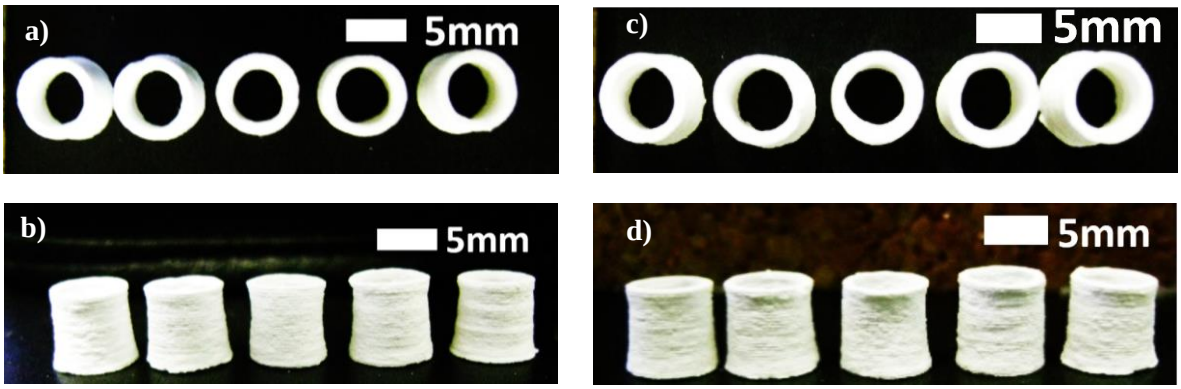

Figure A.17 a) and b) Samples before the SBF, c) and d) Samples after 1 day in SBF.

Table A.10 Samples printed from pastes without binder, 1 day in SBF.

Bottom view	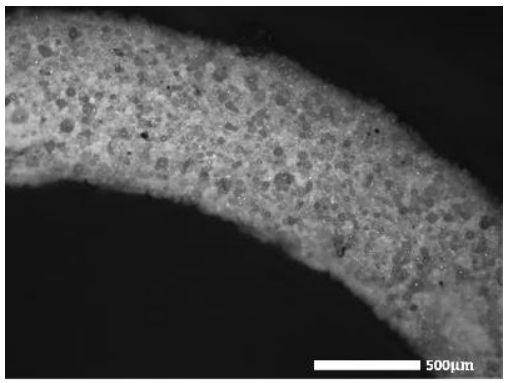	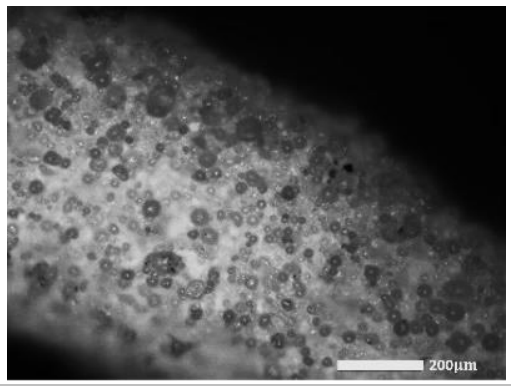
Side view	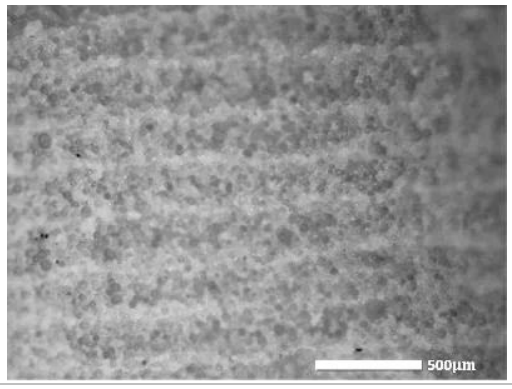	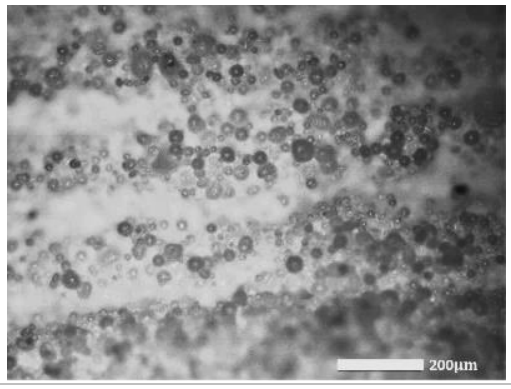

- Paste without binder - 1 week in SBF

Table A.11 Results of samples printed from pastes without binder, 1 week in SBF.

	Samples sintered before SBF				Samples sintered after SBF			
	Height (h) [mm]	Diameter (d) [mm]	Wall (w) [mm]	Weight [g]	Height (h) [mm]	Diameter (d) [mm]	Wall (w) [mm]	Weight [g]
1	6.81±0.01	6.52±0.01	0.92±0.01	0.330±0.005	6.81±0.01	6.52±0.01	0.90±0.01	0.335±0.005
2	6.82±0.01	6.60±0.01	0.92±0.01	0.335±0.005	6.80±0.011	6.60±0.01	0.91±0.01	0.335±0.005
3	6.74±0.01	6.67±0.01	0.93±0.01	0.330±0.005	6.93±0.01	6.89±0.01	0.94±0.01	0.325±0.005
4	6.73±0.01	6.62±0.01	0.95±0.01	0.335±0.005	6.73±0.01	6.63±0.01	0.94±0.01	0.335±0.005
5	6.80±0.01	6.63±0.01	0.87±0.01	0.335±0.005	6.79±0.01	6.63±0.01	0.87±0.01	0.330±0.005

No weight loss after SFB.

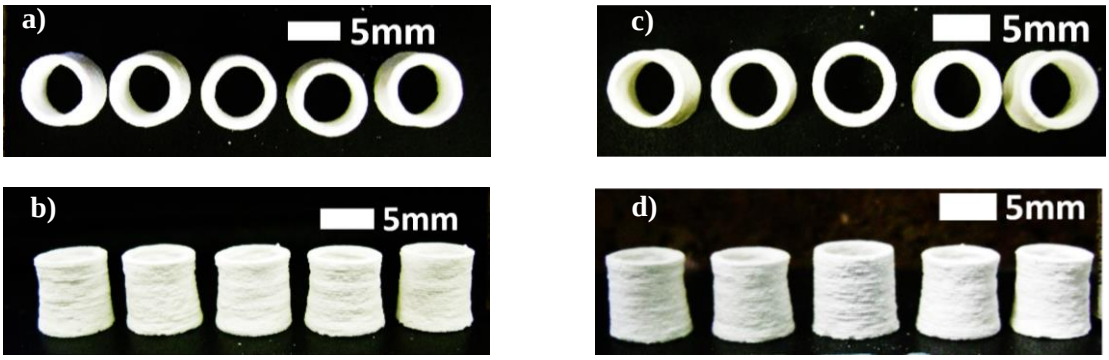

Figure A.18 a) and b) Samples before the SBF, c) and d) Samples after 1 week in SBF.

Table A.12 Samples printed from pastes without binder, 1 week in SBF.

Bottom view	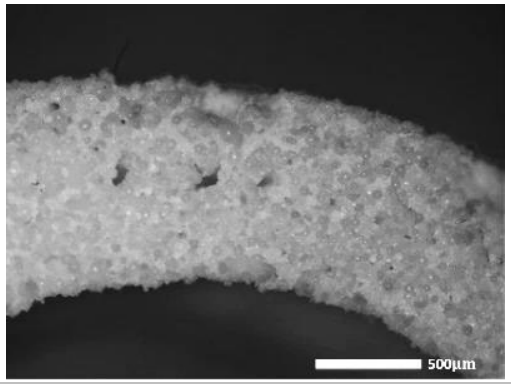	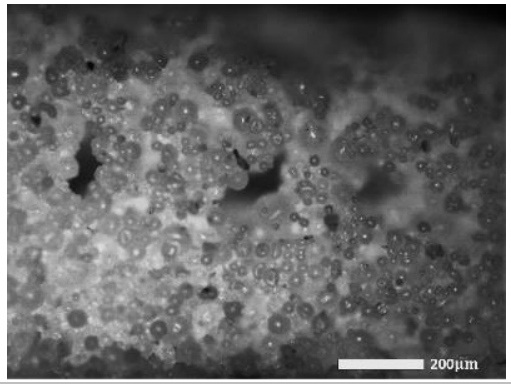
Side view	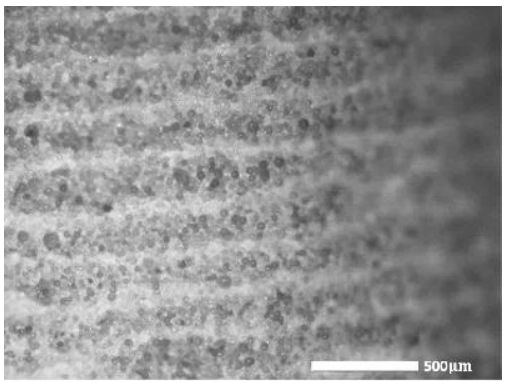	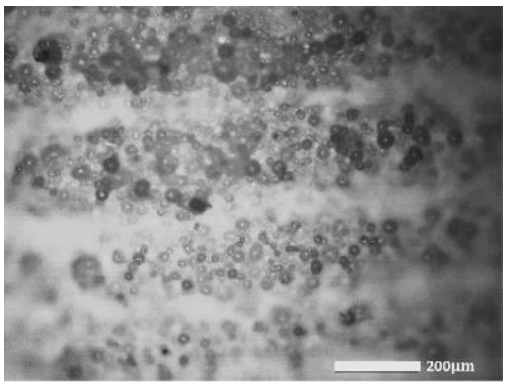

- Paste without binder - 2 weeks in SBF

Table A.13 Results of samples printed from pastes without binder, 2 weeks in SBF.

	Samples sintered before SBF				Samples sintered after SBF			
	Height (h) [mm]	Diameter (d) [mm]	Wall (w) [mm]	Weight [g]	Height (h) [mm]	Diameter (d) [mm]	Wall (w) [mm]	Weight [g]
1	6.73±0.01	6.68±0.01	0.96±0.01	0.335±0.005	6.81±0.01	6.52±0.01	0.90±0.01	0.335±0.005
2	6.81±0.01	6.59±0.01	0.92±0.01	0.340±0.005	6.81±0.01	6.60±0.01	0.91±0.01	0.335±0.005
3	6.83±0.01	6.76±0.01	0.91±0.01	0.335±0.005	6.93±0.01	6.89±0.01	0.94±0.01	0.325±0.005
4	6.88±0.01	6.54±0.01	0.88±0.01	0.325±0.005	6.73±0.01	6.63±0.01	0.94±0.01	0.335±0.005
5	6.79±0.01	6.62±0.01	0.92±0.01	0.340±0.005	6.79±0.01	6.63±0.01	0.87±0.01	0.330±0.005

No weight loss after SFB.

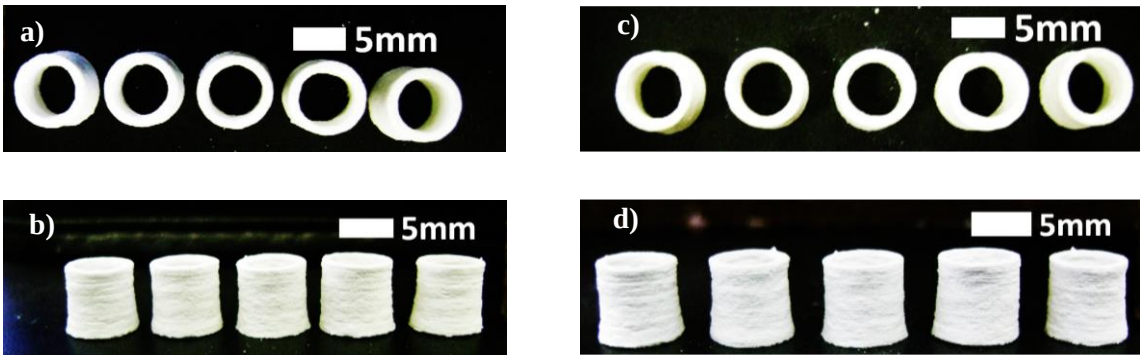

Figure A.19 a) and b) Samples before the SBF, c) and d) Samples after 2 weeks in SBF.

Table A.14 Samples printed from pastes without binder, 2 weeks in SBF.

Bottom view	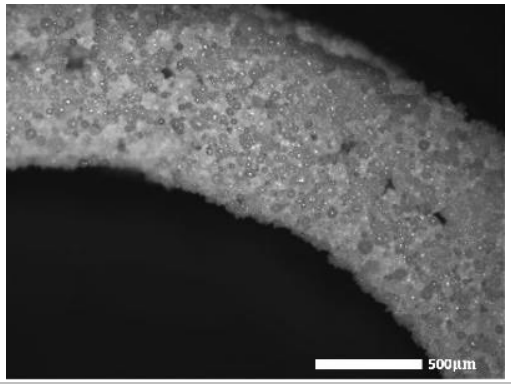	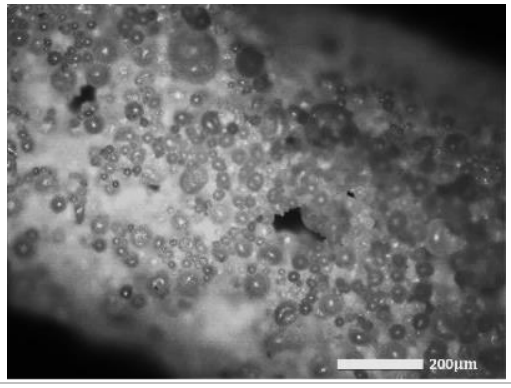
Side view	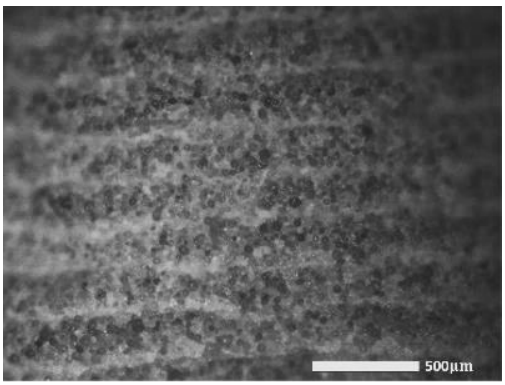	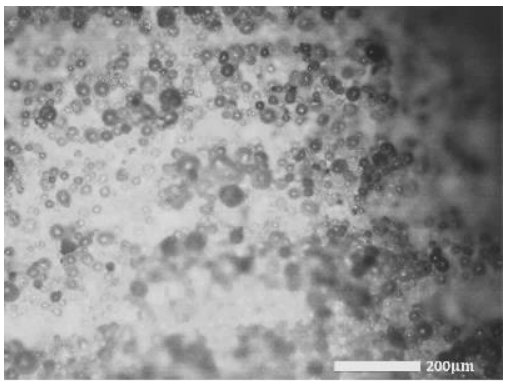

- Paste without binder - 4 weeks in SBF

Table A.15 Results of samples printed from pastes without binder, 4 weeks in SBF.

	Samples sintered before SBF				Samples sintered after SBF			
	Height (h) [mm]	Diameter (d) [mm]	Wall (w) [mm]	Weight [g]	Height (h) [mm]	Diameter (d) [mm]	Wall (w) [mm]	Weight [g]
1	6.93±0.01	6.71±0.01	0.87±0.01	0.335±0.005	6.90±0.01	6.70±0.01	0.87±0.01	0.335±0.005
2	6.92±0.01	6.71±0.01	0.89±0.01	0.340±0.005	6.93±0.01	6.71±0.01	0.88±0.01	0.335±0.005
3	6.81±0.01	6.55±0.01	0.92±0.01	0.335±0.005	6.79±0.01	6.52±0.01	0.92±0.01	0.330±0.005
4	6.83±0.01	6.54±0.01	0.82±0.01	0.330±0.005	6.82±0.01	6.54±0.01	0.89±0.01	0.340±0.005
5	6.90±0.01	6.60±0.01	0.91±0.01	0.345±0.005	6.85±0.01	6.59±0.01	0.92±0.01	0.340±0.005

No weight loss after SFB.

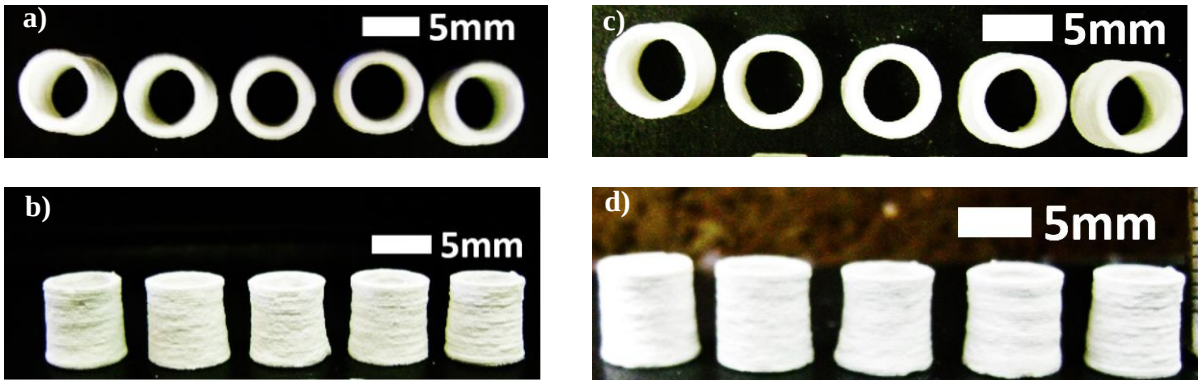

Figure A.20 a) and b) Samples before the SBF, c) and d) Samples after 4 weeks in SBF.

Table A.16 Samples printed from pastes without binder, 4 weeks in SBF.

Bottom view	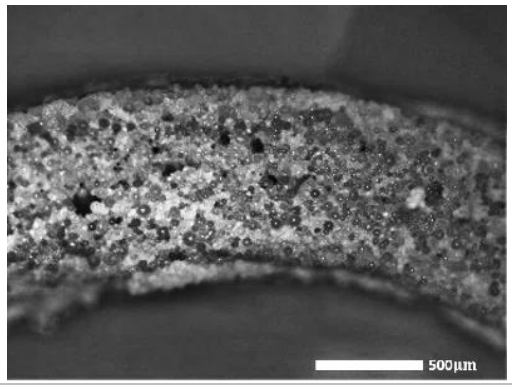	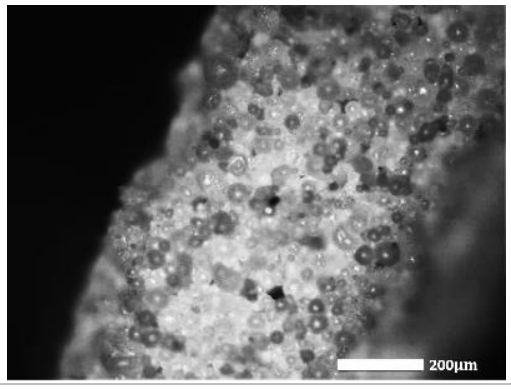
Side view	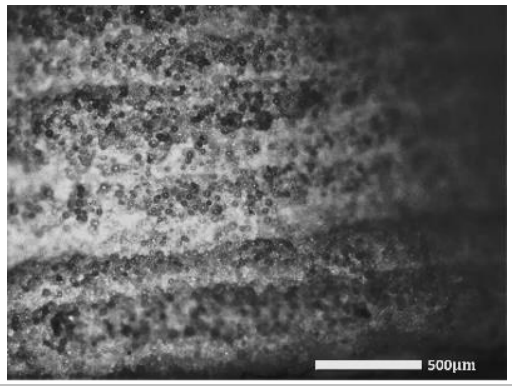	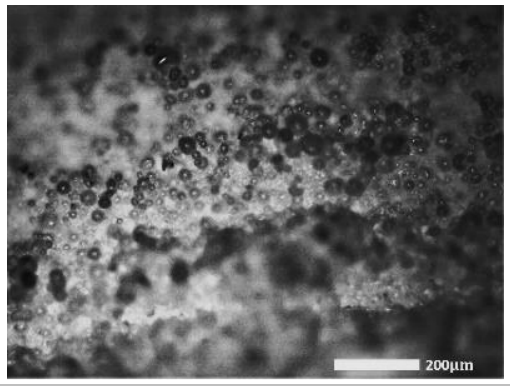

- Paste with binder - Without being in SBF

Table A.17 Results of samples printed from pastes with binder, without being in SBF.

	Samples sintered before SBF				Samples sintered after SBF			
	Height (h) [mm]	Diameter (d) [mm]	Wall (w) [mm]	Weight [g]	Height (h) [mm]	Diameter (d) [mm]	Wall (w) [mm]	Weight [g]
1	5.57±0.01	5.86±0.01	0.80±0.01	-	5.57±0.01	5.86±0.01	0.80±0.01	-
2	5.57±0.01	6.39±0.01	1.00±0.01	-	5.57±0.01	6.39±0.01	1.00±0.01	-
3	5.58±0.01	7.28±0.01	0.95±0.01	-	5.58±0.01	7.28±0.01	0.95±0.01	-
4	5.66±0.01	6.22±0.01	0.83±0.01	-	5.66±0.01	6.22±0.01	0.83±0.01	-
5	6.07±0.01	6.64±0.01	0.85±0.01	-	6.07±0.01	6.64±0.01	0.85±0.01	-

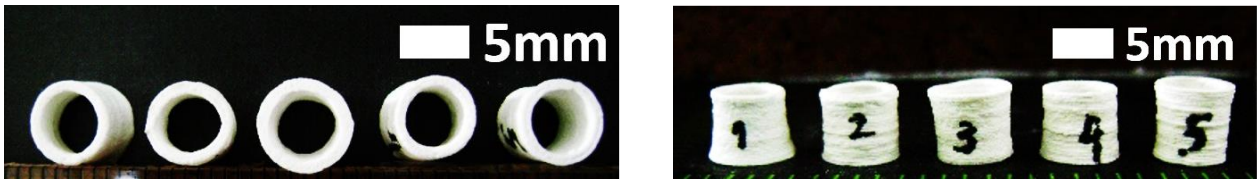

Figure A.21 Samples after the SBF.

Table A.18 Samples printed from pastes with binder, without being in SBF.

Bottom view	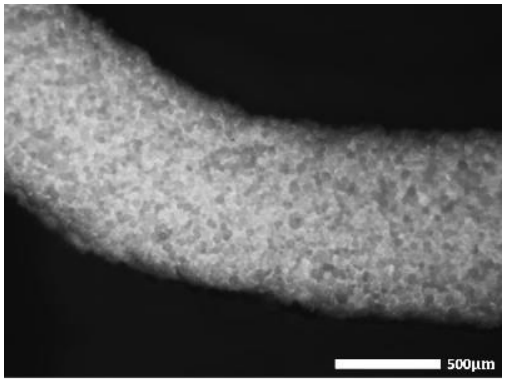	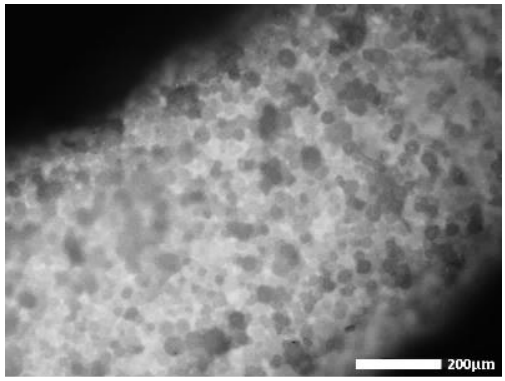
Side view	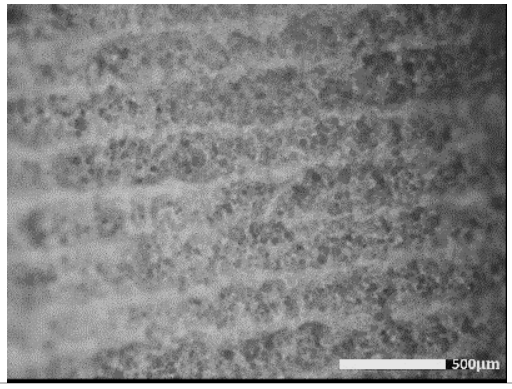	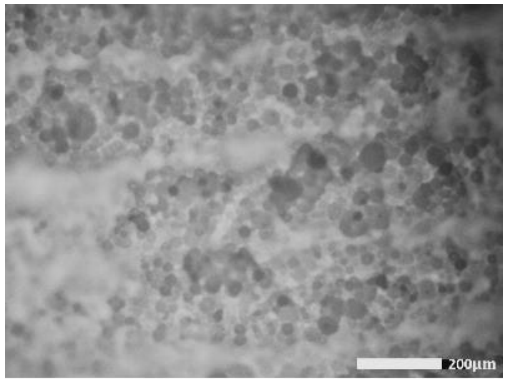

- Paste with binder - 1 day in SBF

Table A.19 Results of samples printed from pastes with binder, 1 day in SBF.

	Samples sintered before SBF				**Samples sintered after SBF**			
	Height (h) [mm]	Diameter (d) [mm]	Wall (w) [mm]	Weight [g]	Height (h) [mm]	Diameter (d) [mm]	Wall (w) [mm]	Weight [g]
1	7.18±0.01	6.79±0.01	0.95±0.01	0.350±0.005	7.15±0.01	6.95±0.01	0.95±0.01	0.350±0.005
2	7.18±0.01	6.95±0.01	0.97±0.01	0.350±0.005	7.17±0.01	6.95±0.01	0.97±0.01	0.350±0.005
3	7.05±0.01	6.80±0.01	0.95±0.01	0.350±0.005	7.07±0.01	6.80±0.01	0.95±0.01	0.350±0.005
4	7.15±0.01	6.91±0.01	0.98±0.01	0.350±0.005	7.15±0.01	6.94±0.01	0.98±0.01	0.350±0.005
5	7.03±0.01	7.02±0.01	0.95±0.01	0.335±0.005	7.01±0.01	7.02±0.01	0.95±0.01	0.335±0.005

No weight loss after SFB.

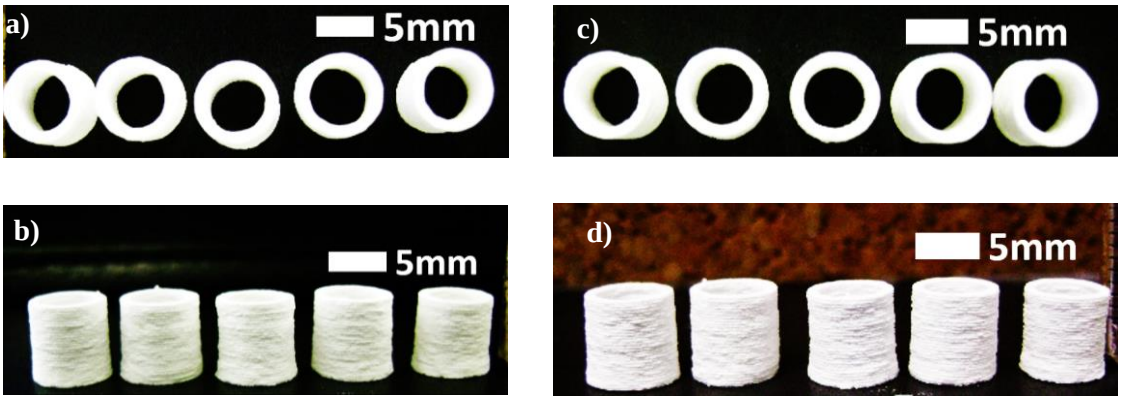

Figure A.22 a) and b) Samples before the SBF, c) and d) Samples after 1 day in SBF.

Table A.20 Samples printed from pastes with binder, 1 day in SBF.

Bottom view	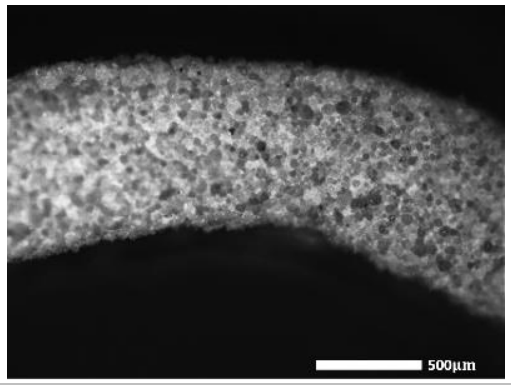	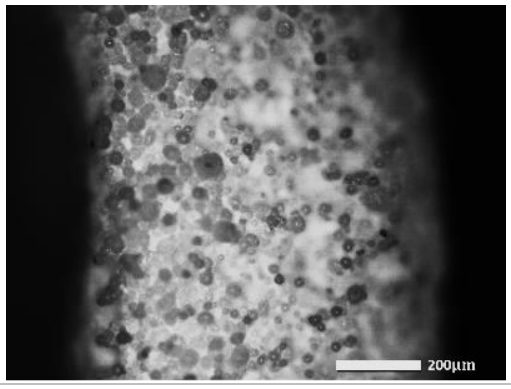
Side view	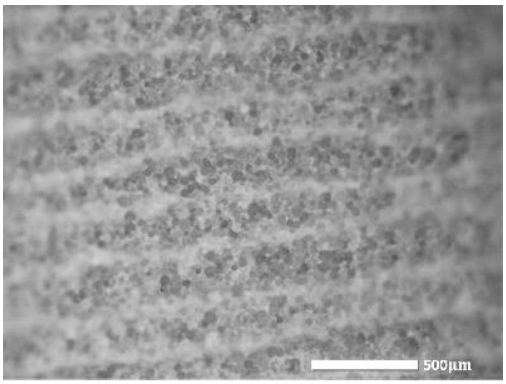	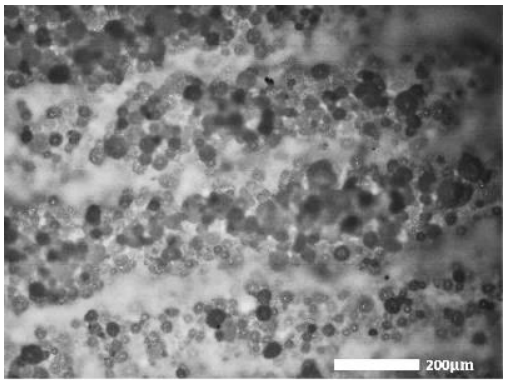

- Paste with binder - 1 week in SBF

Table A.21 Results of samples printed from pastes with binder, 1 week in SBF.

	Samples sintered before SBF				Samples sintered after SBF			
	Height (h) [mm]	Diameter (d) [mm]	Wall (w) [mm]	Weight [g]	Height (h) [mm]	Diameter (d) [mm]	Wall (w) [mm]	Weight [g]
1	7.16±0.01	6.89±0.01	0.98±0.01	0.345±0.005	7.16±0.01	6.89±0.01	0.97±0.01	0.345±0.005
2	7.16±0.01	6.78±0.01	0.98±0.01	0.350±0.005	7.16±0.01	6.86±0.01	0.98±0.01	0.350±0.005
3	6.96±0.01	6.89±0.01	0.92±0.01	0.340±0.005	6.92±0.01	6.75±0.01	0.92±0.01	0.340±0.005
4	6.96±0.01	6.90±0.01	0.99±0.01	0.355±0.005	6.96±0.01	6.93±0.01	0.96±0.01	0.350±0.005
5	7.07±0.01	6.97±0.01	0.94±0.01	0.350±0.005	7.06±0.01	6.97±0.01	0.94±0.01	0.345±0.005

No weight loss after SFB.

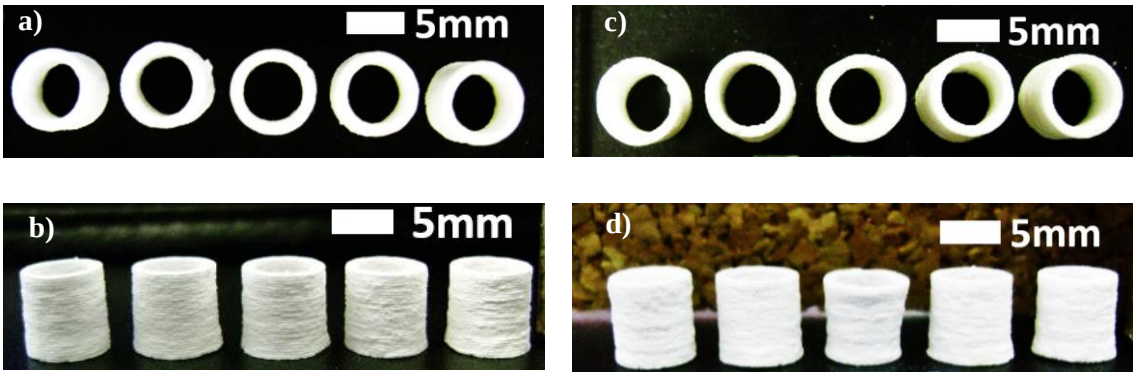

Figure A.23 a) and b) Samples before the SBF, c) and d) Samples after 1 weeks in SBF.

Table A.22 Samples printed from pastes with binder, 1 week in SBF.

Bottom view	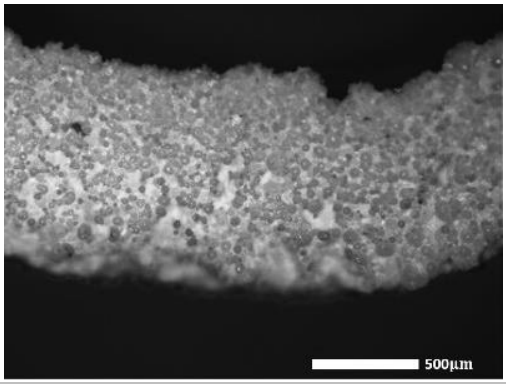	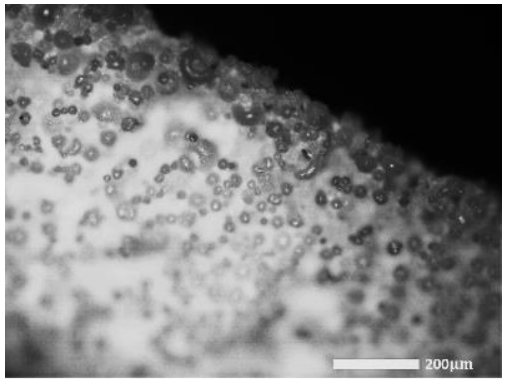
Side view	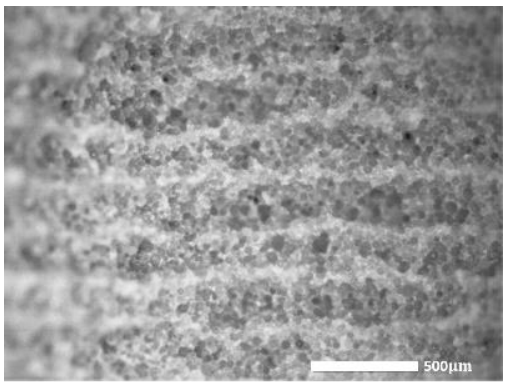	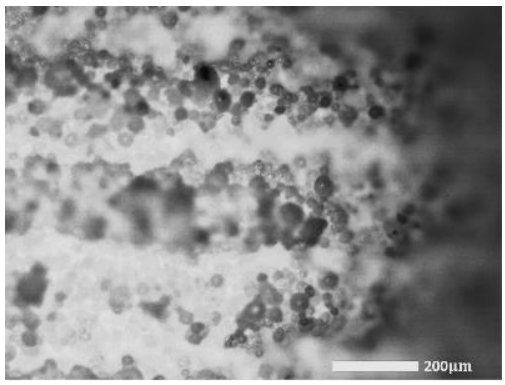

- Paste with binder - 2 weeks in SBF

Table A.23 Results of samples printed from pastes with binder, 2 weeks in SBF.

	Samples sintered before SBF				**Samples sintered after SBF**			
	Height (h) [mm]	Diameter (d) [mm]	Wall (w) [mm]	Weight [g]	Height (h) [mm]	Diameter (d) [mm]	Wall (w) [mm]	Weight [g]
1	7.16±0.01	6.89±0.01	0.98±0.01	0.345±0.005	7.16±0.01	6.89±0.01	0.97±0.01	0.345±0.005
2	7.16±0.01	6.78±0.01	0.98±0.01	0.350±0.005	7.16±0.01	6.86±0.01	0.98±0.01	0.350±0.005
3	6.96±0.01	6.89±0.01	0.92±0.01	0.340±0.005	6.92±0.01	6.75±0.01	0.92±0.01	0.340±0.005
4	6.96±0.01	6.90±0.01	0.99±0.01	0.355±0.005	6.96±0.01	6.93±0.01	0.96±0.01	0.350±0.005
5	7.07±0.01	6.97±0.01	0.94±0.01	0.350±0.005	7.06±0.01	6.97±0.01	0.94±0.01	0.345±0.005

No weight loss after SFB.

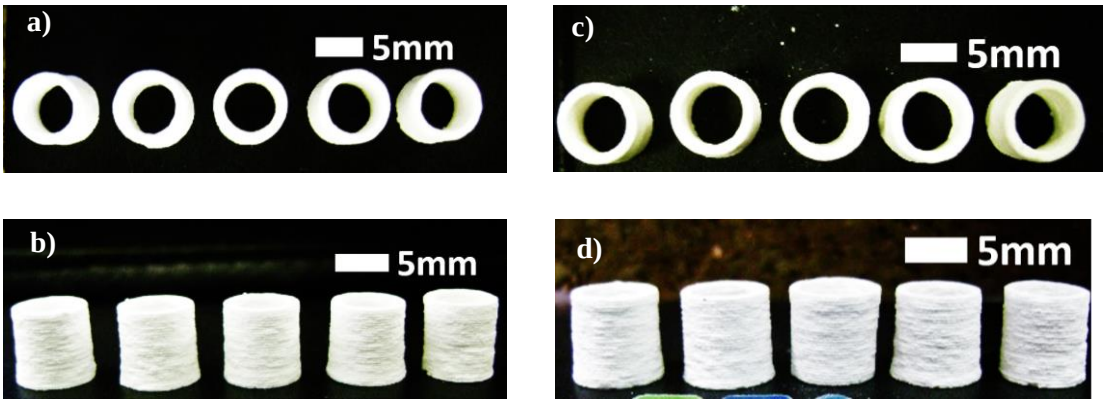

Figure A.24 a) and b) Samples before the SBF, c) and d) Samples after 2weeks in SBF.

Table A.24 Samples printed from pastes with binder, 2 weeks in SBF.

Bottom view	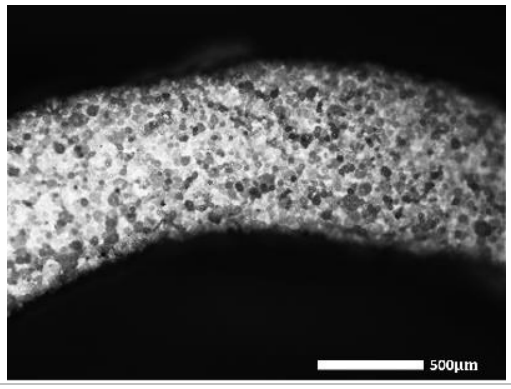	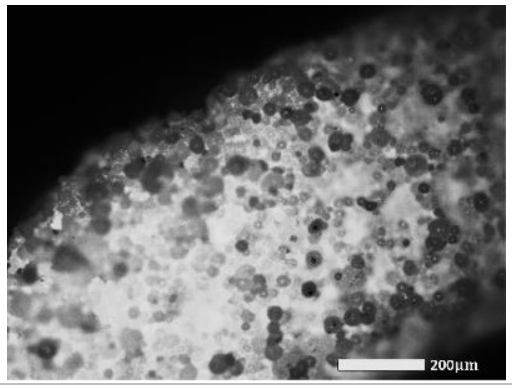
Side view	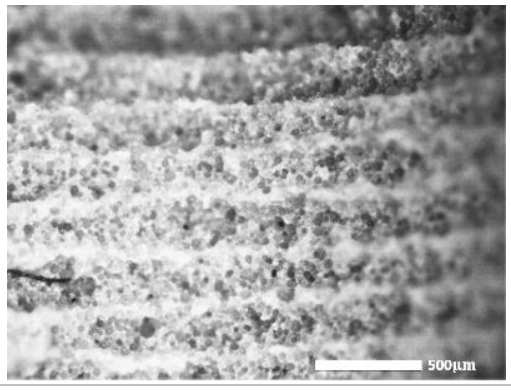	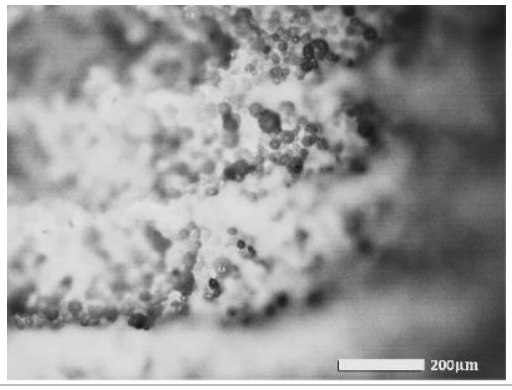

- Paste with binder - 4 weeks in SBF

Table A.25 Results of samples printed from pastes with binder, 4 weeks in SBF.

	Samples sintered before SBF				Samples sintered after SBF			
	Height (h) [mm]	Diameter (d) [mm]	Wall (w) [mm]	Weight [g]	Height (h) [mm]	Diameter (d) [mm]	Wall (w) [mm]	Weight [g]
1	6.83±0.01	6.31±0.01	0.93±0.01	0.335±0.005	6.83±0.01	6.38±0.01	0.94±0.01	0.330±0.005
2	7.03±0.01	7.06±0.01	0.96±0.01	0.325±0.005	6.99±0.01	7.05±0.01	0.96±0.01	0.330±0.005
3	6.79±0.01	6.46±0.01	0.94±0.01	0.325±0.005	6.78±0.01	6.48±0.01	0.93±0.01	0.330±0.005
4	6.88±0.01	6.27±0.01	0.92±0.01	0.335±0.005	6.86±0.01	6.26±0.01	0.92±0.01	0.340±0.005
5	7.09±0.01	6.92±0.01	0.94±0.01	0.365±0.005	7.10±0.01	6.92±0.01	0.93±0.01	0.370±0.005

No weight loss after SFB.

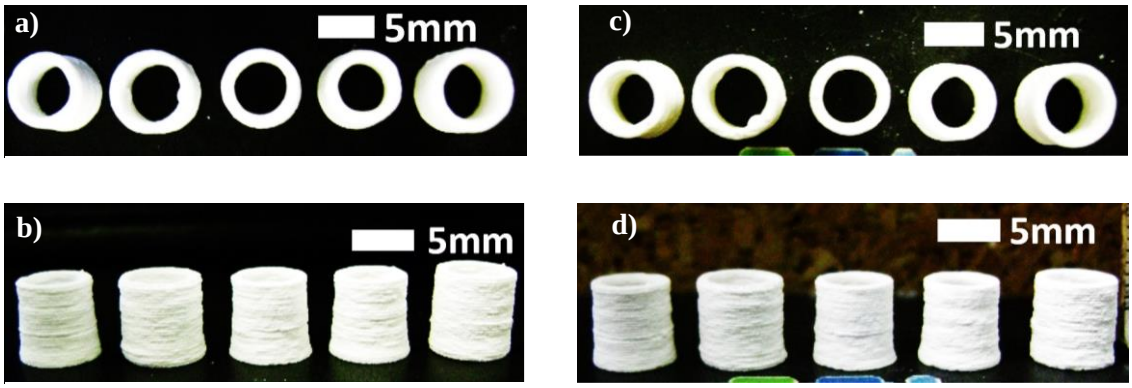

Figure A.25 a) and b) Samples before the SBF, c) and d) Samples after 4 weeks in SBF.

Table A.26 Samples printed from pastes with binder, 4 weeks in SBF.

Bottom view	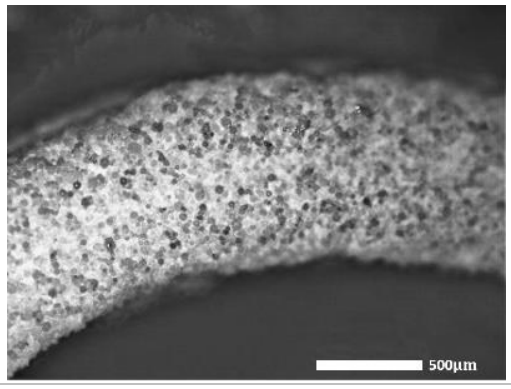	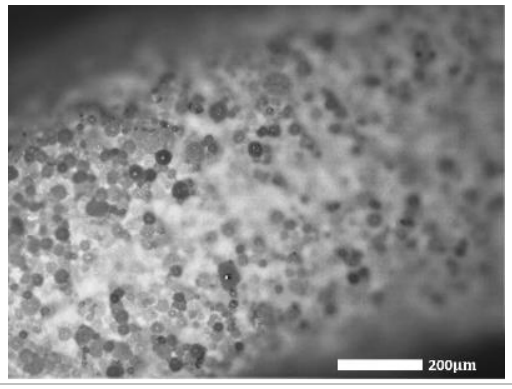
Side view	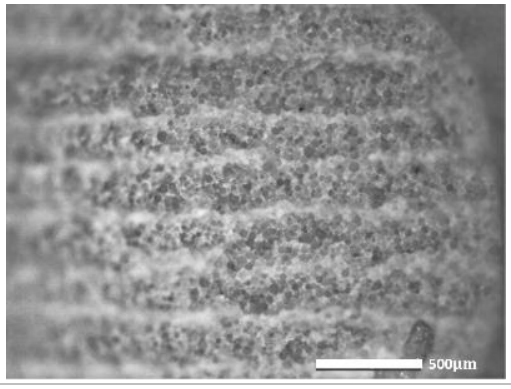	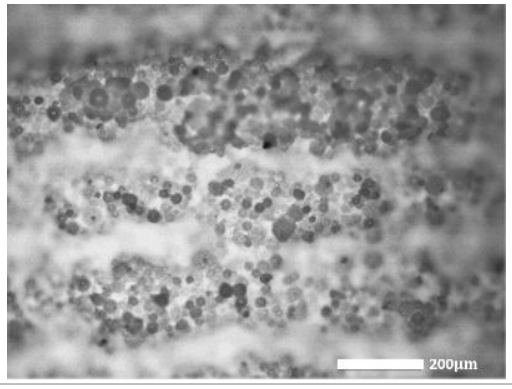

Annex 12

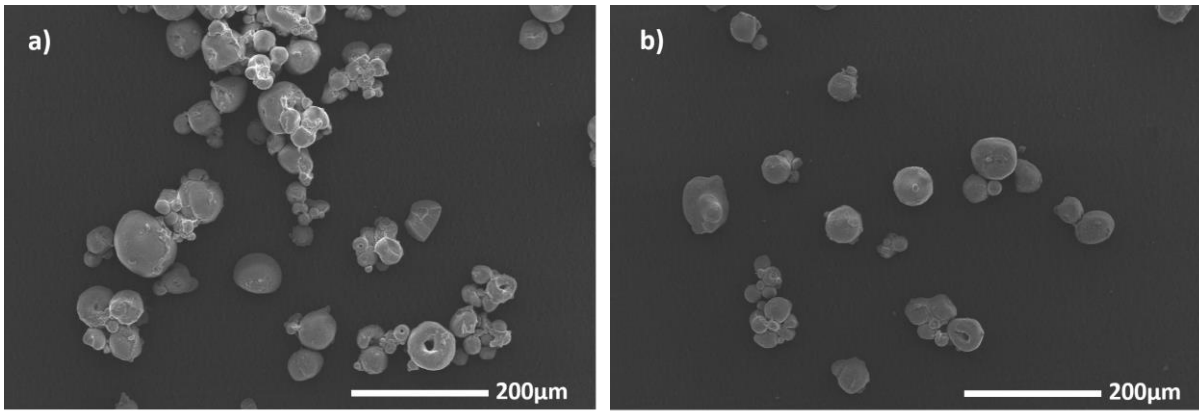

Figure A.26 SEM images, a) Powder of samples printed from pastes without binder and b) Powder of samples printed from pastes without binder, 4 weeks in SBF.

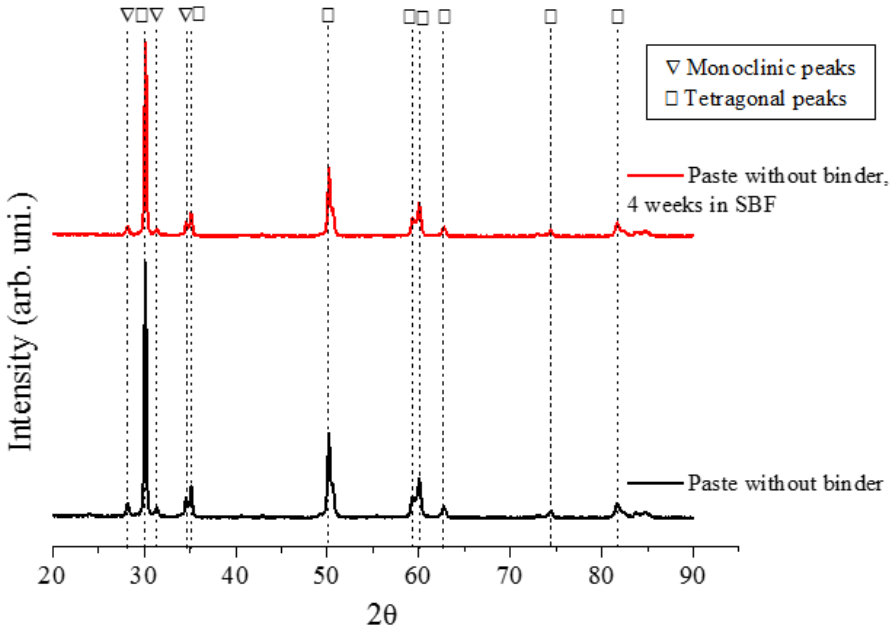

Figure A.27 XDR patterns of samples printed from pastes without binder. [62][37]

Annex 13

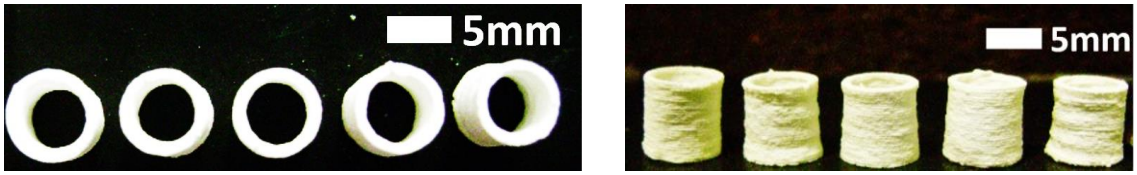

Figure A.28 Samples printed from paste 3YSZ+0.035GO.

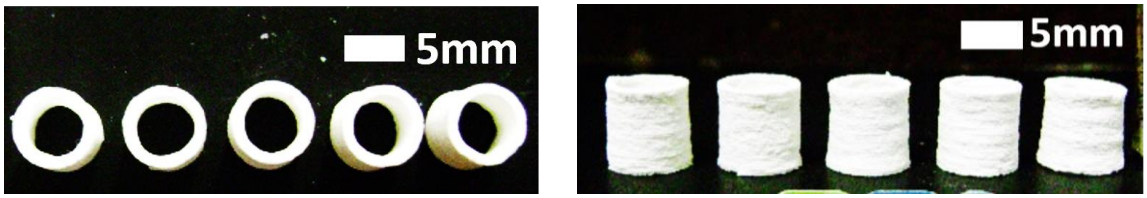

Figure A.29 Samples printed from paste 3YSZ+0.1GO.

Table A.27 Images of solutions and pastes.

0.035GO	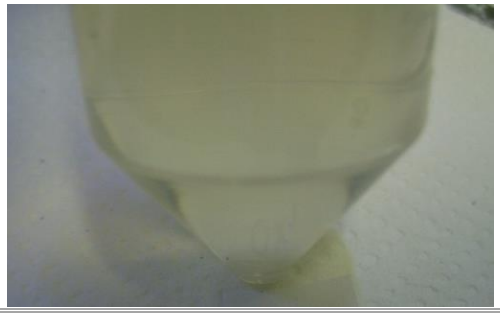	
0.1GO		
0.05GO	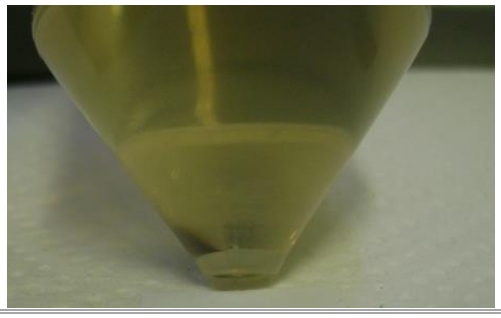	not used to make paste
0.5GO		

Table A.28 Paste 3YSZ+ GO non-sintered.

Paste 3YSZ+0.035GO	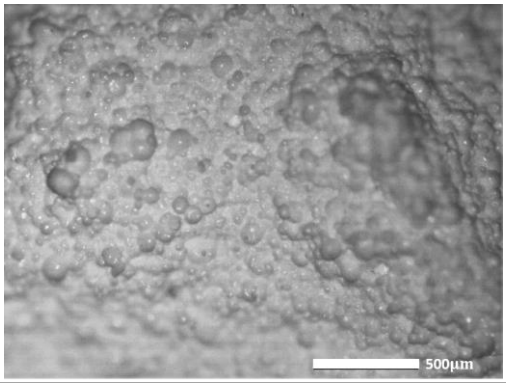	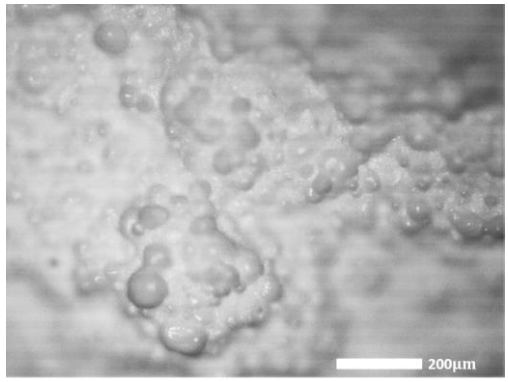
Paste 3YSZ+0.1GO	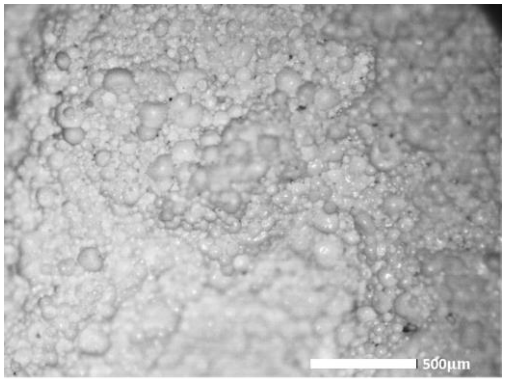	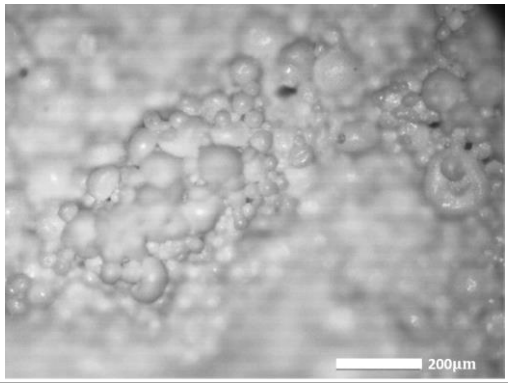
Paste 3YSZ+0.5GO	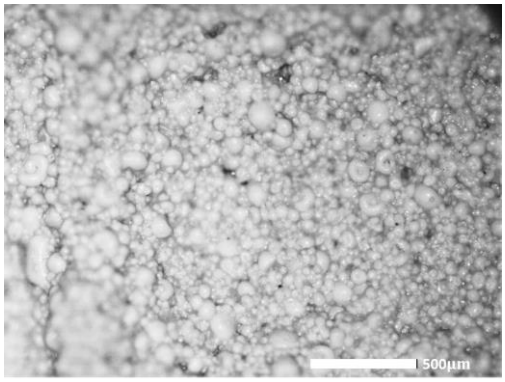	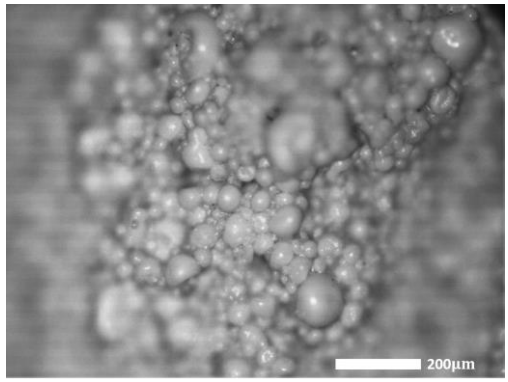

Annex 14

Table A.29 Paste 3YSZ+AgNPs non-sintered.

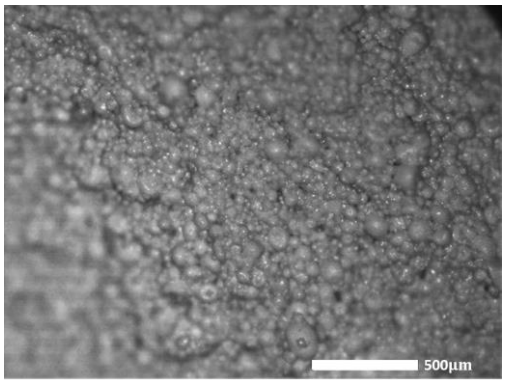

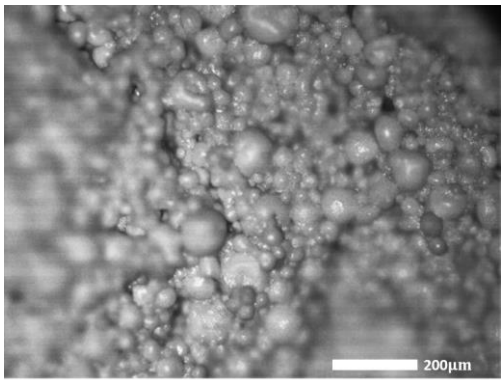

Annex 15

Samples printed with the paste without binder by EDS analysis:

Table A.30 EDS results of samples printed with the paste without binder sintered.

Element	App	Intensity	Weight%	Weight%	Atomic%
	Conc.	Corrn.		Sigma	
O K	15.32	0.3800	27.17	0.81	69.24
Y K	7.64	0.8976	5.74	1.00	2.63
Zr L	81.85	0.9294	59.35	0.99	26.52
Au M	10.78	0.9378	7.75	0.66	1.60
Totals			100.00		

Samples printed with the paste 3YSZ+0.5GO by EDS analysis:

Table A.31 EDS results of samples printed with the paste 3YSZ+0.5GO sintered.

Element	App	Intensity	Weight%	Weight%	Atomic%
	Con.	Corrn.		Sigma	
O K	12.01	0.3693	23.46	1.85	65.05
Y K	9.59	0.9130	7.58	2.74	3.78
Zr L	77.76	0.9372	59.86	2.48	29.12
Au M	11.68	0.9259	9.10	1.52	2.05
Totals			100.00		

Samples printed with the paste 3YSZ+AgNPs by EDS analysis:

Table A.32 EDS results of samples printed with the paste 3YSZ+AgNPs sintered.

Element	App	Intensity	Weight%	Weight%	Atomic%
	Con	Corrn.		Sigma	
O K	12.55	0.3746	24.37	1.08	66.29
Y K	10.34	0.9099	8.27	1.49	4.05
Zr L	74.08	0.9348	57.68	1.36	27.52
Au M	12.18	0.9164	9.68	0.89	2.14
Totals			100.00		

Annex 16

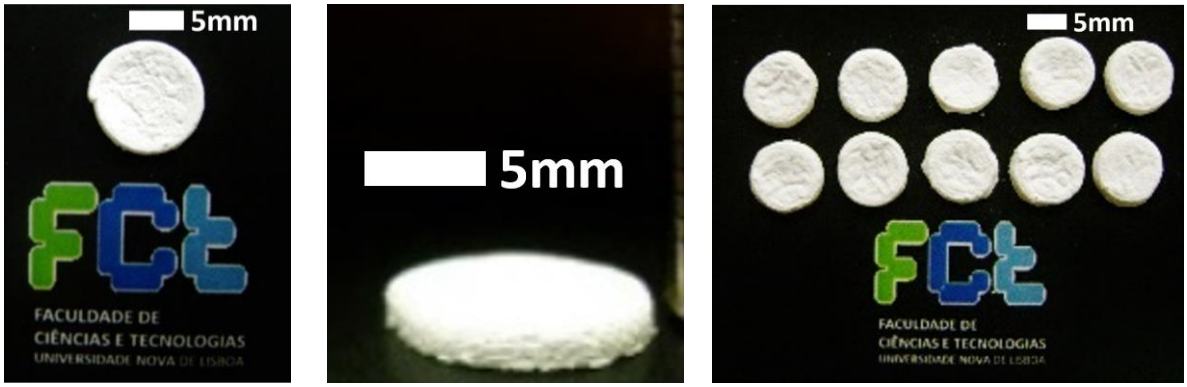

Figure A.30 Example of samples for cytotoxicity assays and adhesion/cell proliferation assays (after sintered, samples printed with the paste without binder).

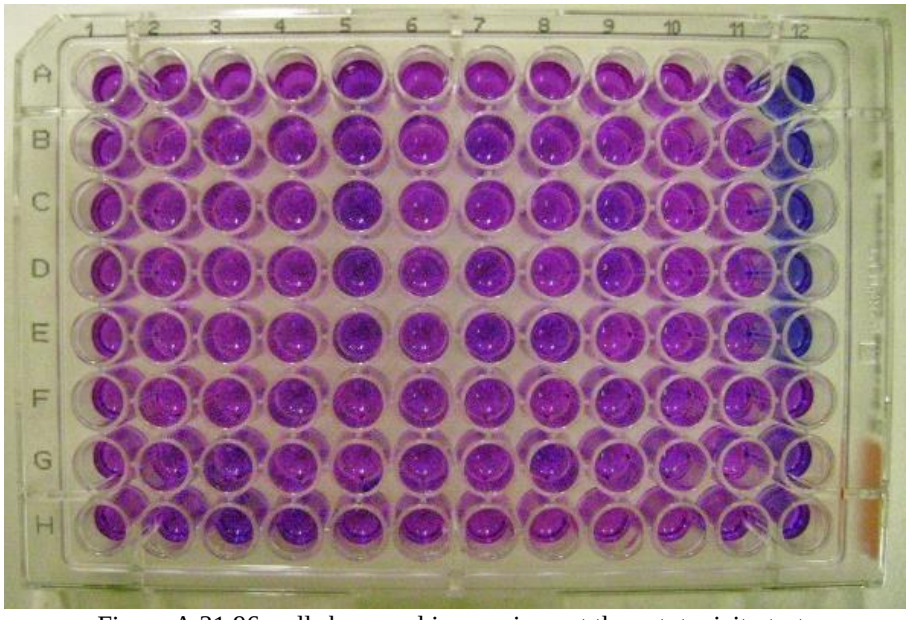

Figure A.31 96 wells box used in carrying out the cytotoxicity test.